Inaugural dissertation

for obtaining the doctoral degree of the

Combined Faculty of Mathematics, Engineering and Natural Sciences

of the Ruprecht-Karls-University Heidelberg

presented by

M. Sc. Alessa Mieg

born in Stuttgart, Germany

Oral examination: 16th December 2022

Aging- and obesity-associated metabolic reprogramming suppresses $CD8^+$ T cell responses

Referees:

Prof. Dr. Britta Brügger

Dr. Guoliang Cui

Abstract

Aging and obesity are growing global health issues and are associated with increased susceptibility towards infectious diseases, increased cancer risk and decreased vaccination efficacy. $CD8^+$ T cells are the main effectors of cell-mediated adaptive immunity and form antigen-specific memory after pathogen clearance. However, upon antigen persistence during cancer or chronic infections, T cells become dysfunctional, a state termed T cell exhaustion. In $CD8^+$ T cells, the transcription factor T cell factor 1 (TCF1, encoded by *Tcf7*) is a stemness marker and high expression is associated with $CD8^+$ T cell longevity and superior functionality. The aim of this study was to identify synergistic effects of aging and obesity on the $CD8^+$ T cell phenotype and function as well as on the plasma metabolite profile to ultimately find a causal relation.

A diet-induced obesity mouse model of young and aged mice was used to study the effect of aging and obesity on the $CD8^+$ T cell phenotype as well as on the plasma metabolite profile. Flow cytometric analysis of naïve $CD8^+$ T cells revealed a terminally differentiated, exhausted $CD8^+$ T cell phenotype with reduced TCF1 expression in aged obese compared to young lean mice. Mass spectrometric analysis of plasma samples identified the tryptophan metabolite 3-Indolepropionic acid (3-IPA) to be synergistically decreased by aging and obesity. Treatment of primary murine and human $CD8^+$ T cells with 3-IPA in therapeutic concentrations, increased TCF1 expression as well as other stemness markers and reversed T cell exhaustion *in vitro*. Using the lymphocytic choriomeningitis virus (LCMV) infection model, 3-IPA pre-treatment of antigen-specific $CD8^+$ T cells rescued aging- and obesity-impaired anti-viral $CD8^+$ T cell effector and memory functions.

To elucidate the molecular mechanism how 3-IPA increases $CD8^+$ T cell stemness, a pull-down experiment was performed and γ-catenin was identified as a 3-IPA-binding protein. Further investigations revealed decelerated degradation of γ-catenin and its close homologue β-catenin upon 3-IPA treatment in activated $CD8^+$ T cells. Moreover, 3-IPA treatment increased *Tcf7* promoter activity in a luciferase assay, while the role of β- and γ-catenin in this context remains elusive.

In summary, aging and obesity synergistically decreased stemness, recall capacity and anti-viral effector functions of $CD8^+$ T cells, thus making them a detrimental combination. Treatment of $CD8^+$ T cells with 3-IPA restored those defects, suggesting a therapeutic potential of 3-IPA to overcome aging- and obesity-mediated $CD8^+$ T cell dysfunctionality.

Zusammenfassung

Hohes Alter und Adipositas sind zunehmende globale Gesundheitsprobleme und gehen mit erhöhtem Infektions- und Krebsrisiko sowie verminderter Wirksamkeit von Impfungen einher. $CD8^+$ T-Zellen sind hauptverantwortlich für die zelluläre Immunantwort des adaptiven Immunsystems. Chronische Infektionen oder Krebs führen zu „T-Zellerschöpfung“, was mit eingeschränkten Effektor- und Gedächtnisfunktionen einhergeht. Der Transkriptionsfaktor TCF1 (Gen: *Tcf7*) ist ein Marker für stammzellartige T-Zellen und eine hohe Expression ist mit Langlebigkeit und verbesserter Funktionalität von $CD8^+$ T-Zellen assoziiert. Ziel dieser Arbeit war es den synergistischen Effekt von Alterung und Adipositas auf den $CD8^+$ T-Zellphänotyp sowie auf das Plasmaproteinprofil zu untersuchen, mit der Absicht einen kausalen Zusammenhang zu identifizieren.

In einem Diät-induzierten Adipositas Mausmodel in jungen und alten Mäusen wurde der synergistische Effekt von Alterung und Adipositas auf den $CD8^+$ T-Zellphänotyp untersucht. Durchflusszytometrische Analysen von $CD8^+$ T-Zellen zeigten einen terminal differenzierten, erschöpften Phänotyp mit erniedrigter TCF1 Expression in alten adipösen Mäusen. Des Weiteren wurde in massenspektrometrische Analysen von Plasmaproben der Tryptophan-Metabolit 3-Indolpropionsäure (3-IPA) als synergistisch erniedrigter Metabolit identifiziert. Behandlung primärer muriner und humaner $CD8^+$ T-Zellen mit 3-IPA in therapeutischen Konzentrationen führte zu erhöhter Expression von TCF1 und weiterer Stammzell-Marker und verhinderte T-Zellerschöpfung *in vitro*. Im lymphozytären Choriomeningitis Virus Model resultierte die Behandlung virus-spezifischer $CD8^+$ T-Zellen aus alten adipösen Mäusen mit 3-IPA in Widerherstellung ihrer anti-viralen Gedächtnis- und Effektorfunktion.

Um den molekularen Mechanismus zu erläutern, wie 3-IPA den $CD8^+$ T-Zellphänotyp beeinflusst, wurde ein Pull-down Experiment durchgeführt und γ-Catenin als 3-IPA-bindendes Protein identifiziert. Weitere Untersuchungen zeigten einen verzögerten Abbau von γ-Catenin und dessen Homolog β-Catenin nach 3-IPA-Behandlung in aktivierten $CD8^+$ T-Zellen. In einem Luciferase-Assay erhöhte 3-IPA des Weiteren die *Tcf7* Promotoraktivität, wobei die Rolle von β- und γ-Catenin in diesem Zusammenhang weiterer Untersuchungen bedarf.

Zusammenfassend zeigt diese Arbeit, dass Alterung und Adipositas in Kombination die Gedächtniszellformierung und anti-virale Funktionen von $CD8^+$ T-Zellen verringern. Diese konnten durch Behandlung mit 3-IPA wiederhergestellt werden, was ein therapeutisches Potential von 3-IPA bei Alter- und Adipositas-assoziierten Krankheiten impliziert.

Acknowledgments

I could not have completed my PhD without the support of the people who accompanied me throughout this exciting journey.

First and foremost, I would like to express my deepest gratitude to my supervisor Dr. Guoliang Cui who gave me the opportunity to conduct this research project in his lab. I am grateful for his constant support and personal supervision whenever I needed it. His excellent knowledge in the field of immunology and overall scientific expertise was inspiring and helped me to develop professionally and personally.

Special thanks to my Thesis Advisory Committee Prof. Dr. Britta Brügger and Prof. Dr. Aurelio Teleman for the valuable input and advice on the project. Furthermore, I'd like to thank Prof. Dr. Hedda Wardemann and Prof. Dr. F. Nina Papavasiliou for being part of my defense committee as additional referees.

Many thanks to my present and former lab colleagues Dr. Nina Weißhaar, Alaa Madi, Marvin Hering, Ferdinand Zettl, Kerstin Mohr, Nora ten Bosch, Dr. Jingxia Wu, Dr. Sicong Ma and Dr. Yanan Ming. I am thankful not only for their support in the lab, but also for the great and fun conversations we had over lunch and coffee, nice activities and motivating words whenever needed. A big thank you also goes to my lab members from HI-TRON in Mainz Dr. Jannis Wißfeld, Dr. Anke Werner and Xin Yan for their scientific input and enjoyable conversations. I'd also like to thank my master student Cecilia Reyneri for her contribution and hard work.

I would like to extend my sincere thanks to the DKFZ flow cytometry core facility, the DKFZ animal core facility, Dr. Gernot Poschet (Centre for Organismal Studies, Heidelberg) and Dr. Aubry Miller (Research Group Cancer Drug Development, DKFZ, Heidelberg) for their experimental and scientific support.

Getting through the PhD required more than just scientific support and therefore a very special thanks goes to my partner, my friends and my family. This journey has been full of ups and downs and I'm very grateful for having such supportive people in my life. Thank you for all the fun times, great conversations, constant motivation and belief in me. Thank you for always having an open ear and just being there.

Table of contents

Abbreviations

2-DG	2-Deoxy glucose
3-IPA	3-Indolepropionic acid
AABA	α-Aminobutyric acid
ACK	Ammonium chloride potassium
ADMA	Asymmetric dimethylarginine
AdPC	*Adenomatous polyposis coli* gene product
AhR	Aryl hydrocarbon receptor
AL	Aged lean
AO	Aged obese
APC	Antigen-presenting cell
APS	Ammonium persulfate
Arm	Armstrong
AT	Adipose tissue
ATP	Adenosine triphosphate
BCR	B cell receptor
BFA	Brefeldin A
BMI	Body mass index
BSA	Bovine serum albumin
BW	Body weight
CD	Cluster of differentiation
cDNA	Complementary DNA
cl13	Clone 13
COVID-19	Coronavirus disease 2019
crRNA	CRISPR RNA

CTL	Cytotoxic T lymphocyte
CTLA-4	Cytotoxic T lymphocyte antigen 4
CXCR3	Chemokine receptor CXC motif 3
DC	Dendritic cell
ddH_2O	Double deionized water
DMSO	Dimethylsulfoxid
dpi	Days post infection
Dvl	Dishevelled
ECAR	Extracellular acidification rate
EGFP	Enhanced green fluorescent protein
Eomes	Eomesodermin
FACS	Fluorescence activated cell sorting
FAO	Fatty acid oxidation
FBS	Fetal bovine serum
FCCP	Carbonyl cyanide 4-(trifluoromethoxy)phenylhydrazone
Foxo1	Forkhead box protein O1
Foxp3	Forkhead box P3
Fzd	Frizzled
GATA3	GATA binding protein 3
GP33	Glycoprotein 33-41
gRNA	Guide RNA
Grz	Granzyme
GSK3	Glycogen synthase kinase 3
HFD	High fat diet
HSC	Hematopoietic stem cell
ICB	Immune checkpoint blockade
IDO	Indoleamine-2,3-dioxygenase
IFNγ	Interferon γ
IL	Interleukin

Ind-SO_4	Indoxyl sulfate
i.p.	Intraperitoneal
IR	Inhibitory receptor
i.v.	Intravenous
KLRG1	Killer-cell lectin like receptor G1
KO	Knockout
LAG-3	Lymphocyte-activation gene 3
LCMV	Lymphocytic choriomeningitis virus
LD	Live/dead
LDL	Low-density lipoprotein
LEF1	Lymphoid enhancer binding factor 1
LRP5/6	Low-density lipoprotein receptor related protein 5/6
mAb	Monoclonal antibody
MDR	MitoTracker™ Deep Red FM
Met-SO	Methionine sulfoxide
MFI	Mean fluorescence intensity
MG	MitoTracker™ Green FM
MHC	Major histocompatibility complex
mTOR	Mechanistic target of Rapamycin
NK	Natural killer cell
OCR	Oxygen consumption rate
OXPHOS	Oxidative phosphorylation
PAGE	Polyacrylamide gel electrophoresis
PBMC	Peripheral blood mononuclear cell
PBS	Phosphate-buffered saline
PCR	Polymerase chain reaction
PD-1	Programmed cell death protein 1
PD-L1	PD-1 ligand 1
pMHC	MHC-bound peptide

RT	Room temperature
SARS-CoV-2	Severe acute respiratory syndrome coronavirus 2
s.c.	Subcutaneous
SDS	Sodium dodecyl sulfate
Slamf6	Signaling lymphocyte activation molecule 6
SRC	Spare respiratory capacity
T-bet	T-box transcription factor TBX21
TCF1	T cell factor 1
T_{cm}	Central memory T cell
TCR	T cell receptor
T_{eff}	Effector T cell
T_{em}	Effector memory T cell
T_{ex}	Exhausted T cell
Tex_{int}	Intermediate exhausted T cell
Tex_{prog}	Progenitor exhausted T cell
TF	Transcription factor
TGFβ	Transforming growth factor-β
Th	T helper cells
TIGIT	T-cell immunoreceptor with immunoglobulin and ITIM domains
TIL	Tumor infiltrating lymphocyte
Tim-3	T cell immunoglobulin and mucin-domain containing-*3*
TME	Tumor microenvironment
T_{mem}	Memory T cell
TNFα	Tumor necrosis factor α
TOX	Thymocyte selection-associated HMG BOX protein
T_{pex}	Progenitor exhausted T cell
tracrRNA	Transactivating crRNA
T_{reg}	Regulatory T cell
T_{rm}	Tissue resident memory T cells

T_{stem}	Stem cell-like T cell
WAT	White adipose tissue
Wnt	Wingless/Integration 1
WT	Wildtype
YL	Young lean
YO	Young obese

1 Introduction

These days, the word “pandemic” has regained increased significance, as since March 2020 novel coronavirus severe acute respiratory syndrome coronavirus 2 (SARS-CoV-2) has induced a global pandemic of enormous extent and the crisis is not over yet.

A pandemic is defined as “an epidemic (occurrence of a disease in a pattern that is clearly in excess of normal expectations) in which a disease spreads worldwide, crossing international boundaries and spreading between continents” [1]. However, nowadays the term “pandemic” is not limited to infectious diseases, but also used for other harmful conditions. Growing incidences of aging, obesity and cancer, for example, are severe global health issues and were therefore labeled as epidemic or pandemic likewise [2-4].

If we take a closer look at different pandemic conditions, one cannot be clearly separated from another since different factors are correlative and potentiate each other. Therefore, it is of great importance to look at the bigger picture to be able to contain existing pandemics and to prevent new pandemics from arising.

1.1 Aging

The global population is aging in all regions of the world. While in 2019, there were 703 million persons aged 65 or above, this number is expected to double in 2050, resulting in a rise in the proportion of aged individuals among the world population from 9 % to 15,5 %. The number of people aged 80 years or older is proposed to even triple by 2050 [5, 6].

Aging is a complex process that is generally defined as a time-dependent progressive decline of various physiological functions of living organisms. This multifactorial process, however, is highly individual. The functional decline on an organ, tissue and cellular level leads to the increased occurrence of malfunctions in aged individuals, making age the biggest risk factor for several diseases such as cancer, cardiovascular disease and neurodegeneration [7]. Furthermore, the frequency and severity of infectious diseases is higher in the elderly compared to young people [8]. A striking example of how age is associated with disease severity is the above-mentioned coronavirus disease 2019 (COVID-19), since patients of age 60 years or older showed significantly higher morbidity and mortality compared to younger patients [9].

One hallmark of aging is cellular senescence. Senescence is defined as a stable cell cycle arrest induced by extrinsic and intrinsic stress stimuli and was discovered almost 60 years ago

by Hayflick and colleagues [10, 11]. Senescent cells secrete various soluble factors such as proinflammatory cytokines [12]. Their accumulation with age results in a constant release of proinflammatory molecules which leads to a systemic, sterile (without infection), chronic low-grade inflammation, termed “inflammaging” [13]. Inflammaging was described to be involved in several of the before-mentioned age-related diseases that are associated with an inflammatory pathogenesis [14].

Life span progressively increases nowadays and is expected to increase further [15], while many of the age-related diseases persist and are still not curable. This leads to increasing disease prevalence making aging a global health issue

1.2 Obesity

Besides aging, another global health issue is the growing rate of overweight and obese people. Obesity is defined as a health-impairing excessive fat accumulation diagnosed by a body mass index (BMI) of ≥30 kg/m^2 [16]. In 2016, 13% of all adults (aged 18 or above) worldwide were obese. In children (aged 5-19) the prevalence of obesity has risen from 4% in 1975 to over 18% in 2016. The overall obesity prevalence nearly tripled between 1975 and 2016, resulting in higher numbers of obese people than underweight people worldwide [17].

Similar to aging, obesity is associated with several co-morbidities such as the metabolic diseases type 2 diabetes mellitus, fatty liver disease, cardiovascular diseases and even some types of cancer [16, 18]. Moreover, obese people are more susceptible to several infectious diseases and once infected, obesity leads to a worse prognosis and higher mortality rates [19]. Again, COVID19 is a striking example of this phenomenon, since Gao *et al.* found a linear correlation between increasing BMI and admission to an intensive care unit [20].

The white adipose tissue (WAT) can be seen as a large endocrine organ which systemically secretes adipokines and cytokines. Adipokines are signaling peptides involved in several metabolic and physiological processes such as insulin signaling, fatty acid oxidation or glucose uptake [21]. Obesity induces a phenotypic switch of the WAT resulting in hypertrophic adipocytes with a mainly inflammatory secretome. The local and systemic secretion of proinflammatory cytokines results in the disruption of normal WAT functions and a systemic low-grade inflammation [22]. This obesity-related inflammation was termed “metaflammation” (metabolically triggered inflammation) [23] and is comparable to the before-described inflammaging.

1.3 The immune system

Both aging and obesity have been described as increasing susceptibility to infectious diseases and to worsen their outcome. Infections are diseases caused by pathogens such as bacteria, viruses, fungi or other microorganisms. We are constantly exposed to pathogens, but yet become ill very rarely due to a complex network of cells, tissues and soluble factors that cooperate to defend the body against diseases. This multi-layered defense mechanism is called “immune system” [24]. Besides external pathogens, own body cells can also do harm by mutating and developing into tumors. It’s the immune system’s job to recognize mutated cells and remove them before tumors can establish [25].

Almost all organisms, including bacteria and plants, have an immune system protecting them from external pathogens [26, 27]. While immune mechanisms of invertebrates, comprising the great majority of animal species on earth, are limited to unspecific defense systems, vertebrates, including mammals, have developed an additional line of defense system, which enables a pathogen-specific response and the development of immunological memory [28]. Those two branches of immunological defense, the unspecific innate and the pathogen-specific adaptive immune system, work tightly together to ensure effective protection from pathogens and cancer.

1.3.1 The innate immune system

The initial defense mechanisms against invading pathogens are anatomic and chemical barriers including skin and mucosal surfaces as well as antimicrobial proteins present at mucosal surfaces. Once a pathogen has breached those initial barriers, further components of the innate immune system come into action, such as the complement system, a network of more than 30 different plasma proteins [24].

Immune cells of the innate immune system are mainly derived from the myeloid lineage and comprise macrophages, dendritic cells (DCs), granulocytes (consisting of neutrophils, eosinophils and basophils) and mast cells [24]. Cells of the innate immune system recognize conserved pathogen-associated molecular patterns, such as lipopolysaccharides of bacterial cell-wall components or viral nucleic acids, by pattern recognition receptors [29, 30]. Macrophages, neutrophils and DCs are phagocytes, which are able to take up pathogenic microorganisms and infected cells, thereby eliminating their target and subsequently presenting fragments of antigens by surface receptors, called major histocompatibility complex (MHC) class I and II [31]. Therefore, those cells were named antigen-presenting cells (APCs). Furthermore, after uptake of the target cell, APCs secrete proinflammatory molecules such as cytokines and chemokines which leads to recruitment and activation of other immune cells [32]. Since the presented antigens are recognized by adaptive immune cells, APCs tightly link

the innate with the adaptive system. Natural killer (NK) cells are another innate immune cell type, deriving from the lymphoid lineage, that are able to directly lyse virus-infected cells and tumor cells [33].

The innate immune system responds to pathogens in an antigen-independent manner and is able to detect and react within hours of antigen encounter, thereby providing an effective first-line defense mechanism [34].

1.3.2 The adaptive immune system

In contrast to the innate immune system, the fundamental trait of the adaptive immune system is the ability to form antigen-specific immunological memory. Two major cell types mediate the adaptive immune response, namely B and T lymphocytes, which develop in the bone marrow (B cells) or thymus (T cells), respectively [35, 36].

Antigens are usually polysaccharides, proteins or glycoproteins [37]. B and T cells recognize their cognate antigen via highly variable antigen-receptors on their surface. B cell receptors (BCRs) and T cell receptors (TCRs) recognize only small fractions of an antigen, the so-called epitope. While BCRs can recognize almost all chemical structures and are able to directly bind to them, TCRs can only recognize protein epitopes which are presented by MHC molecules [24]. Two different MHC molecules are involved in TCR antigen recognition, MHC class I and MHC class II. MHC class I is expressed by all nucleated cells and presents peptides consisting of 8-10 amino acids that mainly derive from degraded cytosolic proteins, such as virus particles. MHC class II is expressed mainly on the surface of APCs and presents peptides with a length of minimum 13 amino acids, that derive from extracellular proteins of the phagocyted cell [38].

Adaptive lymphocytes need to specifically recognize billions of different antigens. In order to be able to encode this huge number of different antigen receptors, they combinate, rearrange and join different gene segments of their antigen receptor during maturation [39, 40]. Before entering the lymphatic system, lymphocytes undergo strict positive and negative selection processes, in order to ensure signaling capacity of the respective antigen receptor on the one hand and to prevent the reaction to “self”-antigens on the other hand, which could result in autoimmunity [41, 42].

After maturation in the primary lymphoid organs, bone marrow and thymus, lymphocytes enter the lymphatic system. They circulate in the blood and lymph and can be found in large numbers in the secondary lymphoid organs, including lymph nodes and spleen. Pathogen antigens are transported to secondary lymphoid organs, mainly by DCs, where they encounter lymphocytes and the immune response is initiated [43]. Both, lymph nodes and spleen are

structurally organized in a way that allows B and T cells to localize in specific zones and to facilitate antigen-encounter and specific activation [44].

Once activated by their specific antigen, B and T cells take on different tasks of the adaptive immune response. While B cells are responsible for antibody-mediated humoral immunity, T cells execute the cell-mediated immune response of adaptive immunity.

1.4 T cells

Two types of T cells are distinguished according to the expression of the cell surface proteins cluster of differentiation 4 (CD4) and 8 (CD8). CD4 and CD8 are co-receptors, which are required for T cell activation mediated by the interaction between the TCR and MHC-bound peptide (pMHC) [45-47]. MHC class I and II have slightly different structures, which can be recognized and bound by CD8 and CD4, respectively. Interaction of CD4 with MHC class II and CD8 with MHC class I increases TCR sensitivity and reduces the amount of peptide required for T cell activation [48-51].

1.4.1 $CD4^+$ T cells

$CD4^+$ T cells recognize antigens presented by APCs and are commonly known as T helper (Th) cells. Once a naïve $CD4^+$ T cell encounters its cognate antigen presented by MHC class II, it can differentiate into different $CD4^+$ T cell subsets, such as Th1, Th2, Th17, T follicular helper or induced regulatory T cells (T_{reg}). The differentiation process is mainly influenced by cytokines produced by cells of the innate immune system [52].

Different $CD4^+$ T cell subsets are helpers of distinct immune cells to improve their function and promote pathogen clearance [53].

In contrast, the function of T_{reg} is to suppress effector T cell (T_{eff}) responses in order maintain peripheral tolerance and prevent autoimmunity. T_{reg} are characterized and maintained by the expression of the transcription factor (TF) Forkhead box P3 (Foxp3) [54].

1.4.2 $CD8^+$ T cells

$CD8^+$ T cells are the main effectors of cell-mediated adaptive immunity and are also referred to as cytotoxic T lymphocytes (CTLs). CTLs are the central players in anti-viral and anti-tumor immunity. Upon antigen encounter, CTLs expand rapidly, differentiate into T_{eff} and and exert their effector functions to clear the infection. After clearance, most of the T_{eff} die, while a small fraction of antigen-specific T cells survives and differentiates into memory T cells (T_{mem}), which are able to rapidly respond to re-infection with the same antigen (Figure 1.1.A). In chronic viral

infections and cancer, however, antigen persists and can't be cleared by CTLs, leading to "T cell exhaustion", further described in chapter 1.5 [55, 56] (Figure 1.1.B).

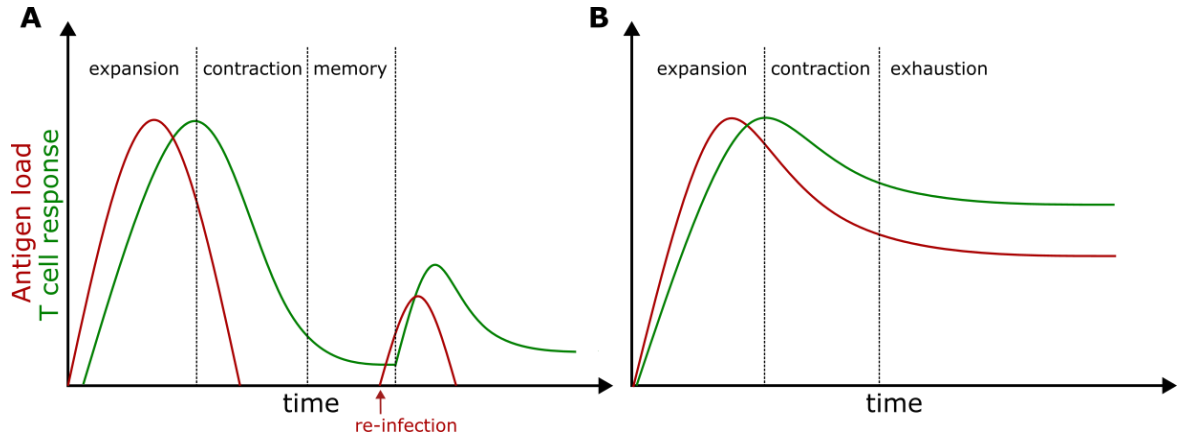

Figure 1.1. Kinetics of CD8⁺ T cell responses (green) following antigen exposure (red) over time. A. *Upon antigen encounter during an acute infection or vaccination, CD8⁺ T cells undergo clonal expansion and clear the antigen, which is followed by a contraction phase and memory formation of the remaining CD8⁺ T cells.* ***B****. During chronic infection or cancer, CD8⁺ T cells are unable to completely clear the antigen, leading to reduced T cell activity of present cells, also referred to as T cell exhaustion. Figure inspired by [57] and [58].*

CTLs mediate killing of their target cells by secreting cytotoxic molecules, such as granzymes and perforins as well as proinflammatory cytokines, such as interleukin 2 (IL-2), interferon γ (IFNγ) and tumor necrosis factor α (TNFα) [59-61].

The effector proteins granzymes and perforins are stored in specialized cytotoxic granules and are released upon antigen recognition and binding. Perforins induce pore formation in the plasma membrane of the target cell through which other effector molecules, such as apoptosis-inducing granzymes, can enter [62]. Besides direct effector proteins, CD8⁺ T cells secrete proinflammatory cytokines. IFNγ released by CTLs, directly inhibits viral replication [63], induces upregulation of MHC class I-expression on target cells [64] and activates and recruits macrophages to the site of the infection, where they act as effector cells and APCs [65]. TNFα can synergize with IFNγ to activate macrophages and is also involved in apoptosis of target cells [66].

1.4.2.1 CD8⁺ T cell differentiation

T cells derive from multipotent hematopoietic stem cells (HSC) in the bone marrow, which migrate over the blood and seed the thymus. Thymic stroma-induced NOTCH signaling promotes T cell lineage commitment of multipotent progenitors [67]. NOTCH signaling induces expression of the TF T cell factor 1 (TCF1) [68] and GATA Binding Protein 3 (GATA3) [69]. Together with another TF, Bcl11b, they further initiate expression of genes specific for the T cell lineage [70]. After a short CD4⁺CD8⁺ double-positive phase, progenitor cells differentiate

into either $CD4^+$ or $CD8^+$ single-positive naïve T cells that are exported from the thymus to the periphery [71].

Naïve $CD8^+$ T cells circulate from the blood to secondary lymphatic organs, especially the lymph nodes. This “homing” process is induced by surface expression of specific homing receptors, such as L-selectin (CD62L) [72]. Naïve T cells are further characterized by high expression levels of TCF1 [73] and the IL-7 receptor α chain CD127 while lacking expression of killer-cell lectin like receptor G1 (KLRG1) and the activation marker CD44 [74, 75].

Once a naïve $CD8^+$ T cell encounters its cognate antigen it becomes activated and undergoes rapid proliferation and clonal expansion. $CD8^+$ T cell activation is initiated by three signals: 1) Interaction between the TCR:CD3 complex and its cognate pMHC as well as CD8 binding to MHC class I [76]. 2) Co-stimulation by APCs by CD28 engagement [77]. 3) Signals by inflammatory cytokines, such as IL-12 or IFNγ [78].

Activated T cells downregulate CD62L and TCF1 and upregulate activation markers CD44 and KLRG1 [79]. Furthermore, activated T cells are characterized by expression of a plethora of effector molecules, such as IL-2, IFNγ, TNFα, granzyme (Grz) A and B as well as perforin [59-61, 80]. The TFs T-box transcription factor TBX21 (T-bet) and Eomesodermin (Eomes) are both involved in IFNγ production and expression of other cytotoxic molecules in $CD8^+$ T cells [81]. Differential expression of T-bet and Eomes, decides T cell fate after the clearance of an infection. While T-bet promotes differentiation to short-lived effector cells with high cytotoxic potential, Eomes rather fosters the development of T_{mem} [82, 83].

After clearance of an infection, most T_{eff} cells die, while a small fraction of antigen-specific T cells remains and differentiates into T_{mem}. The pool of T_{mem}, however, is phenotypically and functionally heterogeneous. Two types of T_{mem} in mice can be well-defined by the expression of CD44 and CD62L. Unlike their naïve counterparts, antigen-experienced T_{mem} generally express CD44, but have differential expression of CD62L. $CD44^{high}CD62^{low}$ T cells have been defined as effector memory T cells (T_{em}), while $CD44^{high}CD62^{high}$ T cells mark the central memory T cell population (T_{cm}) [84]. T_{em} cells have higher prevalence in tissues, display higher cytolytic functions compared to T_{cm} cells and are further identified by KLRG1 expression [85]. T_{cm} cells are found primarily in lymph nodes and have been described to provide a protective immune response against chronic infections [86]. Besides Eomes, TCF1 also plays an important role in T_{cm} differentiation [87]. Another subset of memory T cells are tissue resident memory (T_{rm}) cells, which reside in specific tissues and don’t circulate. T_{rm} cells can be identified by the expression of CD103 and CD69 [88] as well as low expression of TCF1 [89]. A key feature of T_{mem} is IL-7 and IL-15-driven homeostatic proliferation without antigen stimulation, thereby ensuring long-term persistence [90].

A further distinct differentiation state of T cells are exhausted T cells (T_{ex}), which will be further characterized in chapter 1.5.

A schematic and simplified overview of $CD8^+$ T cell differentiation is depicted in Figure 1.2.

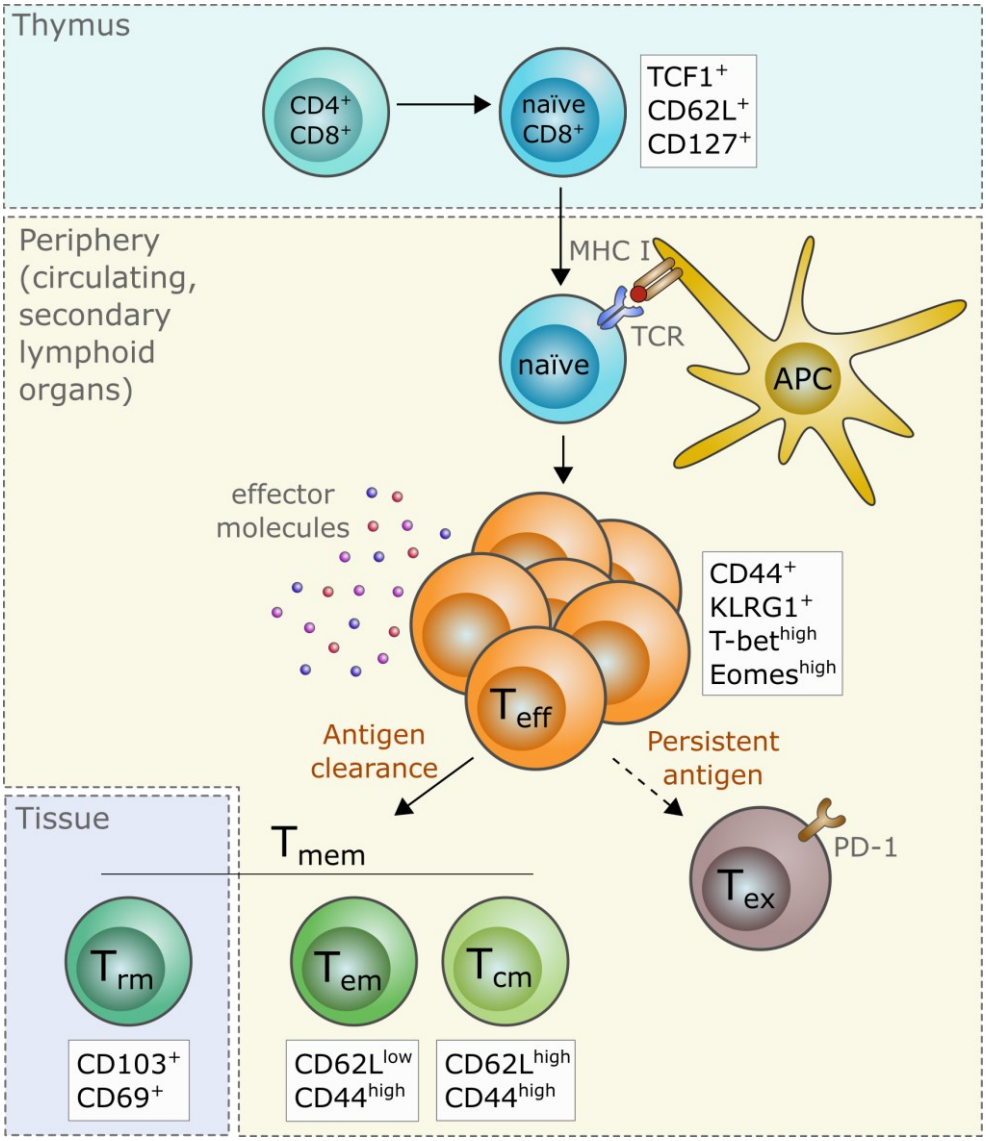

Figure 1.2. $CD8^+$ T cell differentiation model. *In the thymus, $CD4^+CD8^+$ double-positive progenitor cells differentiate into either $CD4^+$ or $CD8^+$ single-positive naïve T cells. Naïve $CD8^+$ T cells, characterized by TCF1, CD62L and CD127 expression, are exported from the thymus to the periphery. Once a naïve T cell encounters and binds with its TCR to its cognate antigen presented by an APC via MHCI, it differentiates into T_{eff}. T_{eff} express high levels of CD44, KLRG1, T-bet and Eomes and exert their effector functions by releasing different effector molecules. Once the antigen has been cleared, a small fraction of T_{eff} differentiates into different T_{mem} subsets, such as T_{em}, T_{cm} and T_{rm}, which can be distinguished by differential surface marker expression. Upon persistent antigen, T cells differentiate into programmed cell death protein 1 (PD-1)-expressing T_{ex}.*

1.4.3 T cell metabolism

During their life span, T cells undergo several differentiation and activation states, which require metabolic flexibility to fulfil their differentiation-specific energetic and biosynthetic demands.

Naïve T cells, which have not encountered their cognate antigen yet, display a quiescent phenotype and primarily use oxidative phosphorylation (OXPHOS) of glucose-derived pyruvate or fatty acid oxidation (FAO) for adenosine triphosphate (ATP) production [91].

Upon activation, T cells undergo metabolic reprogramming and engage aerobic glycolysis for ATP production instead of OXPHOS. This metabolic switch is mainly mediated by CD28-induced phosphoinositide 3-kinase activation and subsequent mechanistic target of Rapamycin (mTOR) stimulation. In the process of aerobic glycolysis, glucose is converted to lactate via the tricarboxylic acid cycle despite the presence of oxygen. From an energetic viewpoint, aerobic glycolysis is less efficient than OXPHOS, as fewer ATP per molecule glucose can be yielded. With regards to the altered energetic and anabolic demands upon activation, however, aerobic glycolysis allows for faster energy production as well as metabolic intermediates required for proliferation and effector functions [92].

T_{mem} persist due to homeostatic self-renewal waiting for re-infection with their cognate antigen. Like naïve T cells, they display a rather quiescent phenotype. T_{mem} depend on FAO using primarily FA from *de novo* synthesis for differentiation, long-term persistence and function. Compared with naïve and T_{eff}, T_{mem} display higher mitochondrial mass as well as greater spare respiratory capacity (SRC), a feature associated with increased cell survival [93, 94].

1.5 T cell exhaustion

Unlike in acute infections, where the infection is cleared by T_{eff} within days or weeks, during chronic infections and cancer, antigen persists and is constantly exposed to antigen-specific T cells. This chronic antigen stimulation leads to a specific differentiation state, termed T cell exhaustion [95]. T_{ex} are identified by several characteristic features, such as the co-expression of various inhibitory receptors (IRs), the progressive loss of effector functions and a distinct transcriptome and epigenetic profile. The exhaustion state is thought to be an adaptation to chronic antigenic stimulation in order to protect from immunopathology or autoreactivity [57, 96]. T cell exhaustion was first described over 20 years ago in the lymphocytic choriomeningitis virus (LCMV) clone 13 (cl13) chronic infection model in mice [97, 98]. The phenomenon of dysfunctional T cells was further discovered and studied in other viral infections [99-101] as well as several cancer entities also in humans [102-105].

T_{ex} derived from either chronic viral infections or cancer share many of the characteristics mentioned above, indicating that constant antigen stimulation is the main driver of T cell exhaustion. However, there are significant differences in the transcriptional profile of T_{ex} derived from either cancer or viral infection indicating that other factors, such as the

suppressive tumor microenvironment (TME), also shape the T_{ex} phenotype [57, 103, 106]. Therefore, one has to be cautious when drawing general conclusions about T_{ex} based on data derived from either setting.

It is important to note that T_{ex} are not inert, but retain reduced effector functions which are crucial to restrict tumor progression and pathogen replication [107]. Furthermore, T cell exhaustion in the early stages is reversible, for example by targeting inhibitory molecules on T_{ex}, which will be discussed later in this chapter.

T cell exhaustion is a differentiation state mainly described for $CD8^+$ T cells, but not limited to this T cell subset. $CD4^+$ T cells have been described to be affected by T cell exhaustion as well, marked by reduced production of effector cytokines and increased expression of IRs in response to chronic antigen stimulation. Exhaustion characteristics partially differ between the two T cell subsets. Virus-specific effector functions of $CD4^+$ T cells decline earlier than the ones of $CD8^+$ T cells. Furthermore, $CD4^+$ T_{ex} upregulate expression of immunosuppressive cytokines such as IL-10 or IL-21 [108-110]. Nevertheless, if not stated differently, only exhausted $CD8^+$ T cells are referred to as T_{ex} in this work.

1.5.1 Characteristics of T cell exhaustion

One hallmark of T_{ex} is the loss of effector functions in a hierarchical manner. Incipient T cell exhaustion is marked by decreased proliferative capacity as well as IL-2 production. This is followed by the loss of TNFα production at an intermediate state of exhaustion. Upon further exhaustion progression, T cells lose their ability to produce the effector molecule IFNγ, succeeded by physical deletion of antigen-specific T cells as the final stage of exhaustion [111, 112].

T_{ex} display several functional and structural alterations of mitochondria, such as increased size or altered levels of reactive oxygen species [113]. Furthermore, T_{ex} accumulate depolarized mitochondria due to decreased mitophagy activity and mitochondrial dysregulation was found to be a driver of T cell exhaustion [114].

In contrast to T_{mem}, T_{ex} aren't able to persist without antigen-stimulation due to IL-7- and IL-15-dependent homeostatic self-renewal as they show low expression levels of CD122 (β-chain of the IL-2 and IL-15 receptor) and CD127 [115].

1.5.1.1 Inhibitory receptors

Expression of various IRs on the cell surface of $CD8^+$ T cells is one of the main characteristics and drivers of T cell exhaustion. Ligands for those IRs are expressed by APCs, other immune cells as well as tissues and cancer cells and their IR binding leads to suppression of T cell effector functions [116-118].

One of the most studied IRs is CD279, better known as PD-1. PD-1 is a member of the CD28 gene family and was discovered 30 years ago by Honjo and colleagues [119]. Two ligands of PD-1 have been identified, PD-1 ligand 1 and 2 (PD-L1, PD-L2), which belong to the B7 family [120, 121]. Deletion of PD-1 causes development of severe autoimmune disease indicating its indispensable role in T cell immunity [122, 123]. PD-1 is transiently expressed on T_{eff}, but decreases with memory differentiation [124]. In the context of chronic infections and cancer, however, $CD8^+$ T cells constantly show high PD-1 expression, which results in suppression of TCR and CD28 signaling, thereby contributing to insufficient effector functions [125]. PD-1 expression is regulated by forkhead box protein O1 (Foxo1) through a positive feedback loop by impaired Akt and mTOR activity leading to antigen desensitization and enhanced survival at the same time [126].

Besides PD-1, cytotoxic T lymphocyte antigen 4 (CTLA-4) is another well-characterized IR, which also belongs to the CD28 family. Two independent labs identified CTLA-4 as negative regulator of T cell function, years after its initial discovery [127-129]. Similar to PD-1, deletion of CTLA-4 results in massive lymphoproliferation implicating its importance in maintaining immunologic homeostasis [127].

Further IRs have been described to be involved in repressing T cell functions in the context of T cell exhaustion, namely lymphocyte-activation gene 3 (LAG-3), 2B4 (CD244), CD160, T cell immunoglobulin and mucin-domain containing-3 (Tim-3) and T-cell immunoreceptor with immunoglobulin and ITIM domains (TIGIT) [130-134].

The pattern and number of IRs co-expressed on the CTL surface can influence the severity of dysfunction [135]. However, it is important to note that T_{ex} can't be identified solely by expression of IRs, since they are also expressed on highly functional T cells [96].

1.5.1.2 Metabolism of T_{ex}

The progressive loss of effector functions during T_{ex} differentiation is accompanied by metabolic dysregulation. While T_{eff} and memory T cells display either a strong glycolytic or a strong oxidative metabolism, T_{ex} display defects in glucose uptake, suppressed cellular respiration as well as dysregulated mitochondrial energetics, resulting in little metabolic reserve [136]. T_{ex} expressed high levels of CD36, a receptor for oxidized low-density lipoproteins (LDL). CD36-mediated uptake and metabolism of oxidized LDL leads to production of peroxides and inhibits T_{ex} effector function [137].

1.5.2 Exogenous immunosuppressive mechanisms

Besides endogenous drivers like mitochondrial deregulation and IRs, exogenous factors also regulate and mediate T cell exhaustion. One example are soluble molecules such as the immunosuppressive cytokines IL-10 and transforming growth factor-β (TGFβ). During chronic

infection, the source of IL-10 includes DCs, monocytes and $CD4^+$ T cells [138-140]. Blockade of the IL-10 receptor results in clearance of chronic viral infection indicating its role in T cell exhaustion [141]. TGFβ has been described to suppress T_{eff} functions via Smad-mediated downregulation of effector genes [142] and through inhibition of Chemokine receptor CXC motif 3 (CXCR3)-mediated trafficking of $CD8^+$ T cells [143].

T_{reg} are known to suppress $CD8^+$ T cells in order to prevent autoimmunity for example by being the source of IL-10 and TGFβ. In chronic infections and cancer, however, T_{reg} numbers at sites of infection as well as in cancer increase, thereby promoting $CD8^+$ T cell exhaustion [144]. T_{reg} are not the only cell type responsible for suppression of CTL functions, since also myeloid-derived suppressor cells, exhausted APCs, $CD8^+$ T_{reg} and NK cells have been reported to compromise CTL function [145-148].

Furthermore, the TME provides a hostile environment to tumor infiltrating lymphocytes (TILs) by depriving them of nutrients and exposing them to metabolic by-products and hypoxia, which restrains their anti-tumor immunity and promotes T cell exhaustion [149].

1.5.3 Transcriptional regulation of T cell exhaustion

Compared to their effector and memory counterparts, T_{ex} have a unique transcriptional and epigenetic profile, supporting the concept that T cell exhaustion is a specific differentiation state [150, 151]. Several TFs have been described to be involved in the process of T cell exhaustion.

In addition to the co-expression of several IRs, T_{ex} have been characterized by the expression pattern of the two specific TFs, T-bet and Eomes. T_{eff} co-express T-bet and Eomes to promote expression of effector molecules, such as IFNγ [152], while T_{ex} display a rather mutually exclusive expression pattern. High expression of T-bet is associated with an intermediate state of exhaustion, whereas a high expression of Eomes has been described to mark terminally differentiated T_{ex} [153].

Another TF crucial for T_{ex} development is thymocyte selection-associated HMG BOX protein (TOX), which is responsible for epigenetic remodeling and involved in upregulation of IRs [154]. Deficiency of TOX leads to activation-induced cell death-mediated extinction of $CD8^+$ T cells in tumors, indicating an important role for TOX in the persistence of T_{ex} [155-157].

Other TFs that have been described to play significant roles in T cell exhaustion are Foxo1, FOXP1, Blimp-1, NFAT and BATF [126, 158-161].

1.5.4 Heterogeneity of the T_{ex} population

The population of T_{ex} within its lineage is heterogenous. Already 10 years ago, Wherry *et al.* reported the co-existence of two distinct T_{ex} subsets. They described a small population characterized by high T-bet and intermediate PD-1 expression (T-bet^{high}PD-1^{mid}) with residual proliferative potential and a large population of Eomes-expressing T_{ex} (Eomes^{high}PD-1^{high}), which displayed higher co-expression of IRs with limited proliferative capacity. They found that the small T-bet^{high}PD-1^{mid} population served as the progenitor pool and gave rise to the big subset of Eomes^{high}PD-1^{high} terminally differentiated T_{ex} [153].

The understanding of T_{ex} subsets was further refined by the identification of C-X-C chemokine receptor type 5 and TCF1 as markers for the T_{ex} progenitor (T_{pex}) population [162]. Since this small T_{pex} population possesses the ability to self-renew and to give rise to terminally differentiated T_{ex}, it is also referred to as “stem”-like T_{pex}. Stem-like T_{pex} differ from terminally differentiated T_{ex} in their transcriptional signature as well as in their chromatin landscape, indicating that stem-like T_{pex} are a distinct population [162-164]. Signaling lymphocyte activation molecule 6 (Slamf6) is another surface molecule marking stem-like TCF1-expressing T_{pex} in chronic viral infections and tumors [165, 166]. A recent study even revealed the presence of two distinct interconverting T_{pex} populations (Tex_{prog1} and Tex_{prog2}), which both express TCF1 and Slamf6, but differ in surface expression of CD69 and their proliferative behavior as well as their ability to further develop into more differentiated T_{ex} populations [167].

In human settings of chronic infection, such as hepatitis C, hepatitis D or human immunodeficiency virus (HIV), the frequency of TCF1$^+$ stem-like CD8$^+$ T cells has been found to positively correlate with clinical outcome and overall survival [165, 168-170]. In the context of anti-tumor immunity, terminally differentiated T_{ex} display a highly cytotoxic phenotype by great production of IFNγ and GrzB but reduced long-term survival. TCF1$^+$ stem-like T_{pex} show lower cytotoxic capacity, but replenish the pool of highly cytotoxic T_{ex}, thereby ensuring long-term tumor control [171]. Furthermore, the subset of TCF1$^+$ T_{pex} has been reported to respond to immunotherapeutic interventions while terminally differentiated T_{ex} don’t, highlighting its importance in the context of chronic viral infections and tumors [172]. Our own work suggests Rgs16, a regulator of G protein signaling, as biomarker for terminally differentiated T_{ex} and shows that Rgs16^{high} CD8$^+$ T cells respond poorly to PD-1/PD-L1 pathway blockade [173].

Recently, the presence of a third, intermediate T_{ex} (Tex_{int}) subset, which lacks TCF1 and Slamf6 expression, but expresses high levels of T-bet and Tim-3, was identified and was described to be responsive towards immunotherapeutic interventions [167, 174], indicating a much more complex T_{ex} subset biology than previously thought. An overview of so far known T_{ex} subpopulations including their hierarchy, specific surface marker and TF profile as well as their localization is shown in Figure 1.3.

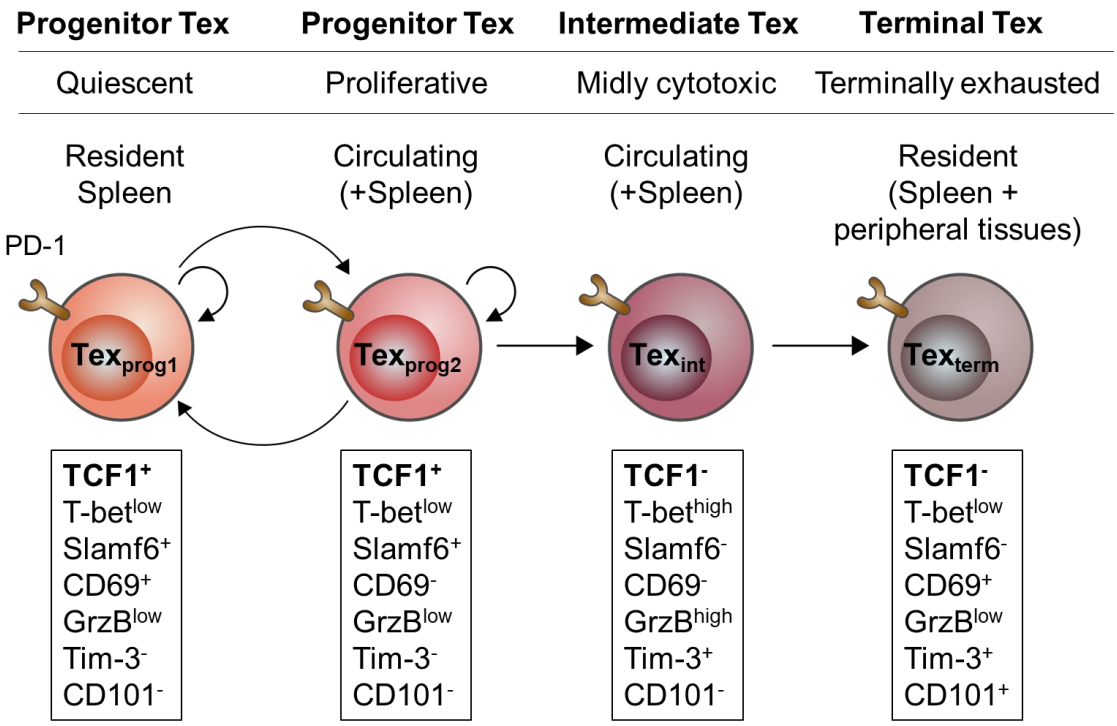

Figure 1.3. Heterogeneity of the T_{ex} population. *Various T_{ex} populations can be distinguished by differential surface marker and TF expression as well as their effector functions and location. Two interconverting progenitor T_{ex} (Tex_{prog}) populations are able to self-renew and to give rise to a more differentiated, intermediate Tex (Tex_{int}) population with residual functionality. This population ultimately differentiates into terminally exhausted Tex_{term}, with reduced functionality and high exhaustion marker expression. Figure inspired by [167] and [174].*

1.5.5 Immunotherapy

IRs expressed on T cells are so-called “immune checkpoints” (IC) which prevent excessive and potentially harmful T cell activation and immune responses under physiological conditions. In the context of chronic viral infections and cancer, however, IRs are upregulated and prevent sufficient immune functions. IC blockade (ICB) using specific monoclonal antibodies (mAb) against IRs or their ligands, respectively, has revolutionized cancer therapy. ICB mAb specifically bind and block IRs, thereby reinvigorating suppressed T cells. In 2018, Tasuku Honjo and James P. Allison received the Nobel Prize in Physiology or Medicine for their pioneering work in this field.

CTLA-4 and PD-1/PD-L1 have been identified as clinically useful targets for ICB [175, 176] and several antibodies have been approved to be used as first-line therapies for solid tumors [177, 178].

Although ICB via specific mAb has shown great success in cancer therapy, only a fraction of patients responds to ICB. Even initially responding patients often develop refractory disease. Therefore, therapeutic resistance is a major issue and its mechanisms are heavily investigated [179]. Clinical response has been reported to correlate with preexisting $CD8^+$ T cell infiltration as well as numbers of circulating $CD4^+$ and $CD8^+$ T cells [180, 181]. Siddiqui and colleagues

found a small population of TCF1$^+$PD-1$^+$CD8$^+$ TILs to be responsible for tumor control in response to immunotherapy [172]. Furthermore, in a study comparing the immune cell transcriptomes from several tumor samples of melanoma patients treated with checkpoint inhibitors, TCF1 expression was associated with increased response to ICB and patient survival [182]. These studies imply a crucial role for TCF1$^+$CD8$^+$ T cells in the context of ICB responsiveness. However, further studies are required to investigate potential therapeutic implementation of this knowledge.

1.6 TCF1 and its role in CD8$^+$ T cells

The TF TCF1 plays a role in various states of T cell development and differentiation. At early stages of T cell development in the thymus, NOTCH-signaling induced TCF1 contributes to T cell fate specification of early thymic progenitors [68, 183]. At later stages of T cell development, TCF1 is also crucial for the establishment of the CD8$^+$ T cell identity as well as for maintenance of CD8$^+$ T cells in a naïve state prior antigen encounter [184]. TCF1^{high} T_{eff} have been described to rather differentiate into T_{cm} than T_{em}, thereby marking the CD8$^+$ T cell subset that is responsible for potent memory formation and durable immune control [185-187]. In the context of chronic viral infections and cancer, TCF1 is the key TF involved in the generation of stem-like CD8$^+$ T_{ex} ensuring long-term persistence and control [162, 163, 165, 172, 188].

Proteins of the TCF family are effector TFs of the Wingless/Integration 1 (Wnt) signaling pathway. In the absence of Wnt signals, cytoplasmic β-catenin levels are regulated by the so-called “destruction complex”, consisting of the scaffold proteins *adenomatous polyposis coli* gene product (AdPC) and Axin as well as the kinases casein kinase 1 (CK1) and glycogen synthase kinase 3 (GSK3). After binding to AdPC and Axin, β-catenin is phosphorylated by CK1 and GSK3, making it recognizable to the E3 ubiquitin ligase subunit β-Trcp, resulting in its ubiquitination and proteasomal degradation [189] (Figure 1.4.A). In the canonical Wnt pathway, Wnt ligands, which are lipid-modified secreted proteins, bind to the cell surface receptors low-density lipoprotein receptor related protein 5/6 (LRP5/6) and/or Frizzled (Fzd), which leads to the recruitment of the scaffolding protein Dishevelled (Dvl) followed by LRP5/6 phosphorylation and Axin recruitment. This results in the disruption of the destruction complex and ultimately leads to accumulation and nuclear translocation of β-catenin [190]. In the nucleus, β-catenin interacts with different DNA-binding proteins, one of them being TCF1. Binding of β-catenin to TCF1 leads to co-activation and expression of TCF1 target genes [191] (Figure 1.4.B).

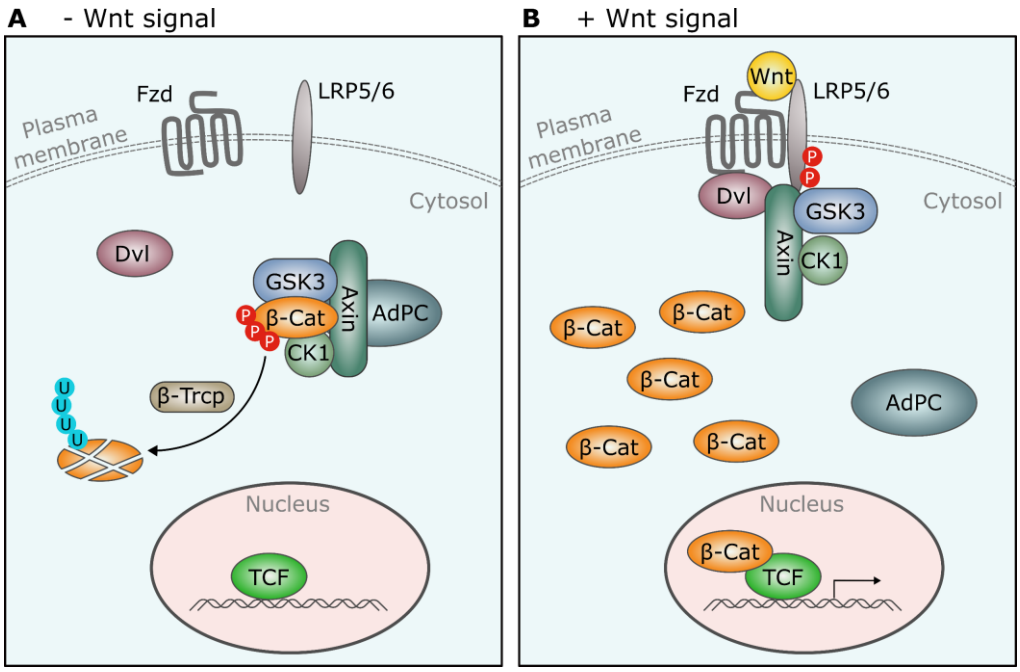

Figure 1.4. The role of β-catenin (β-Cat) and TCF1 in the canonical Wnt signaling pathway. ***A.*** *In the absence of Wnt ligands, cytosolic β-Cat levels are regulated by the destruction complex, consisting of AdPC, Axin, CK1 and GSK3, leading to ubiquitination by β-Trcp and subsequent proteasomal degradation.* ***B.*** *Upon binding of Wnt ligands to the cell surface receptors Fzd and LRP5/6, the destruction complex is disrupted, resulting in accumulation and nuclear translocation of β-Cat. In the nucleus, β-Cat activates TCF1, ultimately leading to target gene expression. Figure inspired by [192].*

In T cells, TCF1 exists in several isoforms, with the long isoform being able to interact with β-catenin through the N-terminal domain [193]. The role of β-catenin in the context of TCF1-dependent T cell development and function is controversially discussed. While some groups describe the Wnt–β-catenin pathway to be crucial for the generation of $CD8^+$ stem-like T_{mem} [194, 195], other groups report β-catenin as well as its homologue γ-catenin (plakoglobin) to be dispensable for $CD8^+$ T cell development and memory formation [196, 197]. Even β-catenin might not be necessarily required for T cell development and memory formation, its activation and interaction with TCF1 may have some beneficial effects on T cells [198].

Besides its role in regulating gene expression as a TF, TCF1 has been reported to exert its functions by having a direct impact on chromatin through its intrinsic histone deacetylase activity [184].

1.7 The immune system in aging

During the course of aging, the immune system loses its functionality, making the human body more susceptible to pathogens and cancer development. This decline in immunological competence was termed “immunosenescence“. In parallel to the functional loss, the

susceptibility to autoimmunity increases with age [199], which seems contradictory, but demonstrates a disbalance in the highly orchestrated immune system. Besides an increased susceptibility to viral infections and cancer, vaccination efficacy is dramatically decreased in the elderly [200-202].

The aged immune system is characterized by a loss of adaptive immune functions and increased unspecific innate immunity [203]. The chronic low-grade inflammation induced by dysregulated innate immune cells is called inflammaging and contributes to several age-related diseases [14]. Alterations in the differentiation potential of HSC contribute to this phenotype. HSC preferentially commit to the myeloid lineage and outnumber lymphoid-prone HSCs with age [204, 205]. Furthermore, thymic involution starts during childhood and results in decreasing numbers of naïve T cells throughout life [206].

In addition to a decreased generation of naïve T cells, a lifetime of antigenic exposure and experienced chronic infections leads to a predominant memory phenotype and the accumulation of terminally differentiated T cells in the elderly [207, 208].

The mechanisms underlying decreased immunological capacity in aging are not fully elucidated yet and are therefore a highly investigated topic in research.

1.8 The immune system in obesity

Similar to the phenomenon of inflammaging, a state of chronic low-grade inflammation is also observed in obese individuals, which increases the risk of developing autoimmune diseases or cancer [209]. In lean adipose tissue (AT) there mainly reside anti-inflammatory immune cells such as M2-type macrophages or T_{reg}. In obese AT, however, rather pro-inflammatory immune cells, such as M1 macrophages, Th1, Th17 and $CD8^+$ T cells with a pro-inflammatory secretome, are found [210].

It has been described that the overall number and of circulating immune cells and immune cell subsets in obese individuals are altered compared to lean subjects. Furthermore adipocyte-derived hormones, such as leptin, are involved in T cell maturation, proliferation and activation [211, 212] and leptin dysregulation in obesity has been described to reduce proliferation of T_{eff} and to increase proliferation of immunosuppressive T_{reg} [213-215].

Besides increased susceptibility to infections in obesity, vaccination efficacy is also decreased, probably due to insufficient T-cell function [216-218].

1.9 Aim of the study

Both aging and obesity, are accompanied by metabolic changes and alterations of the immune system leading to increased susceptibility towards a wide range of diseases and cancer as well as decreased vaccination efficacy. There are several studies focusing on either aging or obesity in the context of $CD8^+$ T cell immunity in anti-viral infections or cancer. However, there are no studies considering the combination of the two different factors. Since both populations, the elderly (≥65 years) as well as the obese population (BMI ≥30 kg/m^2), have dramatically grown over the last years and are expected to increase further in an exponential manner, the number of aged obese individuals will also rise. To face this growing global health issue, studies on the combinatorial outcome of those two conditions are required.

This work aims to shed light on the potential synergistic effect of aging and obesity on the immune system with a specific focus on $CD8^+$ T cells. The ultimate goal of this study was to find a link between a potentially altered plasma metabolite profile and the immunological changes observed in aging and obesity. Furthermore, the therapeutic potential of synergistically altered metabolites was explored using *in vitro* cell culture systems as well as well-established *in vivo* mouse models of cancer and infection.

2 Materials

2.1 Chemicals, reagents and diets

Deionized water was taken from the laboratory water supply. Double deionized water (ddH2O) was purified by an ion-exchanger (TKA GenPure, JWT, Jena, Germany).

Table 2.1. Overview of used chemicals and reagents.

Material	Company	Identifier
1H-indole-3-propanamide	BIOZOL Diagnostica Vertrieb GmbH (Eching, Germany)	1817-100
2-Deoxy glucose	Cayman Chemical (Ann Arbor, MI, USA)	14325-5
3-(1H-Indol-3-yl)butanoic acid	Abcr GmbH (Karlsruhe, Germany)	AB499210
3-(1-Methyl-1H-indol-3-yl)propanoic acid	Abcr GmbH (Karlsruhe, Germany)	AB417282
3-(2-Oxo-2,3-dihydro-1H-indol-3-yl)propanoic acid	Abcr GmbH (Karlsruhe, Germany)	AB376564
3-(5-Methoxy-1H-indol-3-yl)propanoic acid	Abcr GmbH (Karlsruhe, Germany)	AB595952
3-Indolepropionic acid (3-IPA)	Sigma-Aldrich/ Merck KGaA (Darmstadt, Germany)	57400-5G-G
30% Acrylamide/Bis Solution, 29:1	Serva (Heidelberg, Germany)	10687.01
α-Aminobutyric acid (AABA)	Sigma-Aldrich/ Merck KGaA (Darmstadt, Germany)	A1879-1G
Ammonium persulfate (APS)	Bio-Rad Laboratories (Hercules, CA, USA)	161-0700
Ampicillin	Sigma-Aldrich/ Merck KGaA (Darmstadt, Germany)	A5354-10ML

Asymmetric dimethylarginine (ADMA)	MedChemExpress LLC (Monmouth Junction, NJ, USA	HY-113216-10mg
Betaine	Sigma-Aldrich/ Merck KGaA (Darmstadt, Germany)	B2629-50G
Biocoll® Trennlösung	Bio&SELL (Feucht, Germany)	BS.L 6115
Bovine serum albumin (BSA)	Sigma-Aldrich/ Merck KGaA (Darmstadt, Germany)	A9647
Brefeldin A Solution	Abcam (Cambridge, UK)	Ab193369
Carbonyl cyanide 4-(trifluoromethoxy)phenylhydrazone (FCCP)	Cayman Chemical (Ann Arbor, MI, USA)	15218-50
CHIR-99021 trihydrochloride	BIOZOL Diagnostica Vertrieb GmbH (Eching, Germany)	HLB-HB1262
Clarity™ Western ECL Substrate	Bio-Rad Laboratories (Hercules, CA, USA)	1705060S
Dimethylsulfoxid (DMSO)	Sigma-Aldrich/ Merck KGaA (Darmstadt, Germany)	D8418
Dithiothreitol (DTT)	Sigma-Aldrich/ Merck KGaA (Darmstadt, Germany)	10708984001
Dynabeads™ M-280 Streptavidin	Thermo Fisher Scientific (Waltham, MA, USA)	11205D
eBioscience™ Foxp3/transcription factor staining buffer set	Thermo Fisher Scientific (Waltham, MA, USA)	00-5523-00
Fetal bovine serum (FBS)	Sigma-Aldrich/ Merck KGaA (Darmstadt, Germany)	F0804
Fixation Buffer	BioLegend (San Diego, CA, USA)	420801
FzM1	Sigma-Aldrich/ Merck KGaA (Darmstadt, Germany)	5343580001
G-418 Sulfate	Sigma-Aldrich/ Merck KGaA (Darmstadt, Germany)	345810-1GM
GeneRuler 1 kb Plus DNA ladder	Thermo Fisher Scientific (Waltham, MA, USA)	SM1331

Gibco® 0.25 % Trypsin-EDTA (1X)	Thermo Fisher Scientific (Waltham, MA, USA)	25200-055
Gibco® 2-Mercaptoethanol (1000X)	Thermo Fisher Scientific (Waltham, MA, USA)	21985-023
Gibco® ACK Lysing Buffer	Thermo Fisher Scientific (Waltham, MA, USA)	A10492-01
Gibco® DMEM (1X) (4,5 g/l D-Glucose, L-Glutamine, no pyruvate)	Thermo Fisher Scientific (Waltham, MA, USA)	41965-039
Gibco® DPBS (1X)	Thermo Fisher Scientific (Waltham, MA, USA)	14040-091
Gibco® MEM NEAA (100X)	Thermo Fisher Scientific (Waltham, MA, USA)	11140050
Gibco® Penicillin-Streptomycin (PenStrep)	Thermo Fisher Scientific (Waltham, MA, USA)	14140-122
Gibco® RPMI Medium 1640	Thermo Fisher Scientific (Waltham, MA, USA)	21875-034
Glucose	Sigma-Aldrich/ Merck KGaA (Darmstadt, Germany)	G7021-1KG
Hydrochloric acid (1N)	VWR International (Radnor, DE, USA)	30024.290
Indole-3-acetic acid	BIOZOL Diagnostica Vertrieb GmbH (Eching, Germany)	PTL-I885-5G
Indole-3-butyric acid	BIOZOL Diagnostica Vertrieb GmbH (Eching, Germany)	APE-B5985
Indoxyl sulfate (Ind-SO_4)	Cayman Chemical (Ann Arbor, MI, USA)	Cay16926-100
Invitrogen™ Permeabilization Buffer 10X	Thermo Fisher Scientific (Waltham, MA, USA)	00-8333-56
L-Glutamine solution	Sigma-Aldrich/ Merck KGaA (Darmstadt, Germany)	G7513-100ML
Laemmli Sample Buffer (4x)	Bio-Rad Laboratories (Hercules, CA, USA)	1610747
LB-Agar	Carl Roth (Karlsruhe, Germany)	X965.2

Live/dead fixable red dead cell stain kit	Thermo Fisher Scientific (Waltham, MA, USA)	L23102
Mdivi-1	Sigma-Aldrich/ Merck KGaA (Darmstadt, Germany)	M0199
Melatonin	Sigma-Aldrich/ Merck KGaA (Darmstadt, Germany)	M5250
Methionine sulfoxide (Met-SO)	MP Biomedicals LLC (Santa Ana, CA, USA)	102296.1
MitoTracker™ Deep Red FM	Thermo Fisher Scientific (Waltham, MA, USA)	M22426
MitoTracker™ Green FM	Thermo Fisher Scientific (Waltham, MA, USA)	M7514
Nuclease Free Duplex Buffer	Integrated DNA Technologies (Coralville, IA, USA)	11-05-01-12
Oligomycin	Merck Millipore (Burlington, MA, USA)	495455-10mg
Orange DNA Loading Dye (6x)	Thermo Fisher Scientific (Waltham, MA, USA)	R0631
PageRuler™ Prestained Protein Ladder	Thermo Fisher Scientific (Waltham, MA, USA)	26616
Passive Lysis 5X Buffer	Promega (Madison, WI, USA)	E1941
Percoll™	GE Healthcare (Chalfont, UK)	17-0891-01
Poly D-Lysine	Merck Millipore (Burlington, MA, USA)	A-003-E
Poly(I:C) (HMW) VacciGrade™	Invivogen (San Diego, CA, USA)	vac-pic
Propidium Iodide Solution	BioLegend (San Diego, CA, USA)	421301
rCutSmart™ Buffer	New England Biolabs (Ipswich, MA, USA)	B6004S
RIPA Lysis Buffer System	Santa Cruz Biotechnology (Santa Cruz, CA, USA)	sc-24948
Rodent Diet With 10 kcal% Fat (Chow)	Research Diets, Inc. (New Brunswick, NJ, USA)	D12450Hi

Rodent Diet With 45 kcal% Fat (HFD)	Research Diets, Inc. (New Brunswick, NJ, USA)	D05122301i
Rotenone	Cayman Chemical (Ann Arbor, MI, USA)	13995-5
Screening compound ($C_{15}H_{20}N_2O$)	Enamine ltd (Kyiv, Ukraine)	Z31763241
SeaKem® ME Agarose	Lonza (Basel, Switzerland)	50014
Serotonin	Toronto Research Chemicals Inc (Toronto, Canada)	H977043
Skim milk powder	GERBU Biotechnik (Heidelberg, Germany)	16020500
Sodium azide	Sigma-Aldrich/ Merck KGaA (Darmstadt, Germany)	S2002-5G
Sodium dodecyl sulfate (SDS)	Sigma-Aldrich/ Merck KGaA (Darmstadt, Germany)	L3771-100G
Sodium hydroxide (1N)	VWR International (Radnor, DE, USA)	35256-1L
Sodium pyruvate	Sigma-Aldrich/ Merck KGaA (Darmstadt, Germany)	P5280
SYBER safe DNA stain	Thermo Fisher Scientific (Waltham, MA, USA)	S33102
T4 DNA Ligase Reaction Buffer	New England Biolabs (Ipswich, MA, USA)	B0202S
TEMED	Bio-Rad Laboratories (Hercules, CA, USA)	161-0801
Trans-Indole-3-acrylic acid	Thermo Fisher Scientific (Waltham, MA, USA)	11430113
Tris base	Sigma-Aldrich/ Merck KGaA (Darmstadt, Germany)	10708976001
Triton™ X-100	Sigma-Aldrich/ Merck KGaA (Darmstadt, Germany)	X100-500ML
Trypan Blue solution	Sigma-Aldrich/ Merck KGaA (Darmstadt, Germany)	T81544-100ML
Trypton/Pepton aus Casein	Carl Roth (Karlsruhe, Germany)	91079-40-2
XF Base Medium	Agilent Technologies (Santa Clara, CA, USA)	102353-100

XF Calibrant	Agilent Technologies (Santa Clara, CA, USA)	100840-000
X-tremeGENE™ HP	Sigma-Aldrich/ Merck KGaA (Darmstadt, Germany)	6366236001
Yeast extract	Thermo Fisher Scientific (Waltham, MA, USA)	211929

2.2 Commercial Kits

Table 2.2. Commercially available kits used in the study.

Kits	Company	Identifier
Dual-Glo® Luciferase Assay System	Promega (Madison, WI, USA)	E2920
MxP® Quant 500 kit	BIOCRATES Life Sciences AG (Innsbruck, Austria)	21094.12
P3 Primary Cell 4D-Nucleofector® X Kit	Lonza Bioscience (Basel Switzerland)	V4XP-3024
Pierce™ BCA™ Protein Assay Kit	Thermo Fisher Scientific (Waltham, MA, USA)	23225
Plasmid Mini Kit	QIAGEN (Venlo, Netherlands)	12123
QIAquick Gel Extraction Kit	QIAGEN (Venlo, Netherlands)	28704
QIAquick PCR Purification Kit	QIAGEN (Venlo, Netherlands)	28104
RNase-Free DNase Set	QIAGEN (Venlo, Netherlands)	79254
RNeasy Mini Kit	QIAGEN (Venlo, Netherlands)	74106
SuperScript™ III system	Thermo Fisher Scientific (Waltham, MA, USA)	18080051

2.3 Antibodies

Table 2.3. Fluorescence-labeled antibodies for flow cytometry and respective dilutions.

Antibody	Company	Identifier	Dilution
AF488 anti-human/mouse TCF1	Cell Signaling Technology (Danvers, MA, USA)	6444S	1:400
AF488 Donkey anti-rabbit IgG	BioLegend (San Diego, CA, USA)	406416	1:1000

AF647 Donkey anti-rabbit IgG	BioLegend (San Diego, CA, USA)	406414	1:1000
APC anti-human CD45RA	BioLegend (San Diego, CA, USA)	983004	1:400
APC anti-mouse CD4 Antibody	BioLegend (San Diego, CA, USA)	100412	1:400
APC anti-mouse CD25	BioLegend (San Diego, CA, USA)	101910	1:400
APC anti-mouse CD45.1 (Ly5.1)	BioLegend (San Diego, CA, USA)	110714	1:400
APC anti-mouse CD223 (LAG-3)	BioLegend (San Diego, CA, USA)	12510	1:400
APC anti-mouse Foxp3	eBioscience™, Thermo Fisher Scientific (Waltham, MA, USA)	17-5773-82	1:400
APC anti-mouse T-bet	Miltenyi Biotec (Bergisch Gladbach, Germany)	130-098-607	1:100
APC/Cyanine7 anti-human CD4	BioLegend (San Diego, CA, USA)	357416	1:400
APC/Cy7 anti-mouse CD4	Becton Dickinson (Franklin Lakes, NJ, USA	552051	1:400
APC/Cy7 anti-mouse CD45.1 (Ly5.1)	BioLegend (San Diego, CA, USA)	110716	1:400
APC/Cy7 anti-mouse/human CD44	BioLegend (San Diego, CA, USA)	103028	1:400
APC/Vio770 anti-mouse CD45.2 (Ly5.2)	Miltenyi Biotec (Bergisch Gladbach, Germany)	130-118-951	1:200
APC/Vio770 anti-mouse CD352 (Slamf6)	Miltenyi Biotec (Bergisch Gladbach, Germany)	130-127-490	1:100
BV421 anti-human CD45RO	Miltenyi Biotec (Bergisch Gladbach, Germany)	130-113-560	1:400
BV421 anti-mouse CD4	BioLegend (San Diego, CA, USA)	562891	1:400
BV421 anti-mouse CD44	BioLegend (San Diego, CA, USA)	103040	1:400
BV421 anti-mouse CD45.1 (Ly5.1)	BioLegend (San Diego, CA, USA)	110732	1:400

BV421 anti-mouse CD45.2 (Ly5.2)	BioLegend (San Diego, CA, USA)	109832	1:400
BV421 anti-mouse CD62L	Miltenyi Biotec (Bergisch Gladbach, Germany)	130-102-425	1:100
BV421 anti-mouse IL-2	BioLegend (San Diego, CA, USA)	503825	1:400
BV421 anti-mouse CD366 (Tim-3)	BioLegend (San Diego, CA, USA)	134019	1:400
BV421 Donkey anti-rabbit IgG	BioLegend (San Diego, CA, USA)	406410	1:1000
BV650 anti-mouse CD45.2 (Ly5.2)	BioLegend (San Diego, CA, USA)	109835	1:400
BV711 anti-mouse CD45	BioLegend (San Diego, CA, USA)	103147	1:400
BV711 anti-mouse CD45.1 (Ly5.1)	BioLegend (San Diego, CA, USA)	110739	1:800
BV711 anti-mouse CD90.1 (Thy1.1)	BioLegend (San Diego, CA, USA)	202539	1:800
FITC Annexin V	Miltenyi Biotec (Bergisch Gladbach, Germany)	130-093-060	1:200
FITC anti-human CD62L Antibody	BioLegend (San Diego, CA, USA)	304804	1:400
FITC anti-mouse CD4	BioLegend (San Diego, CA, USA)	100406	1:400
FITC anti-mouse CD8b	BioLegend (San Diego, CA, USA)	126606	1:400
FITC anti-mouse CD62L Antibody	BioLegend (San Diego, CA, USA)	104406	1:400
FITC anti-mouse CD244	BioLegend (San Diego, CA, USA)	133504	1:400
FITC anti-mouse TCR-vα2	BioLegend (San Diego, CA, USA)	127806	1:400
FITC anti-mouse TNF-α	Miltenyi Biotec (Bergisch Gladbach, Germany)	130-102-294	1:200
PE anti-mouse CD45.2 (Ly5.2)	BioLegend (San Diego, CA, USA)	109808	1:400

PE anti-mouse Eomes	Miltenyi Biotec (Bergisch Gladbach, Germany)	130-102-419	1:100
PE anti-mouse TIGIT	BioLegend (San Diego, CA, USA)	142104	1:400
PE anti-mouse TNF-α	BioLegend (San Diego, CA, USA)	506306	1:400
PE Donkey anti-rabbit IgG	BioLegend (San Diego, CA, USA)	406421	1:1000
PE/Cyanine7 anti-mouse CD25	BioLegend (San Diego, CA, USA)	101916	1:400
PE/Cy7 anti-mouse CD62L	BioLegend (San Diego, CA, USA)	104418	1:400
PE/Cy7 anti-mouse IFN-γ	BioLegend (San Diego, CA, USA)	505826	1:400
PE/Cy7 anti-mouse Ki67	BioLegend (San Diego, CA, USA)	652426	1:400
PE/Cy7 anti-mouse PD-1	BioLegend (San Diego, CA, USA)	135216	1:400
PerCP anti-human CD8a	BioLegend (San Diego, CA, USA)	300922	1:200
PerCP/Cy5.5 anti-mouse CD8a	BioLegend (San Diego, CA, USA)	100734	1:200

Table 2.4. Biotinylated and HRP-conjugated antibodies and respective dilutions.

Antibody	Company	Identifier	Dilution
Biotin anti-mouse CD8a (53-6.7)	BioLegend (San Diego, CA, USA)	100704	1:1000
HRP Donkey anti-rabbit IgG	BioLegend (San Diego, CA, USA)	406401	1:5000
HRP Goat anti-mouse IgG	BioLegend (San Diego, CA, USA)	405306	1:5000

Table 2.5. Unconjugated antibodies and respective dilutions.

Antibody	Company	Identifier	Dilution/concentration
β-Actin (C4)	Santa Cruz Biotechnology (Santa Cruz, CA, USA)	sc-47778	1:1000

β-Catenin	BD Biosciences (Franklin Lakes, NJ, USA)	610154	1:1000
γ-Catenin	BD Biosciences (Franklin Lakes, NJ, USA)	610253	1.1000
GRP94 (D6X2Q)	Cell Signaling Technology (Danvers, MA, USA)	20292	1:1000
LEF1 (C18A7)	Cell Signaling Technology (Danvers, MA, USA)	2286	1.1000
TCF1/TCF7 (C63D9)	Cell Signaling Technology (Danvers, MA, USA)	2203S	1:1000 (Western Blot) 1:400 (flow cytometry)
Ultra-LEAF™ Purified anti-human CD2	BioLegend (San Diego, CA, USA)	309235	0.1 µg/ml
Ultra-LEAF™ Purified anti-human CD3	BioLegend (San Diego, CA, USA)	317349	0.1 µg/ml
Ultra-LEAF™ Purified anti-human CD28	BioLegend (San Diego, CA, USA)	302933	0.1 µg/ml
Ultra-LEAF™ Purified anti-mouse CD16/32	BioLegend (San Diego, CA, USA)	101330	1:1000

2.4 Proteins, Enzymes and Peptides

Table 2.6. Overview of used enzymes, proteins, and peptides.

Proteins, enzymes and peptides	Company	Identifier
Alt-R® CRISPR-Cas9 crRNAs	Integrated DNA Technologies (Coralville, IA, USA)	
Alt-R® CRISPR-Cas9 tracrRNA, ATTO™ 550	Integrated DNA Technologies (Coralville, IA, USA)	1075928
DNA Polymerase I, Large (Klenow) Fragment	New England Biolabs (Ipswich, MA, USA)	M0210S
GP(33-41) peptide	GenScript (Piscataway Township, NJ, USA)	RP20091
HpaI	New England Biolabs (Ipswich, MA, USA)	R0105
IFNγ	PeproTech (Rocky Hill, NJ, USA)	315-05-20

MluI-HF®	New England Biolabs (Ipswich, MA, USA)	R3198S
Phusion® High-Fidelity PCR Master Mix	New England Biolabs (Ipswich, MA, USA)	M0531S
Primers	Eurofins Scientific (Luxemburg, Luxemburg)	
Recombinant Mouse IL-2 (carrier-free)	BioLegend (San Diego, CA, USA)	575408
Recombinant Mouse IL-7 (carrier-free)	BioLegend (San Diego, CA, USA)	577808
Recombinant Mouse IL-12 (p70) (carrier-free)	BioLegend (San Diego, CA, USA)	577004
Recombinant Mouse IL-15 (carrier-free)	BioLegend (San Diego, CA, USA)	566304
T4 DNA Ligase	New England Biolabs (Ipswich, MA, USA)	M0202S
XhoI	New England Biolabs (Ipswich, MA, USA)	R0146S

2.5 Plamids and Oligonucleotides

Table 2.7. Overview of used plasmids and oligonucleotides.

Plasmids and oligonucleotides	Provided by / purchased from	Identifier/Reference
Alt-R® CRISPR-Cas9 crRNAs	Integrated DNA Technologies (Coralville, IA, USA)	
Alt-R® CRISPR-Cas9 tracrRNA, ATTO™ 550	Integrated DNA Technologies (Coralville, IA, USA)	1075928
MigR1-GFP	Prof. Dr. Susan Kaech (Salk Institute for Biological Sciences, La Jolla, CA, USA)	
pcDNA6-N-3XFLAG-*Ctnnb1*	Addgene (Watertown, MA, USA)	123586
Tcf7 pGL3 reporter plasmid	Dr. Ken Oestreich (Ohio State University, Ohio, USA)	[219]

2.6 Buffers and Solutions

Table 2.8. Overview over used buffers and solutions and the respective composition.

Buffer/Solution	Composition
1x Annexin V staining buffer	0.01 M HEPES 0.14 M NaCl 2.5 mM $CaCl_2$ pH 7.4
Complete RPMI	10 % (v/v) FBS 1 % (v/v) PenStrep 1 % (v/v) NEAA 0.1 % (v/v) 2-Mercaptoethanol RPMI 1640
FACS buffer	2 % FBS 0.1 % (w/v) NaN_3 PBS
Freezing medium	10 % (v/v) DMSO FBS
1x LB medium	170 mM NaCl 1 % Tryptone 0,05 % Yeast extract
1x Phosphate-buffered saline (1x PBS)	137 mM NaCl 8.1 mM KCl 2.7 mM Na_2HPO_4 1.5 mM KH_2PO_4 pH 7.4
PBS-T	0.01 % (v/v) Triton X-100 PBS
1 % RPMI	1 % (v/v) FBS 1 % (v/v) Pen Strep RPMI 1640
1x SDS running buffer	25 mM Tris base 0.19 M Glycine 1 % (w/v) SDS
SDS-PAGE Resolving gel (12 %)	12 % Acrylamide/Bis Solution 375 mM Tris-HCl pH 8.8 0.1 % (w/v) SDS

	0.1 % (w/v) APS
	0.04 % (v/v) TEMED
SDS-PAGE Stacking gel (5 %)	5 % Acrylamide/Bis Solution
	125 mM Tris-HCl pH 6.8
	0.1% (w/v) SDS
	0.1% (w/v) APS
	0.01% (v/v) TEMED
1x Tris acetate EDTA buffer (1x TAE)	40 mM Tris base
	1 mM EDTA
	pH 7.4
1.0 M Tris-HCl pH 6.8	1.0 M Tris base
	pH 6.8
1.5 M Tris-HCl pH 8.8	1.5 M Tris base
	pH 8.8
1x Western blot transfer buffer	25 mM Tris base
	190 mM Glycine
	20 % (v/v) MeOH or EtOH

2.7 Cell culture Media compositions

Table 2.9. Cell culture growth medium composition for immortalized cell lines.

Cell line	Medium composition
B16F10-gp$_{33-41}$	10 % (v/v) FBS
	1 % (v/v) PenStrep
	200 µg/ml G-418
	DMEM
EL4	10 % (v/v) FBS
	1 % (v/v) PenStrep
	1 % (v/v) NEAA
	1 % (v/v) sodium pyruvate
	DMEM
HEK293T	10 % (v/v) FBS
	1 % (v/v) PenStrep
	DMEM

2.8 Biological material

2.8.1 Cell lines and competent bacteria

Table 2.10. Overview of used immortalized cell lines.

Cell line	Provided by / purchased from	Identifier
B16F10-gp$_{33-41}$	Prof. Dr. Hanspeter Pircher (University Freiburg, Freiburg, Germany)	
EL4	ATCC, Rockville, USA	TIB-39™
HEK293T	ATCC, Rockville, USA	CRL-1573™
Subcloning Efficiency™ DH5α Competent Cells	Thermo Fisher Scientific (Waltham, MA, USA)	18265017

2.8.2 Viral strains

Table 2.11. Viral strains for in vivo infections.

Viral strain	Reference	Provided by
LCMV Armstrong (Arm)	[220]	Prof. Dr. Susan Kaech (Salk Institute for Biological Sciences, La Jolla, CA, USA)
LCMV clone 13 (cl13)	[221]	

2.8.3 Mouse strains

Mice were housed in the pathogen-free facility at DKFZ at an age of 6-12 weeks if not indicated otherwise. For experiments using knockout mice, age- and sex-matched littermates were used. The studies were performed after approval of the Regierungspräsidium Karlsruhe.

Table 2.12. Used mouse lines.

Mouse strain	Short name	Provider, Reference	Identifier
B6-Tg(Cd4-cre)1Cwi Foxo1tm1Rdp Tg(TcrLCMV)327Sdz / Glcui	CD4-Cre x Foxo1 flox/flox x P14		DKFZ ID: 4292
B6-Tg(TcraTcrb)1100Mjb Ahrtm1Bra / Off	AhR-/- OT-I		DKFZ ID: 3616
B6-Tg(TcrLCMV)327Sdz Tg(Cd4-cre)1Cwi Gt(ROSA)26Sortm1(CAG-xstpx-cas9,-EGFP)Fezh/ Glcui	P14 x CD4-Cre x Rosa-Cas9-GFP		DKFZ ID: 4695
C57BL/6		Charles River	027
Tg(TcrLCMV)327Sdz	P14	[222]	MGI:2665105

2.9 Consumables

Table 2.13. Overview of consumables used in the study.

Consumable	Company	Identifier
Cellstar® White 96 Well Cell Culture Microplate	Greiner Bio-One (Kremsmünster, Austria)	655073
Costar® 50 ml Reagent Reservoir	Corning (Corning, New York, USA)	4870
Falcon™ 15 ml Polypropylene Conical Tube	Thermo Fisher Scientific (Waltham, MA, USA)	352096
ColiRollers™ Plating Beads	Merck Millipore (Burlington, MA, USA)	71013
Cryovials, 2 ml	Biozym Scientific GmbH (Hessisch Oldendorf, Germany)	710522
Falcon™ 50 ml Polypropylene Conical Tube	Thermo Fisher Scientific (Waltham, MA, USA)	352070
Falcon™ Cell Strainer 70 µm Nylon	Thermo Fisher Scientific (Waltham, MA, USA)	352350
Micro-Probengefäß Citrat 3,2%	Sarstedt AG & Co. KG (Nümbrecht, Germany)	41.1506
Millex®-GS Filter Unit 0.22 µm	Merck Millipore (Burlington, MA, USA)	SLGS033SS
NORM-JECT®-F Luer Solo Syringe	B.Braun (Melsungen, Germany)	NJ-9166017
Nylon Mesh SEFAR NITEX	Sefar (Edling, Germany)	3A03-0150-115-00
Petri dish, PS, 94 x 16 mm	Greiner Bio-One (Kremsmünster, Austria)	GB633180
Pierce™ Blotting Paper	Thermo Fisher Scientific (Waltham, MA, USA)	LC2010
PVDF membrane	Santa Cruz Biotechnology (Santa Cruz, CA, USA)	sc-358811
Safe Lock Tube 0,5 ml	Eppendorf (Eppendorf, Germany)	0030121023
Safe Lock Tube 1,5 ml	Eppendorf (Eppendorf, Germany)	0030120086
Safe Lock Tube 2 ml	Eppendorf (Eppendorf, Germany)	0030120094

Safe Lock Tube 5 ml	Eppendorf (Eppendorf, Germany)	0030119487
Seahorse XFe96 FluxPak	Agilent Technologies (Santa Clara, CA, USA)	102416-100
TipOne 10 µl Graduated Tip	StarLab (Hamburg, Germany)	S1111-3700
TipOne 1000 µl Graduated Tip	StarLab (Hamburg, Germany)	S1111-6701
TipOne 200 µl Yellow Tip	StarLab (Hamburg, Germany)	S1111-0706
Tube, 14 ml, PP, 18/95 mm, round bottom	Greiner Bio-One (Kremsmünster, Austria)	187261
Zellkulturflasche 75cm^2	Techno Plastic Products TPP (Trasadingen, Switzerland)	90076
Zellkulturtestplatte 6 Well	Techno Plastic Products TPP (Trasadingen, Switzerland)	92006
Zellkulturtestplatte 12 Well	Techno Plastic Products TPP (Trasadingen, Switzerland)	92012
Zellkulturtestplatte 24 Well	Techno Plastic Products TPP (Trasadingen, Switzerland)	92024
Zellkulturtestplatte 96F Well	Techno Plastic Products TPP (Trasadingen, Switzerland)	92696
Zellkulturtestplatte 96U Well	Techno Plastic Products TPP (Trasadingen, Switzerland)	92697

2.10 Instruments

Table 2.14. Instruments for analysis and experiments.

Instrument	Company
4D-NucleofectorTM Core and X Unit	Lonza Bioscience (Basel Switzerland)
Agilent 2100 Bioanalyzer	Agilent Technologies (Santa Clara, CA, USA)
Caliper TWIN-CAL IP67	Tesa Technology (Ludwigsburg, Germany)
Cell incubator Heraeus Hera cell 150	Thermo Fisher Scientific (Waltham, MA, USA)
Centrifuges:	
Centrifuge 5810R	Eppendorf (Eppendorf, Germany)
Centrifuge 5920R	
Megafuge3.0RS	Heraeus (Hanau, Germany)
Chemi-Smart 5100	Vilber Lourmat (Eberhardzell, Germany)
Flow cytometers:	
FACS Canto II	Becton Dickinson (Franklin Lakes, NJ, USA)

FACS Fortessa	
FACS LSR II	
Fusion FX chemiluminescence imager	Vilber Lourmat (Eberhardzell, Germany)
Heatblock:	
VWR Digital Heatblock	VWR (Radnor, DE, USA)
Block heater SBH130D	Cole-Parmer (Staffordshire, UK)
Thermomixer compact	Eppendorf (Eppendorf, Germany)
Horizon®11.14 Gibco BRL Gel Electrophoresis Apparatus	Thermo Fisher Scientific (Waltham, MA, USA)
Manual pipettes:	
Research® Plus (0.1-2.5µl; 1-10µl; 2-20µl;10-100µl; 20-200µl; 100-1000µl)	Eppendorf (Eppendorf, Germany)
Rainin Classic™ Pipette (1-10µl; 10-100µl; 100-1000µl)	Mettler-Toledo (Columbus, OH, USA)
Transferpette®S-12 and S-8 (20-200µl)	Brand (Wertheim, Germany)
Measures:	
Sartorius Universal	Sartorius (Göttingen, Germany)
Sartorius Analytic	
Microscope brightfield Nikon eclipse TS100	Nikon (Minato, Japan)
Microwave R-941STW	Sharp (Osaka, Japan)
Mini-PROTEAN® Tetra cell	Bio-Rad Laboratories (Hercules, CA, USA)
Molecular Imager GelDoc XR+	Bio-Rad Laboratories (Hercules, CA, USA)
OneTouch Select® Plus blood measuring device	LifeScan Inc (Malvern, PA, USA)
Orion L Microplate Luminometer	Berthold Detection Systems (Pforzheim, Germany)
PCR machine:	
T100™ Thermal Cycler	Bio-Rad Laboratories (Hercules, CA, USA)
Mastercycler	Eppendorf (Eppendorf, Germany)
PH meter ProfiLine pH 3210	Consort (Turnhout, Belgium)
Pipetboy acu	Integra biosciences (Zizers, Switzerland)
Power supply:	
Electrophoresis Power supply E864	Consort (Turnhout, Belgium)
peQPOWER	VWR (Radnor, DE, USA)
PowerPac	Bio-Rad Laboratories (Hercules, CA, USA)

Seahorse XFe96 analyzer	Agilent (Santa Clara, CA, USA)
Shaker	Edmund Bühler (Bodelshausen, Germany)
Stirrer D-6010	NeoLab (Heidelberg, Germany)
Table centrifuges:	
Hearaeus Pico17 (for 24 tubes)	Thermo Fisher Scientific (Waltham, MA, USA)
Centrifuge 5415R (for 24 tubes)	Eppendorf (Eppendorf, Germany)
Tube rotator	Thermo Fisher Scientific (Waltham, MA, USA)
Vortexer Vortex Genie 2	Scientific industries (Bohemia, NY, USA)
Waterbath WNE 7	Memmert (Schwabach, Germany)

2.11 Software

Table 2.15. Used software and software versions.

Software	Company
EndNote 20	Thomson Reuters (Toronto, Canada)
FACS Diva™	Becton Dickinson (Franklin Lakes, NJ, USA)
FlowJo V10.1	Becton Dickinson (Franklin Lakes, NJ, USA)
FUSION FX software	Vilber Lourmat (Eberhardzell, Germany)
Graph Pad Prism 7.05	GraphPad Software (San Diego, CA, USA)
Inkscape 1.2	Inkscape (RRID:SCR_014479)
Integrative Genomics Viewer	Broad Institute (Cambridge, MA, USA)
Microsoft Office Standards 2019	Microsoft (Redmond, WA, USA)
SnapGene® Viewer 6.0.2	Dotmatics (Bishop's Stortford, GB)
Wave 2.6.0	Agilent (Santa Clara, CA, USA)

3 Methods

3.1 Cell biology

3.1.1 General cell culture practice

Handling of cells and all cell culture experiments were performed under sterile conditions using a Heraeus Hera Safe laminar flow hood (Thermo Fisher Scientific, Waltham, MA, USA).

3.1.1.1 Maintenance of cells

B16F10-gp_{33-41} (B16-gp33), HEK293T and EL4 cells or primary cells were cultured at 37 °C with 5 % CO_2 in a humidified incubator in the respective growth media (Table 2.9). To inactivate complement factors, fetal bovine serum (FBS) for the growth medium was heated for 30 min at 56 °C. Cell lines were cultivated and maintained in 20 ml growth medium in 75 cm^2 cell culture treated polystyrene flasks if not indicated otherwise. Cell growth was monitored daily by microscopy. Cell lines were passaged at a dilution from 1:2 to 1:20, when they reached 90 % confluency. Adherent cell lines were detached from the culture flasks by removing the medium, carefully rinsing the cells with 5 ml DPBS to remove dead cell residues and all traces of serum and digesting them with 2 ml 0.25 % Trypsin-EDTA for 2-5 min. Detached cells were collected in 6 ml cell culture medium. After centrifugation, the supernatant was removed, and cell pellet was resuspended in fresh growth medium. Cells were seeded as indicated for the respective experiment or passaged as described above.

Centrifugation of cells (e.g. for pelleting or washing steps) was performed at 2000 rpm (684-818 g) for 2 min at room temperature (RT), if not specified else.

3.1.1.2 Determination of cell numbers

Cell numbers were determined using a Brand™ Neubauer counting chamber (Thermo Fisher Scientific, Waltham, MA, USA). Prior counting, cells were stained with Trypan Blue solution at a 1:10 to 1:100 dilution to discriminate between viable and dead cells. Cells were counted in all four outer quarters under a light microscope. The final cell number was calculated according to the following equation:

Cells / ml = (Counted cell number / 4) x 10 000 x dilution factor

3.1.1.3 Freezing and thawing of eukaryotic cells (cell lines and primary cells)

For freezing, 1-5x10^6 cells were resuspended in 1 ml freezing medium and transferred to cryotubes. For gentle freezing (stepwise decrease of temperature, 1 °C/min), tubes were placed in a Thermo Scientific™ Mr. Frosty™ Freezing Container (Thermo Fisher Scientific, Waltham, MA, USA) at -80 °C.

Frozen cells were thawed rapidly in a 37 °C water bath. To remove DMSO, the cell suspension was transferred to a 50 ml conical tube and washed with 20 ml of the respective pre-warmed cell culture medium. The cells were cultivated as described above. Medium was changed 24 h after thawing to remove dead cells.

3.1.2 Primary cell preparation from mouse organs

To prepare single cell suspensions from the organs of interest, mice were sacrificed by cervical dislocation and the respective organs (e.g. spleen, kidney) were removed. Organs were collected in 1-5 ml 1 % RPMI and placed on ice immediately. Single cell suspensions were prepared by grinding the organs with the plunger of a 1 ml syringe through a 70 µm cell strainer and flushing the cell strainer with 5-10 ml 1 % RPMI. Single cells were pelleted and the supernatant was removed.

To remove red blood cells, the cell pellet was resuspended in 1 ml Ammonium-Chloride-Potassium (ACK) Lysing buffer for 1 min. The reaction was stopped by adding 4 ml of 1% RPMI. The cell pellet was resuspended in 1 ml complete RPMI and filtered through a nylon mesh to a fresh 15 ml conical tube.

3.1.3 Preparation of TILs from B16-gp33 mouse tumors

After isolation, tumors were collected in 5 ml 1% RPMI. The tumors were grinded with the plunger of a 1 ml syringe through a 70 µm cell strainer and the cell strainer flushed with 15-20 ml 1 % RPMI. Single cells were pelleted and the supernatant was removed.

For flow cytometry analysis, cells were resuspended in 1 ml ACK Lysing buffer for 1 min and the reaction was stopped by adding 4 ml 1% RPMI. Cells were pelleted and resuspended in 1-10 ml complete RPMI. Cell suspensions were incubated with anti-CD16/CD32 (1:1000) for 10 min on ice to block unspecific binding of fluorescently labeled antibodies to receptors for the fragment crystallizable (Fc) region of antibodies.

For sorting of TILs, the cell pellet was resuspended in 6 ml 30 % Percoll™ diluted in plain DMEM. The suspension was carefully overlaid on 3 ml 80 % Percoll™ diluted in plain DMEM in a conical 15 ml tube. The gradient was centrifuged for 15 min at 2000 rpm (684-818 g), RT, with the breaking speed reduced to 2. The middle layer containing the TILs was collected in a fresh conical 15 ml tube and washed once with 10 ml 1 % RPMI. The pellet was resuspended

in 1 ml ACK Lysing buffer for 1 min. To stop the reaction, 4 ml complete RPMI were added. Cells were pelleted and resuspended in 1 ml 1% RPMI.

3.1.4 Isolation of peripheral blood mononuclear cells (PBMCs) from human buffy coat

Human buffy coat was obtained from the Institut für Klinische Transfusionsmedizin und Zelltherapie (IKTZ) Heidelberg. Buffy coats were diluted 1:4 with DPBS. A volume of 25 ml diluted buffy coat was overlaid to 20 ml of Biocoll® separating solution in a conical 50 ml tube and centrifuged for 15 min at 2000 rpm (684-818 g), RT, with the breaking speed reduced to 2. The middle layer containing the PBMCs was collected in a fresh conical 50 ml tube and washed once with 20 ml DPBS. The resulting pellet was resuspended with 2 ml ACK Lysing buffer for 1 min. The reaction was stopped by adding 8 ml 1% RPMI. Cells were pelleted and the supernatant was removed. After counting, PBMCs were frozen as described before (50 million PBMCs/vial).

3.1.5 *In vitro* culture of primary cells

3.1.5.1 *In vitro* activation of P14 cells with antigen

For *in vitro* stimulation, per well $2x10^5$ splenocytes from a P14 mouse were cultivated in 96-well plates with round bottom in 200 µl complete RPMI with 10 ng/µl of their cognate antigen peptide gp_{33-41} (GP33) and IL-2, respectively. Cells were incubated for 3 days.

Additional drugs or chemicals were added at the indicated concentration and time points.

3.1.5.2 *In vitro* exhaustion of P14 cells by repeated antigen stimulation

For repeated stimulation of P14 cells, per well $2x10^5$ splenocytes from a P14 mouse were cultivated in 96-well plates with round bottom in 200 µl complete RPMI with 5 ng/µl IL-7/IL-15 and 10 ng/µl GP33 for 5 days. For repeated stimulation, GP33 was added daily, 5 times in total. Cells were splitted 1:2 at day 3.

Additional drugs or chemicals were added at the indicated concentration.

3.1.5.3 *In vitro* exhaustion of P14 cells by mitochondrial impairment

For stimulation of P14 cells, per well $4x10^6$ splenocytes from a P14 mouse were cultivated in 6-well plates in 4 ml complete RPMI with 10 ng/µl IL-2 and GP33, respectively. Cells were incubated for 3 days. To induce exhaustion *in vitro* by mitochondrial damage and mitophagy inhibition, oligomycin in a concentration of 5 µM and Mdivi-1 in a concentration of 100 µM were added to the culture and incubated for additional 6 h.

3.1.5.4 *In vitro* activation of human PBMCs with anti-CD2, anti-CD3 and anti-CD28

Per well, 2,5x10^5 freshly thawed PBMCs were cultivated in 96-well plates with round bottom in 200 µl complete RPMI with 2 ng/µl anti-CD2, anti-CD3 and anti-CD28, respectively. Cells were incubated for 4 days and re-stimulated with 2 ng/µl anti-CD2, anti-CD3 and anti-CD28 at day 2.

3.1.5.5 Treatment of cells with metabolites

For treatment of cells, different metabolites identified from the mass spectrometry screen were purchased in powder form and diluted in dimethyl sulfoxide (DMSO) to a stock concentration of 100 mM. Cells were treated with the diluted metabolites in a maximal concentration of 100 µM (1:1000). Control cells were treated with the diluent DMSO (1:1000).

The metabolite 3-IPA was investigated in more detail. To be able to treat cells in higher concentrations, an aqueous 3-IPA solution was produced. Therefore, the powder was diluted in 0.2 M NaOH and vortexed until dissolved. To get a stock concentration of 100 µM, the respective amount of ddH_2O was added and the solution was titrated with 1 M HCl to a pH of 7. The solution was aliquoted and a freshly thawed vial was used for each experiment.

All metabolites were stored at -20 °C (for up to 6 months) or -80 °C (long term).

To treat cells, metabolites were added in the indicated concentration to the cell culture medium at the time point of *in vitro* activation and cultured for 72 h, if not indicated otherwise.

3.1.5.6 CRISPR/Cas9 knockout in P14 cells

To knockout specific genes identified in a screening experiment, the CRISPR/Cas9 system was applied. Therefore, the mouse strain P14 x CD4-Cre x Rosa-Cas9-GFP, further referred to as P14-Cas9 was used. P14-Cas9 mice harbor P14 $CD8^+$ T cells that endogenously express the Cas9 enzyme coupled to enhanced green fluorescent protein (EGFP).

The guide RNA (gRNA) consists of a CRISPR RNA (crRNA) and a transactivating crRNA (tracrRNA). The crRNA contains a specific protospacer sequence which targets the gene of interested and the tracrRNA, labeled with the fluorescent dye ATTO™550, binds the Cas9 enzyme, ultimately leading to blunt-ended cuts in genomic DNA and subsequent DNA repair. The gene-specific crRNAs were selected from predesigned Alt-R® CRISPR-Cas9 crRNAs from Integrated DNA Technologies (IDT™) (*Jup*: TACGACTCGGGCATCCACTC CGG; *Dsp*: CCACCCGCGGATCAACACGC TGG).

To form a functional gRNA duplex, crRNAs and tracrRNA ATTO™550 were diluted in Nuclease-Free Duplex Buffer to 100 µM, respectively. A volume of 10 µl of each solution was combined and annealed by heating the solution to 90 °C for 5 min and then reducing temperature stepwise in a polymerase chain reaction (PCR) cycler as indicated in table 3.1.

Table 3.1. PCR cycler program for gRNA duplex formation.

Step	Time	Temperature [°C]
1	5 min	90
2	5 min	85
3	5 min	80
…		
15	5 min	20
16	hold	4

Annealed duplexes were stored at -20 °C until used.

Splenocytes from P14-Cas9 mice were isolated as described in chapter 3.1.2.

$1x10^7$ freshly isolated splenocytes were nucleofected with 3 µl of the respective gRNA duplex or control crRNA using the P3 Primary Cell 4D-Nucleofector® X Kit and the 4D-Nucleofector™ Core and X Unit according to manufacturer's instructions. Nucleofected cells were immediately transferred to 6-well plates containing 3 ml prewarmed complete RPMI with IL-7 (5 ng/ml) and cultured for 24 h. Transfection efficacy was determined 24 h after nucleofection using flow cytometry by detection of ATTO™550-positive cells.

After confirmation of successful nucleofection, P14 cells were activated and treated with 3-IPA (75 µM) as described in chapter 3.1.5.1 and 3.1.5.5. After 72 h, cells were stained for flow cytometry as described in chapter 3.1.6 and analyzed.

3.1.6 Staining for flow cytometry and sort

3.1.6.1 Surface staining

For fluorescence activated cell sorting (FACS) staining, single cell suspensions were transferred to a round bottom 96-well plate (not more than $2x10^6$ cells/well) and briefly centrifuged for 2 min at 2000 rpm (684-818 g), RT and the supernatant was removed. The antibodies of choice were diluted in FACS buffer and 50 µl was added to each well. Cells were gently resuspended in the staining solution using a multi-channel pipette and incubated for 25 min at 4 °C. Afterwards, cells were washed once with 200 µl FACS buffer/well. For direct acquisition, cells were resuspended in 50 µl FACS buffer/well. For later acquisition or intracellular staining, cells were fixed with 50 µl Fixation Buffer/well at RT for 5 min and subsequently washed twice with 200 µl FACS buffer/well.

3.1.6.2 Staining of mitochondria

To investigate the mitochondrial activity per mitochondrial mass, the two stains MitoTracker™ Green FM (MG), which allows for examination of mitochondrial mass and

MitoTracker™ Deep Red FM (MDR), a dye used to investigate the membrane potential of cells, were used.

Per well, 50 µl of a staining solution containing 50 nM MitoTracker™ dyes and other surface staining antibodies of interest in FACS buffer were added and incubated for 30 min at 37 °C. Cells were washed once with 200 µl FACS buffer/well and resuspended in 50 µl FACS buffer/well. Cells were kept on ice and acquired freshly without prior fixation.

3.1.6.3 Fixation and intracellular staining

For staining of cytokines or TFs, fixation and permeabilization of cells is required. Surface staining was performed as described above and followed by the respective procedure for intracellular staining.

For staining of cytokines, cells were fixed with 50 µl Fixation Buffer/well at RT for 5 min and subsequently washed twice with 200 µl Permeabilization (PERM) Buffer/well to transiently permeabilize their plasma membrane. The respective intracellular staining antibodies were diluted in PERM Buffer and 50 µl staining solution was incubated for 15 min at RT. The cells were washed once with 200 µl PERM Buffer/well, resuspended in 50 µl PERM Buffer/well and acquired on a flow cytometer.

For TF staining, cells were fixed with 200 µl eBioscience™ Fixation/Permeabilization solution/well at 4 °C for 1 h. Cells were washed twice with 200 µl FACS buffer/well. The respective intracellular staining antibodies were diluted in PERM Buffer and 50 µl staining solution was added per well and incubated for 15 min at RT. Cells were washed once with 200 µl PERM Buffer/well, resuspended in 50 µl PERM Buffer/well and acquired on a flow cytometer.

Non-fluorescently coupled staining antibodies (primary antibodies) were included in the respective staining solution. After incubation as indicated above, cells were washed twice with the respective buffer and 50 µl staining solution containing a fluorophore-conjugated secondary antibody reactive towards species-specific IgG for the primary antibody. After incubation for 15 min at RT, cells were washed once with 200 µl of the respective buffer/well, resuspended in 50 µl and acquired on a flow cytometer.

Fixed cells were stored up to 72 h at 4 °C before acquisition at a flow cytometer.

3.1.6.4 *in vitro* re-stimulation for cytokine analysis

For cytokine analysis, primary P14 cells were re-stimulated with the LCMV-specific peptide GP33 (10 ng/ml) and in the presence of 5 µg/ml Brefeldin A (BFA) to prevent proteins from being secreted. Cells were incubated in 200 µl complete RPMI/well in a round bottom 96-well plate for 4-6 h. Cells incubated in 200 µl complete RPMI/well without GP33 were included as unstimulated negative controls.

3.1.7 Metabolic analysis

To investigate the effect of metabolite treatment on the metabolism of cells, per well $4x10^6$ P14 cells were seeded in 6 ml complete RPMI in 6-well plates. Cells were *in vitro* activated with 10 ng/ml GP33 and IL-2 for 3 days and cultured with or without 3-IPA in the concentration of 75 µM.

One day prior the assay, Seahorse Cartridges were hydrated according to manufacturer's description. Seahorse 96 well cell culture plates were coated with 50 µl Poly-D-Lysine/well (1:20 diluted in XF calibrant buffer) and incubated at 4 °C overnight.

On the day of the assay, Poly-D-Lysine buffer was removed from the cell culture plate, and the plate was washed once with 200 µl plain Seahorse base medium per well. *In vitro* activated cells were pelleted, washed once with 10 ml DPBS and subsequently resuspended in 1 ml plain Seahorse medium. Per well, $4x10^5$ cells were seeded in 180 µl plain Seahorse medium (glycolytic stress test) or 180 µl Seahorse medium with 10 mM glucose and 1 mM pyruvate (mitochondrial stress test). After seeding of the cells, the culture plate was spun for 1 min at 2000 rpm (684-818 g), RT and incubated for 30-60 mins in a 37 °C incubator without CO_2. The Seahorse cartridge was loaded with the respective drugs as described in Table 3.2 and Table 3.3, and run on the analyzer follwing the program in Table 3.4.

Table 3.2. Portal injections for the mitochondrial stress test [in Seahorse medium + 10 mM glucose + 1 mM pyruvate].

Port	Drug	Final concentration [µM]	Injection volume [µl]
A	Oligomycin	2	20
B	FCCP	2	22
C	Rotenone	2	25

Table 3.3. Portal injections for the glycolytic stress test [in plain Seahorse medium].

Port	Drug	Final concentration	Injection volume [µl]
A	Glucose	10 mM	20
B	Oligomycin	2 µM	22
C	2-DG	2 mM	25

Table 3.4. Assay program for mitochondrial and glycolytic stress tests.

Step	Time	Repeats
Calibration	Standard	-
Equilibration	Standard	-
Baseline	Mix 5 min Measure 5 min	3
Injection Port A	Mix 5 min Measure 5 min	3
Injection Port B	Mix 5 min Measure 5 min	3
Injection Port C	Mix 5 min Measure 5 min	3
Final measurement	Mix 5 min Measure 5 min	3

3.2 Molecular biology

3.2.1 Cloning of overexpression plasmid

To generate a *Jup* overexpressing plasmid, the *Jup* gene was amplified from prior synthesized complementary DNA (cDNA) and cloned into a MigR1-GFP backbone plasmid containing 4 additional restriction sites (for the restriction enzymes SggI, AscI, RsrII and MluI), therefore further referred to as MigR1-SARM.

3.2.1.1 RNA extraction and cDNA synthesis

RNA from a mouse kidney was extracted using the Qiagen RNAeasy mini kit according to manufacturer's instructions. A DNA digestion step using the Qiagen RNase-Free DNase Set was included, before mRNA was eluted. 1.5 µg RNA/sample were used for reverse-transcription to cDNA using the SuperScript™ III system, according to manufacturer's description.

3.2.1.2 PCR

Two PCR primers were designed to amplify the coding region of the *Jup* gene with additional restriction sites for the restriction enzymes XhoI and MluI (table 3.5).

Table 3.5. Primer for Jup amplification.

primer	sequence
forward	5'-AA ACGCGT atggaggtgatgaaccttat-3'
reverse	5'-AA CTCGAG ctaggccagcatgtggtctg-3'

The PCR was performed using the Phusion High-Fidelity PCR Master Mix (Thermo Scientific) by preparing the mix as depicted in table 3.6 and using the PCR cycler program depicted in table 3.7. Optimal annealing temperature of 62 °C was determined by a prior performed temperature gradient PCR.

Table 3.6. PCR Mix for Jup amplification.

Component	Volume [µl]
Phusion High-Fidelity PCR Master Mix	25
Forward primer (10µM)	2,5
Reverse primer (10µM)	2,5
cDNA (600 ng)	1
ddH_2O	19

Table 3.7. PCR cycler program for Jup amplification.

Step	Time	Temperature [°C]	
1	30 s	98	
2	10 s	98	32 repeats
3	30 s	62	
4	1 min 30 s	72	
5	10 min	72	
6	hold	4	

The PCR product was purified using the QIAquick PCR Purification Kit according to manufacturer's instructions.

3.2.1.3 Restriction and ligation

Both, the MigR1-SARM backbone vector as well as the PCR product were restricted using the reaction mix indicated in table 3.8 for 2h at 37 °C.

Table 3.8. Restriction reaction setup.

Component	Amount
DNA	1 µg
10X rCutSmart Buffer	5 µl
MluI-HF	1 µl (20 units)
XhoI	1 µl (20 units)
ddH_2O	to 50 µl

The restricted MigR1-SARM vector and PCR product were mixed with 6x Loading Dye each and together with a DNA ladder (GeneRuler 1 kb Plus) loaded on a 1 % agarose gel containing 0.005 % SYBER safe DNA stain in TAE. The DNA was separated at 120 V for 30-40 min. The agarose gel was imaged using UV light and a control band at the size of the band of interest (MigR1-SARM or Jup gene) was cut. To prevent mutations due to UV light, DNA that was used for further procedure was not exposed to UV light and cut at the size of the control band.

DNA was recovered from the gel using the QIAquick Gel Extraction Kit according to manufacturer's instructions.

Recovered and restricted MigR1-SARM plasmid and PCR product (insert) were ligated using the T4 DNA Ligase as described in table 3.9 overnight at 16 °C.

Table 3.9. Ligation reaction setup.

Component	Amount
Vector DNA	50 ng
Insert DNA	37,5 ng
T4 DNA Ligase Buffer (10X)	2 µl
Nuclease-free H_2O	to 20 µl
T4 DNA Ligase	1 µl

3.2.1.4 Transformation of competent DH5α cells and plasmid isolation

To transform competent DH5α cells, cells were thawed on ice and 5 µl ligation product was added to 50 µl cell suspension and shortly mixed without pipetting. Cells were incubated on ice for 30 min and subsequently exposed to a temperature of 42 °C for 40 s. After heat shock, cells were placed on ice for 2 min. Cell suspensions were filled up to 1 ml with LB medium and incubated for 1 h at 37 °C. Afterwards, cell suspensions were centrifuged (8000 rpm, RT, 3 min) and supernatant was removed. The cell pellet was resuspended in the residual liquid and equally distributed on an agar plate containing Ampicillin [100 µg/ml] using plating beads. Plates were incubated over night at 37 °C.

Single colonies were picked using a sterile pipette tip and placed into a tube containing 4 ml LB medium with Ampicillin [100 µg/ml] (LB-Amp) and cultured overnight in an incubator shaker at 37 °C and 180 rpm.

The next day, plasmids from overnight cultures were extracted using the QIAGEN Plasmid Mini Kit according to manufacturer's instructions. To check for positive clones, isolated plasmids were digested as described in chapter 3.2.1.3 and loaded on a 1 % agarose gel containing 0.005 % SYBER safe DNA stain in TAE, and separated at 120 V for 30-40 min. The agarose gel was imaged using an agarose gel documentation system. In case of two visible bands, one for the MigR1-SARM backbone plasmids and the other one at the size of the insert, clones were defined as positive and sent for sequencing using two sequencing primers for the MigR1-SARM backbone (fw and rev) and one sequencing primer starting in the middle of the target gene (*Jup*) (table 3.10)

Table 3.10. Sequencing primers for Jup MigR1-SARM.

primer	sequence
MigR1-SARM fw	CCTTGAACCTCCTCGTTCGAC
MigR1-SARM rev	CTCACATTGCCAAAAGACG
Jup	GAACAACCCTAAGTTCCTGGC

3.2.2 Generation of pcDNA6-N-3XFLAG-*Ctnnb1* control plasmid

The purchased overexpression plasmid pcDNA6-N-3XFLAG-*Ctnnb1* was restricted using the two restriction enzymes HpaI and XhoI and the bigger fragment gel-purified as described in 3.2.1.3.

Since HpaI generates blunt ends while XhoI restriction results in sticky ends, DNA Polymerase I, Large (Klenow) Fragment was used to fill up the sticky ends generated by XhoI to have blunt ends for later ligation. Gel-purified linear plasmid DNA was dissolved in T4 DNA Ligase Reaction buffer supplemented with 33 µM of each dNTP. One unit of Klenow was added per µg DNA and the mixture was incubated at 25 °C for 15 min. The reaction was stopped by adding EDTA to a final concentration of 10 mM and heating at 75 °C for 20 minutes.

Ligation to a linear plasmid was performed as described in chapter 3.2.1.3 and amplification of the control plasmid as described in chapter 3.2.1.4.

3.2.3 Western Blot

3.2.3.1 Sample preparation

Cells to be analyzed by Western blot were pelleted and washed twice with 10 ml DPBS. The cell pellet was lysed with 50 µl RIPA lysis buffer per 10^6 cells for 30 min on ice on an orbital

shaker. Cell debris of lysed cells was pelleted by centrifugation (13000 rpm, (16100 - 17000 g), RT, 5 min) and the lysate (supernatant) transferred to a new sterile 1.5 ml tube. Protein concentration of the lysates were determined using the Pierce™ BCA™ Protein Assay kit, according to the manufacturer instructions. Volumes of the protein solution with equal amounts of total protein (20-100 µg) were adjusted to a total volume of 12 µl with ddH_2O and were subsequently solubilized in 4x SDS sample buffer and heat denatured at 95 °C for 5 minutes. The samples were cooled on ice for 2 min and loaded in a volume of 16 µl on a SDS–polyacrylamide gel.

3.2.3.2 Gel preparation and electrophoresis

12% SDS-polyacrylamide gel electrophoresis (PAGE) gels were casted using casting chambers (Bio-Rad Laboratories, Hercules, CA, USA). In a first step, the resolving gel mixture (table 3.11) was prepared and immediately poured between two glass slides (with 1.5 mm spacer) using a serological pipette before the mixture started to polymerize. To smoothen the surface and remove air bubbles, the gel was overlaid with isopropanol. After 15-30 min of polymerization, the isopropanol was removed. In a second step, the stacking gel mixture (table 3.11) was freshly prepared and poured on top of the resolving gel using a serological pipette. A 10 or 15-well comb was carefully inserted. After 15-30 min of polymerization, the gel was either used immediately or stored in wetted tissue paper in the fridge at 4 °C for up to one week.

Table 3.11. Composition of SDS-polyacrylamide gels.

	Resolving gel (12 %)	Stacking gel (5 %)
Component	Final concentration	Final concentration
Acrylamide/Bis Solution	12 %	5 %
Tris-HCl pH 8.8	375 mM	-
Tris-HCl pH 6.8	-	125 mM
SDS (w/v)	0,1 %	0,1 %
APS (w/v)	0,1 %	0,1 %
TEMED (v/v)	0,04 %	0,01 %

At the day of electrophoresis, the gel was installed in a Mini-PROTEAN Tetra Cell (Bio-Rad Laboratories, Hercules, CA, USA) and the chamber was filled with 500 ml SDS running buffer. After removal of the combs, samples or 3 µl PageRuler™ Prestained Protein Ladder were loaded to the wells. Gel run was performed at 70 V for 20 min and then 60-90 min at 120 V, until the desired separation was reached.

3.2.3.3 Transfer and blot

After separation, the gel was removed from the glass slides and the stacking gel was cut and discarded. Proteins were transferred on PVDF membranes by wet transfer.

To activate the membrane, it was incubated with 100 % MeOH for 30 s prior assembly of the blotting sandwich. The sandwich was assembled as followed from bottom to top: blotting pad, filter paper, membrane, SDS-PAGE gel, filter paper, blotting pad. After assembly, it was inserted in a Mini-PROTEAN Tetra Cell (Bio-Rad Laboratories, Hercules, CA, USA) and the chamber was filled with 500 ml wet blot transfer buffer. An ice pack was added in order to prevent heating and denaturation of proteins while blotting. The electrophoretic transfer of proteins was performed at 100 V and constant amperage for 2 h.

After transfer, the membrane was blocked with 5 % skim milk powder in PBS-T or for 60 min at RT on a shaker. The membrane was washed with PBS-T and incubated with the respective primary antibodies diluted in 5 % BSA with PBS-T with 0.2 mg/ml NaN_3 over night at 4 °C on a shaker.

3.2.3.4 Detection

After transfer, the membrane was blocked with 5 % skim milk powder in PBS-T or for 60 min at RT on a shaker. The membrane was washed with PBS-T and incubated with the respective primary antibodies diluted in 5 % BSA with PBS-T with 0.2 mg/ml NaN_3 over night at 4 °C on a shaker.

Probed blots were washed 3x 10 min with PBS-T at RT on a shaker. The HRP-conjugated secondary antibody was diluted to the indicated concentration (table 2.5) in 5 % skim milk powder in PBS-T and incubated for 60 min at RT on a shaker. The blots were washed 3x 10 min with PBS-T at RT on a shaker. For detection, 1 ml Clarity™ Western ECL Substrate was applied to the membrane and the signals were imaged using the Fusion FX chemiluminescence imager.

3.2.4 Streptavidin-Bead Pulldown

To identify potential 3-IPA binding proteins, a new compound was designed and synthesized by linking 3-IPA to biotin-PEG3-Amine, further referred to as 3-IPA-Biotin-PEG3-Amine (designed and synthesized with the help of Dr Aubry Miller, Research Group Cancer Drug Development, DKFZ, Heidelberg).

P14 cells were isolated and cultured in 24-well plates (0.5 $x10^6$ cells/well in 1 ml complete RPMI with 10 ng/µl GP33 and IL-2) for 3 days. After *in vitro* activation, cells were lysed as described in chapter 3.2.3.1. Lysates were incubated with either 3-IPA-Biotin-PEG3-Amine or control Biotin-PEG3-Amine for 2 h at RT. Afterwards, lysates were incubated with

Dynabeads™ M-280 Streptavidin for 30 min at RT on a tube rotator. Beads were washed five timed with PBS-T. Per tube, 65 µl of 4x Laemmli Sample Buffer (including 50 nM DTT) were added to the beads and boiled at 95 °C for 12 min. Boiled beads were vortexed five times and pelleted by centrifugation (13000 rpm, (16100 - 17000 g), RT, 1 min). Supernatant was transferred to a new sterile 1.5 ml tube and sent to the EMBL Proteomics Core Facility for mass spectrometry analysis.

3.2.5 Luciferase Assay

To determine the effect of different proteins in combination with 3-IPA on *Tcf7* gene expression, the Dual-Glo® Luciferase Assay System (Promega) was performed in HEK293T and EL4 cells.

HEK293T were seeded in 96-well (flat bottom) plates ($2x10^4$ cells/well in 100 µl growth medium) 24 h prior transfection. On the day of transfection, 100 µl of cell culture medium containing 3-IPA (final concentration 75 µM) or control medium were added to each well. Cells were transfected with a total amount of 0.1 µg DNA (see table 3.13) per well using X-tremeGENE™ HP DNA Transfection Reagent according to the manufacturer's instructions.

EL4 cells ($2x10^5$) were transfected with 5 µg total DNA (see table 3.13) using X-tremeGENE™ HP DNA Transfection Reagent according to the manufacturer's instructions. Cells were seeded in 96-well plates ($2x10^4$ in 200 µl growth medium) and cultured with or without 75 µM 3-IPA the same day.

Table 3.12. DNA amounts transfected per well for luciferase assay.

	DNA amount [µg] / well ($2x10^4$ cells)	
Plasmid	HEK293T	EL4
Tcf7 pGL3 reporter plamid	0,04	0,18
pRL *Renilla* Luciferase Control Reporter plasmid	0,01	0,02
pcDNA6-N-3XFLAG-*Ctnnb1*	0,025	0,15
pcDNA6-N-3XFLAG control	0,025	0,15
MigR1-SARM-*Jup*	0,025	0,15
MigR1-SARM control	0,025	0,15

Three days post transfection, cells were washed twice with 200 µl DPBS, and 40 µl of Passive Lysis 5X Buffer were added to each well. After a freeze/thaw cycle, 20 µl of lysate were transferred to a 96-well solid white plate and the assay was performed according to the manufacturer's instructions and measured using a microplate luminometer.

To minimize sample variability, the firefly luciferase signal of the experimental reporter plasmids was normalized to the Renilla signal of the control reporter plasmid.

3.3 *In vivo* studies

3.3.1 Genotyping of congenic markers

Genotyping of congenic markers was performed using blood samples of mice. A volume of 50 µl of the samples was transferred from a sodium-citrate containing collection tube to a round bottom 96-well plate. After centrifugation (2000 rpm, 2 min, RT), the supernatant was discarded. To remove red blood cells, cell pellets were resuspended in 200 µl ACK Lysing buffer and incubated for 1 min. The plate was centrifuged at 2000 rpm (684-818 g), 2 min, RT and the supernatant was discarded. The ACK lysis was repeated 2 times. The final pellet was washed with 200 µl FACS buffer and cells were stained using the standard panel from table 3.13

as described in chapter 3.1.6.

Table 3.13. Standard flow cytometry staining for congenic marker genotyping.

Antigen	Fluorophore	Dilution
CD8a	PerCP-Cy5.5	1:400
TCR-vα2	FITC	1:400
CD45.1	APC	1:400
CD45.2	PE	1:400
CD90.1	BV421	1:800
CD90.2	PE-Cy7	1:400

3.3.2 High fat diet (HFD) experiments

3.3.2.1 Feeding of mice

Young (6 weeks) and aged (15 months) mice were fed either a HFD enriched in saturated fatty acids (Research Diets, Inc, 45 kcal% Fat, mostly hydrogenated coconut oil) or a standard chow control diet (Research Diets, Inc, 10 kcal% Fat) in pellet form for 110 days (~ 4 months). Mice were fed *ad libitum* and food intake as well as body weights were monitored weekly.

3.3.2.2 Blood glucose measurement

Mice were fasted for 12 h prior blood sampling. Blood was collected from the submandibular vein and one drop was used to measure the blood glucose levels using the OneTouch Select® Plus blood measuring device.

3.3.2.3 Preparation of plasma samples for mass spectrometry analysis

Blood was taken from the submandibular vein right before sacrificing the mice and collected into 1.5 ml tubes containing 60 µl sodium citrate to prevent coagulation. Volume of collected blood was measured using a mechanical pipette. Samples were centrifuged at 13000 rpm (16100 - 17000 g) for 5 min and the clear supernatant (plasma) was transferred to new 1.5 ml tubes. Samples were stored at -80 °C until analysis. In collaboration with Dr. Gernot Poschet from the centre for organismal studies (COS) Heidelberg, samples were analyzed by mass spectrometry using the MxP® Quant 500 Kit from Biocrates.

3.3.2.4 Immune characterization of mice from different age and diet groups

Mice from all age and diet groups were sacrificed by cervical dislocation. Spleens were isolated and splenocytes isolated as described in chapter 3.1.2 and stained for flow cytometry analysis as described in chapter 3.1.6.

3.3.3 Viral infection experiments

3.3.3.1 LCMV Arm and adoptive transfer

P14 T cells of donor mice with mismatched congenic markers (to the acceptor mice) were purified as described in chapter 3.1.2 or isolated from tumors (chapter 3.1.3) and subsequently *in vitro* activated and cultured with or without 3-IPA (chapter 3.1.5.1 and 3.1.5.5). To induce mitochondrial impairment cells were additionally treated with oligomycin and Mdivi-1 for 6 h as described in chapter 3.1.5.3. The proportion of viable activated donor cells was determined by flow cytometry and cell concentrations were adjusted accordingly.

Acceptor C57BL/6 mice were infected with $2x10^5$ pfu LCMV Armstrong (Arm) (intraperitoneally (i.p.) in 200 µl RPMI).

$1x10^5$ activated donor cells per group were adoptively transferred to acceptor mice the same day (intravenously (i.v.), in 200 µl plain RPMI).

Acceptor mice were sacrificed 8 days or 24 days after infection (days post infection, dpi) and the splenic T cells were stained for flow cytometry. Donor cells were identified by their congenic markers.

3.3.3.2 LCMV cl-13 and adoptive transfer

Splenocytes from LCMV Arm-infected mice were isolated on 30 dpi. P14 donor cells were identified by their congenic marker and their percentage among total splenocytes determined by flow cytometry. Donor cell numbers were calculated using the donor cell percentage and splenocyte count. A number of $1x10^5$ activated donor cells per group were adoptively transferred to a new batch of congenically mismatched acceptor mice (i.v. in 200 µl plain RPMI).

Acceptor C57BL/6 mice were infected with 2x10^6 pfu LCMV cl13 (i.p. in 200 µl RPMI) the same day.

Acceptor mice were sacrificed 8 dpi and splenic T cells were stained for flow cytometry. Donor cells were identified by their congenic markers.

3.3.4 Tumor experiments

3.3.4.1 Tumor implantation

B16-gp33 cells were cultivated in respective cell culture medium (table 2.9) and passaged 3-4 times before inoculation. On the day of tumor implantation, the cells were detached from the flask and washed twice with plain medium to remove residual FBS. For tumor inoculation, C57BL/6 mice were anesthetized with 1.5-3 % isoflurane. The injection site was shaved and 0.2x10^6 B16-gp33 cells in 100 µl plain DMEM were subcutaneously injected above the right flank.

3.3.4.2 Tumor measurements

Tumor growth was monitored and measured using a digital caliper every 2-3 days. The tumor volume was calculated by $V = D \times d \times \frac{1}{2} d$ (V = tumor volume, D = larger tumor diameter, d = smaller diameter).

3.3.4.3 Adoptive transfer and vaccination

P14 T cells of donor mice with mismatched congenic markers (to the acceptor mice) were purified as described in chapter 3.1.2 and subsequently *in vitro* activated and cultured with or without 3-IPA (chapter 3.1.5.1 and 3.1.5.5) for 3 days. After activation, the proportion of viable activated donor cells was determined by flow cytometry and cell concentrations were adjusted accordingly.

0.3x10^6 activated donor cells per group were adoptively transferred to tumor-bearing acceptor mice (i.v. in 200 µl plain RPMI) 9 days after tumor implantation.

For vaccination, acceptor mice were injected with 50 µg adjuvant TLR3 ligand [poly(I:C)] and 10 µg GP33 in 40 µl DPBS in the right posterior paw (subcutaneously (s.c.)) the same day.

4 Results

4.1 Aging and obesity synergistically alter the T cell phenotype and metabolic profile in mice

To investigate the synergistic effect of aging and obesity on the immune system and more specifically on $CD8^+$ T cells as well as the overall metabolism, I fed young (6 weeks) and aged (15 months) C57BL/6 mice either a chow control diet or a HFD enriched in saturated fatty acids, resembling a “Western diet” [223] for 4 months (Figure 4.1A).

Body weight (BW) was monitored weekly. Over the course of the experiment, young mice which received the chow diet increased their BW due to physiological growth, while aged mice receiving the same diet maintained their weight. After 4 months, young and aged mice receiving the chow diet did not show a difference in their weight. Both age groups receiving the HFD started gaining weight already one week after diet start. Similar to the chow diet groups, both young and aged mice receiving the HFD did not show a weight difference but were significantly heavier compared to the groups receiving the chow diet (Figure 4.1B). After the course of the experiment, there were four groups of mice: young lean (YL), young obese (YO), aged lean (AL) and aged obese (AO). (Figure 4.1A and B). These four groups represented the optimal model to identify changes in the T cell compartment as well as in the metabolic profile induced by aging and obesity alone or by their combination. Parallel identification of T cell phenotypic alterations and metabolic changes allowed the identification of potential correlations.

All mice were fasted for 12 h prior blood sampling and blood glucose levels were determined shortly before sacrificing the mice. Lowest blood sugar levels were measured in YL mice, while the highest levels were observed in YO mice, indicating a strong effect of an obese condition on blood sugar levels. Surprisingly, there was no difference in blood sugar levels between AL and AO mice. While there was no difference in blood sugar levels between the two lean age groups, AO mice displayed significantly lower levels compared to YO mice (Figure 4.1C).

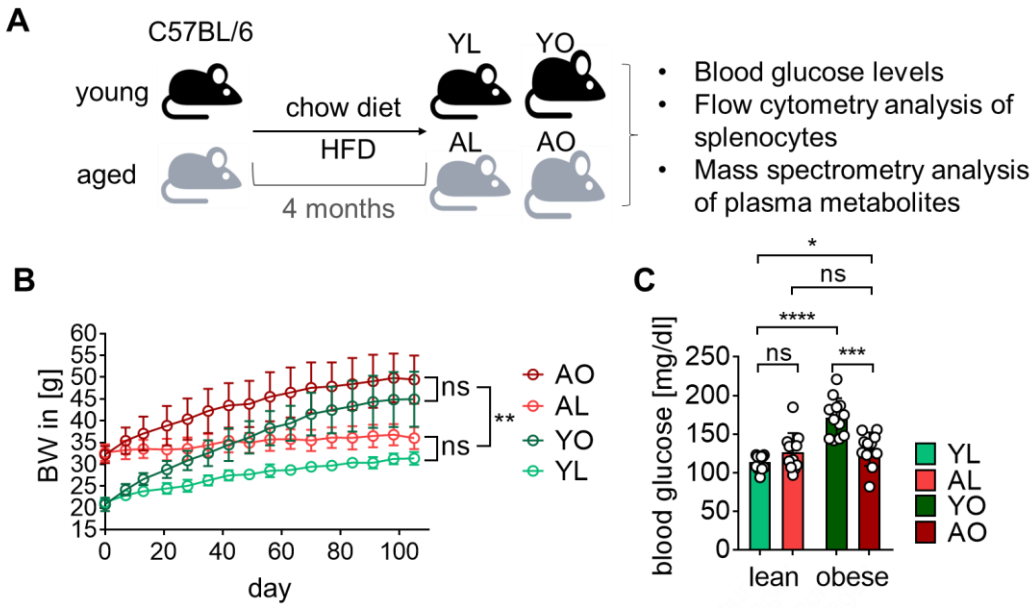

Figure 4.1. Feeding a HFD for 4 months induces obesity and increases blood sugar in mice. ***A****. Experimental setup. Young (6 weeks) and aged (15 months) mice were fed a HFD or chow diet for 4 months. Analysis of splenocytes and plasma samples were conducted as described above (YL = young lean, YO = young obese, AL = aged lean, AO = aged obese).* ***B****. BWs were monitored weekly. Data are pooled from two independent experiments (n=10-12).* ***C****. Blood glucose levels were measured after a fasting period of 12h. Data are means ± s.d. of 10-12 measurements and were analyzed by two-way ANOVA. Statistically significant changes are indicated by ns: not significant, *P ≤ 0.05, **P ≤ 0.01, ***P ≤ 0.001, ****P ≤ 0.0001.*

4.1.1 Effects on T cell phenotype

To investigate the influence of aging and obesity on the T cell phenotype, splenocytes of all groups were isolated and analyzed by flow cytometry. While obese mice showed decreased percentages of $CD8^+$ T cells among all lymphocytes, this proportion was not influenced by the age of the mice. By contrast, the percentage of $CD4^+$ T cells was significantly lower in aged mice compared to their young counterparts, and less affected by the diet of the mice (Figure 4.2A and B). The proportion of $CD8^+$ T cell-suppressing T_{reg} (defined by co-expression of CD25 and Foxp3 [224]) among $CD4^+$ T cells was significantly increased in AO mice compared to all other groups (Figure 4.2B and D). Based on the well-defined surface markers CD62L and CD44, T cells can be divided into naïve, T_{cm} and T_{em} cells [84] (Figure 4.2E (left)). While YL mice had the highest percentage of naïve $CD8^+$ T cells, AO displayed the lowest proportion of this population. Naïve $CD8^+$ T cells were mainly reduced by HFD and even more by the combination of HFD and aging. In general, aged mice displayed higher percentages of T_{mem} compared to their young counterparts. More specifically, T_{cm} cells were significantly increased in both aged groups while there was no difference between the AL and AO groups. In young mice, however, this percentage was decreased by obesity. T_{em} cells, the most differentiated among those three populations, was highest in AO mice (Figure 4.2E). Furthermore, $CD8^+$ T cells from aged mice displayed a more activated phenotype compared to $CD8^+$ T cells from

young mice, marked by increased expression of the surface marker CD44, the effector molecule GrzB as well as co-expression of the TFs T-bet and Eomes. This activated phenotype was even more increased by the combination of aging and obesity (Figure 4.2F (left)). While showing the most activated phenotype, AO mice also held the highest percentage of T_{ex}, marked by co-expression of the IRs PD-1 and TIGIT. The proportion of stem-like T-bet$^-$TCF1$^+$ CD8$^+$ T cells was significantly decreased in aged mice and even lower in AO compared to AL animals.

In summary, both aging and obesity altered proportions of CD4$^+$ and CD8$^+$ T cells in different manners. In combination, aging and obesity skewed T cells towards an activated phenotype (CD44, cytokines, T-bet$^+$Eomes$^+$) and increased immunosuppressive mechanisms (T_{reg}, IR expression). Furthermore, stem-like cells (T-bet$^-$TCF1$^+$) were significantly decreased in AO mice compared to all other groups.

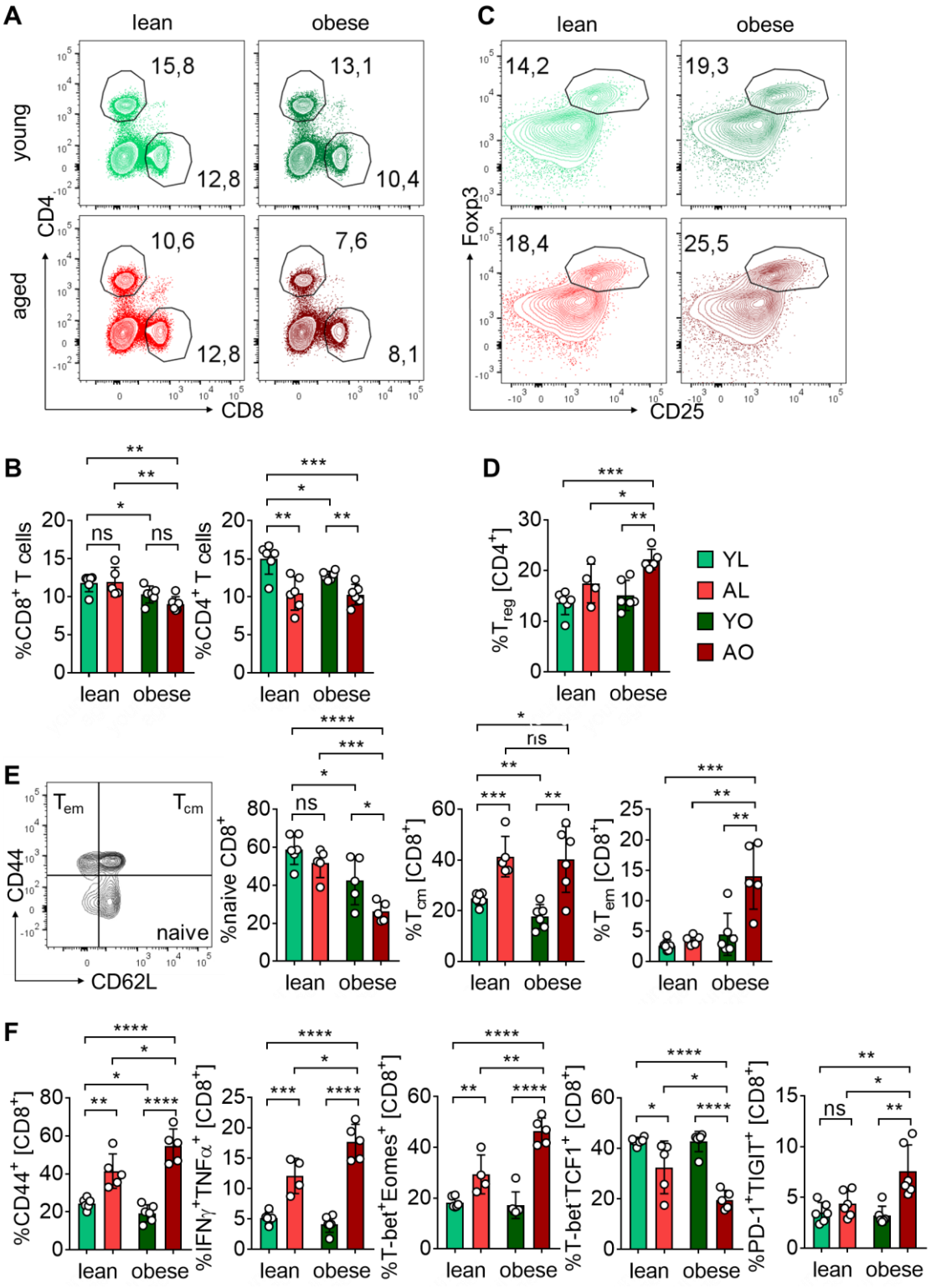

Figure 4.2. Aging and obesity skew T cells towards a terminally differentiated phenotype. *Flow cytometry analysis of T cells isolated from spleen.* ***A****. Representative FACS plots of CD4⁺ and CD8⁺ T lymphocytes.* ***B****. Quantification of cell ratios of CD8⁺ (left) and CD4⁺ (right) T lymphocytes* ***C****. Representative FACS plots of CD25⁺Foxp3⁺ T_{reg}.* ***D****. Quantification of cell ratios of CD25⁺Foxp3⁺ T_{reg}.* ***E****. Schematic representation of CD8⁺ T cell populations according to CD62L and CD44 surface expression (left). Quantification of cell ratios of CD8⁺ T cell populations (right).* ***F****. Quantification of cell ratios of selected CD8⁺ T cell markers, cytokine and TF expression (n=6). Data are means ± s.d. and were analyzed by two-way ANOVA. Statistically significant changes are indicated by ns: not significant, *P ≤ 0.05, **P ≤ 0.01, ***P ≤ 0.001, ****P ≤ 0.0001.*

4.1.2 Effects on metabolic profile

In parallel to T cell phenotypic characterization, plasma concentrations of 630 different metabolites from 26 biochemical classes were determined using the MxP® Quant 500 Kit (Biocrates). In two independent experiments, 29 metabolites were significantly decreased, while 142 were found to be significantly increased in AO compared to YL mice (Figure 4.3A).

Six metabolites were exemplarily chosen for presentation and further analysis. α-Aminobutyric acid (AABA) and asymmetric dimethylarginine (ADMA) were found to be significantly increased in AO compared to YL mice, while aging and obesity alone did not significantly alter plasma concentrations. The metabolites betaine and methionine sulfoxide (Met-SO) were significantly decreased only by the combination of aging and obesity. 3-Indolepropionic (3-IPA) and indoxyl sulfate (Ind-SO_4) were already decreased by obesity alone in young mice and the combination of aging and obesity reduced plasma concentrations even more (Figure 4.3B).

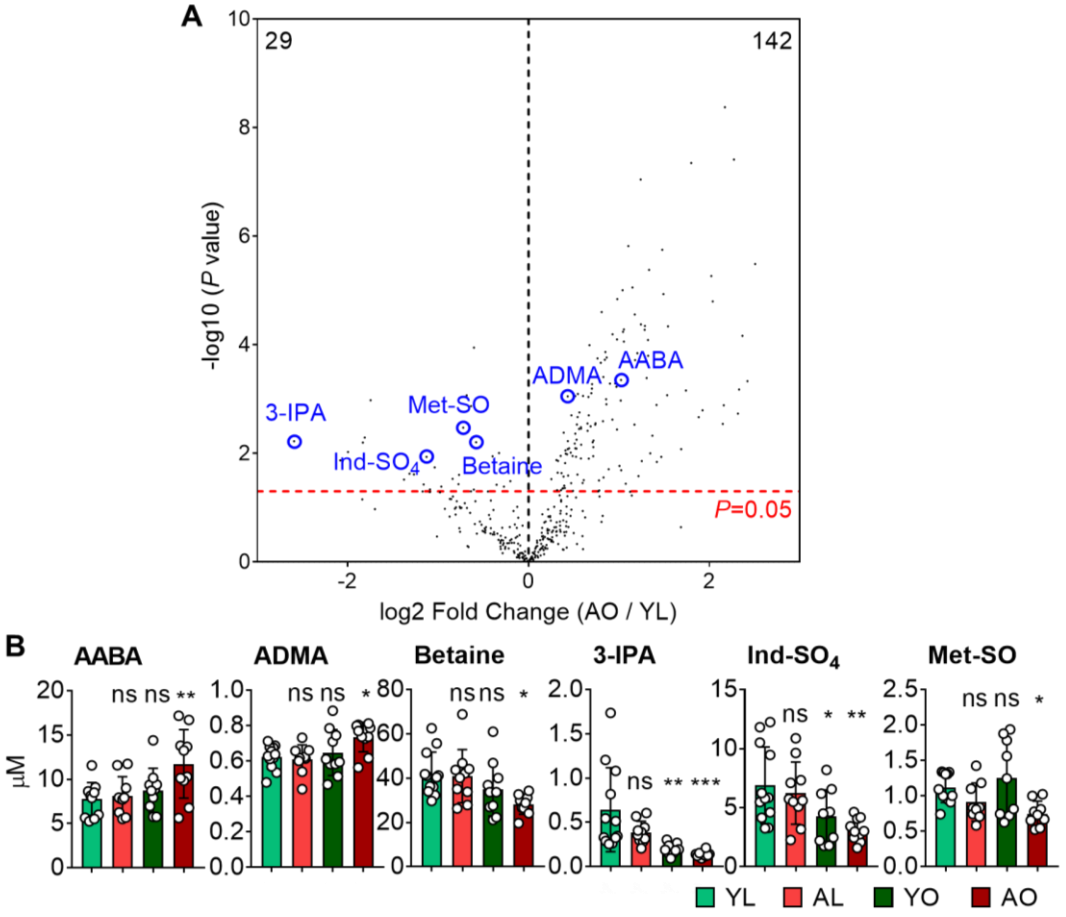

Figure 4.3. Plasma metabolites are synergistically altered by aging and obesity. ***A.*** *Concentrations of 630 metabolites in plasma samples were obtained using the MxP® Quant 500 Kit (Biocrates). Volcano plot showing synergistically altered plasma metabolites comparing YL and AO samples. Data sets were analyzed using two-tailed unpaired Student's t-test (P ≤ 0.05).* ***B****. Plasma concentrations of six exemplary metabolites (AABA = α-Aminobutyric acid, ADMA = Asymmetric dimethylarginine, 3-IPA = 3-Indolepropionic acid, Ind-SO_4 = Indoxyl sulfate, Met-SO = Methionine sulfoxide). Data are means ± s.d. of 10-12 measurements and were analyzed by one-way ANOVA. Statistically significant changes are indicated by ns: not significant, *P ≤ 0.05, **P ≤ 0.01, ***P ≤ 0.001, ****P ≤ 0.0001.*

4.2 The synergistically deprived metabolite 3-IPA alters murine CD8$^+$ T cell phenotype and function *in vitro*

The ultimate goal of this experiment was to find a link between a potentially altered metabolite profile and the T cell phenotype. To find this link, six synergistically altered metabolites were chosen according to their plasma concentrations and commercial availability.

For this and all further *in vitro* experiments splenocytes from the Tcrα Knockout (KO)/Transgenic LCMV P14 T Cell Receptor mouse line, further referred to as "P14" were used [222, 225]. CD8$^+$ P14 cells bear a transgenic TCR that is specific for the GP_{33-41} epitope of LCMV and stimulating them with the GP33 peptide induces antigen-specific CD8$^+$ T cell activation.

To investigate a potential effect on T cells, P14 splenocytes were cultivated with the chosen metabolites (Figure 4.3B) and in the presence of GP33 and IL-2 for 3 days. Subsequently, various T cell markers were analyzed by flow cytometry (Figure 4.4A). Cells were treated with different metabolites in four concentrations each (2, 10, 50 and 100 µM) covering roughly the range of plasma concentrations of all selected metabolites. Surface expression of the T cell markers CD62L as well as the two IRs PD-1 and LAG-3 were assessed and the percentage of marker-expressing CD8$^+$ T cells after treatment was compared to the untreated control. While treatment with AABA, ADMA, betaine, Ind-SO_4 and Met-SO in any tested concentration did not induce changes of the investigated markers, 3-IPA treatment significantly increased the proportion of CD62L-expressing CD8$^+$ T cells and significantly reduced the percentage of PD-1$^+$LAG-3$^+$ CD8$^+$ T cells in concentrations of 50 and 100 µM (Figure 4.4B and C).

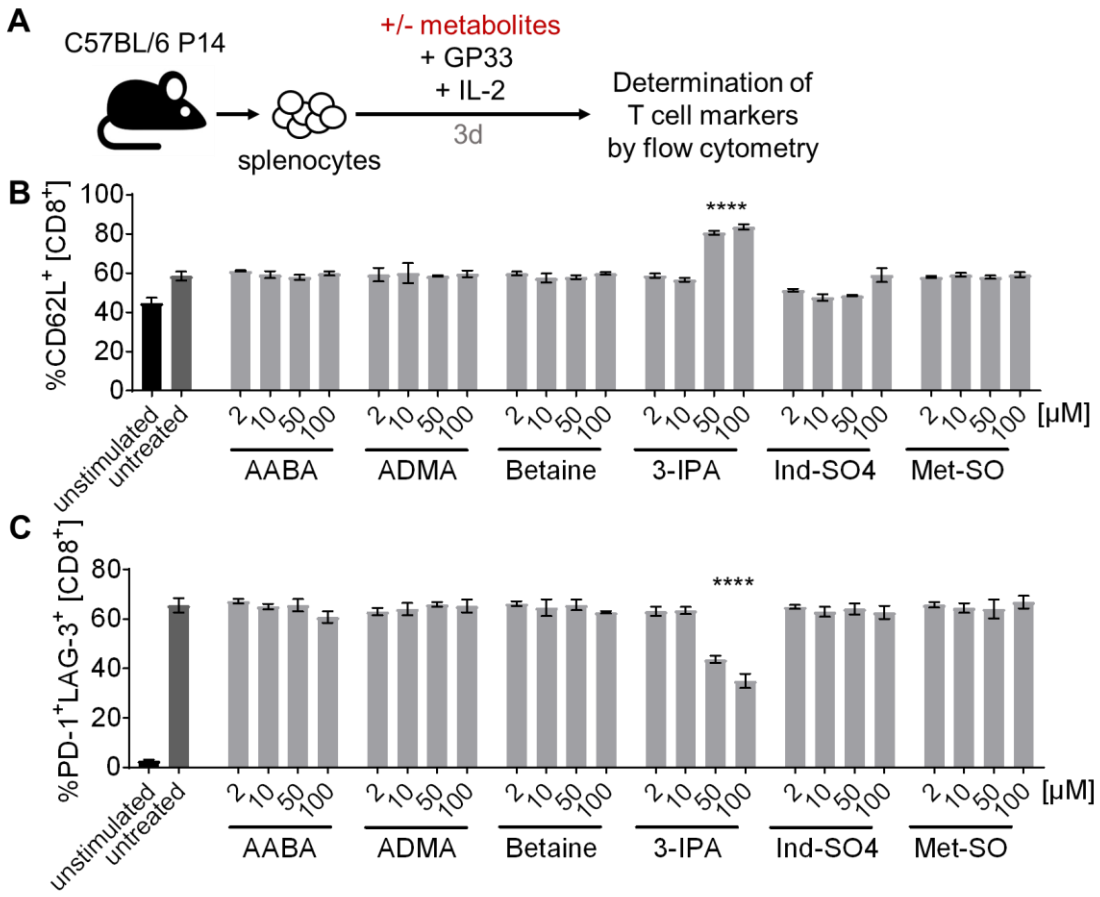

Figure 4.4. 3-IPA treatment affects CD8⁺ T cell marker expression. A. *Experimental setup. P14 cells were in vitro stimulated with GP33 and IL-2 and cultured for 3 days with synergistically altered metabolites in different concentrations. Surface markers were analyzed by flow cytometry.* ***B****. Quantification of cell ratios of CD62L⁺ CD8⁺ T cells.* ***C****. Quantification of cell ratios of PD-1⁺LAG-3⁺ CD8⁺ T cells. Data are means ± s.d. and were analyzed by one-way ANOVA. Statistically significant changes are indicated by ****P ≤ 0.0001.*

Due to the strong and reproducible effect of 3-IPA on the CD8⁺ T cell phenotype, this metabolite was chosen for further investigation.

3-IPA is a tryptophan metabolite that is detectable in mammalian plasma only in the presence of very few bacterial strains of the gut microbiome, most importantly *Clostridium sporogenes* [226, 227]. 3-IPA was described as a potent scavenger of hydroxyl radicals with neuro- and cytoprotective properties [228]. Moreover. 3-IPA was identified as potential biomarker for several metabolic diseases [229-231]. So far, no studies mention this metabolite in the context of CD8⁺ T cell immunity.

4.2.1 Determining optimal treatment concentration of 3-IPA

In a first step, the optimal treatment concentration of 3-IPA was determined using CD62L and TCF1 expression as reference markers. Those two markers were chosen since they were upregulated consistently upon 3-IPA treatment in all experiments. Using the experimental setup as described in Figure 4.4A, cells were treated with 3-IPA in concentrations ranging from

10 to 150 µM. The least effective concentration in upregulating both CD62L and TCF1, was determined to be 50 µM, while maximal marker expression was reached at concentrations from 75 µM on (Figure 4.5A and B). Therefore, 75 µM was determined to be the optimal treatment concentration for $CD8^+$ T cells and if not stated otherwise, all further experiments were performed using this concentration.

Measured plasma concentrations of 3-IPA ranged from 0.1 to 1.7 µM (Figure 4.3B). Using physiological concentrations for treatment, however, did not alter $CD8^+$ T cell markers. Optimal treatment concentration as determined before is roughly 100-fold higher than the physiological one. Due to the strong and reproducible effect on T cell marker expression, however, the therapeutical potential of this metabolite was further explored.

Since no decrease in cell viability was observed in the so far tested concentrations, in the next experiment potential toxicity was investigated by treating P14 cells in different concentrations up 1000 µM (1 mM). The percentage of viable and dead $CD8^+$ T cells among all cells was analyzed after treatment. Surprisingly, not even the highest of the tested concentrations was toxic to cells in this experimental setup. The proportion of dead $CD8^+$ T cells was even decreased compared to the untreated control in all tested concentrations. The proportion of viable $CD8^+$ T cells was increased in all tested concentration compared to the control, while this number decreased in a dose-dependent manner with rising concentrations. This observation is probably due to decreased proliferation of cells upon 3-IPA treatment, which is supported by the fact that the culture medium of untreated cells was more yellowish compared to the treatment wells (data not shown), indicating an overgrowth of cells in the control wells, but not in the treatment wells. Therefore, reduced percentages of dead cells are rather due to decreased proliferation and lower cell death related to overgrowth. Nevertheless, no toxicity was observed in all tested concentrations (Figure 4.5C).

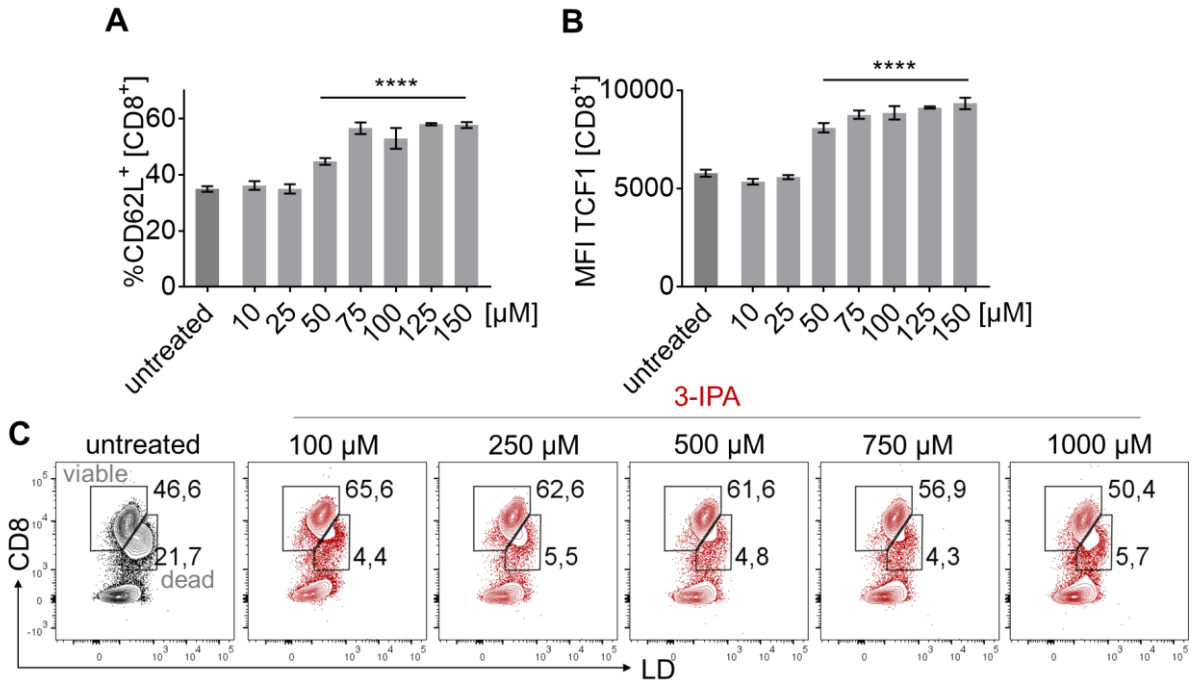

Figure 4.5. Determining the optimal 3-IPA treatment concentration. ***A****. Quantification of cell ratios of CD62L⁺ CD8⁺ T cells.* ***B****. Quantification of TCF1 mean fluorescence intensity (MFI) values of CD8⁺ T cells. Data are means ± s.d. and were analyzed by one-way ANOVA. Statistically significant changes are indicated by ****P ≤ 0.0001.* ***C****. Representative FACS plots of viable and dead CD8⁺ T lymphocytes after treatment with different concentrations of 3-IPA (LD = live/dead).*

4.2.2 3-IPA induces a stem-like CD8⁺ T cell phenotype *in vitro*

To explore the effect on the CD8⁺ T cell phenotype, P14 cells were treated with 3-IPA and cultured in the presence of GP33 and IL-2 for 3 days. T cell markers were assessed by flow cytometry (Figure 4.6A).

While the proportion of viable CD8⁺ T cells was similar between untreated and treated P14 cells (Figure 4.6B), the MFI of CD8 was increased upon 3-IPA treatment (Figure 4.6C), indicating a higher CD8 expression per cell, which has been described to be a marker of cells with stem cell-like features [232].

Furthermore, 3-IPA treatment induced upregulation of the stemness marker TCF1, which was observed both in Western Blot (Figure 4.6D) and flow cytometry analysis (Figure 4.6E). Interestingly, only TCF1 was upregulated upon 3-IPA treatment, while expression of its homologue lymphoid enhancer binding factor 1 (LEF1) was unaffected (Figure 4.6D). In addition to TCF1, other typical markers of naïve and stem-like CD8⁺ T cells, such as CD62L and Slamf6 were upregulated upon treatment with 3-IPA (Figure 4.6F and G), while the activation marker CD44 was downregulated (Figure 4.6H).

Taken all analyzed phenotypic markers in consideration, 3-IPA treatment of CD8⁺ T cells induced a stem-like phenotype *in vitro*.

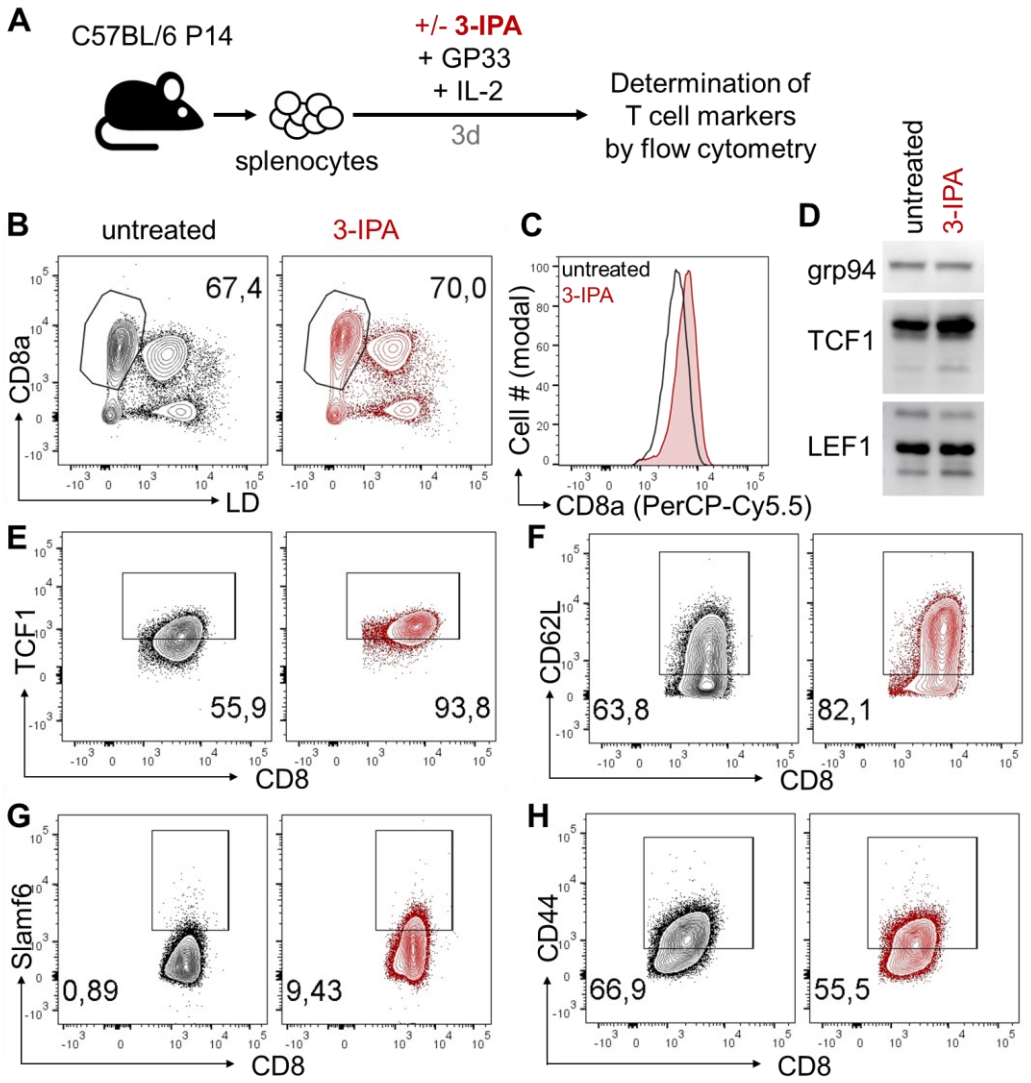

Figure 4.6. 3-IPA treatment induces a stem cell-like CD8⁺ T cell phenotype in vitro. ***A****. Experimental setup. P14 splenocytes were cultivated with or without 3-IPA in the presence of IL-2 and GP33 for 3 days. T cell markers were analyzed by flow cytometry.* ***B****. Representative FACS plots of viable CD8⁺ T cells.* ***C****. Representative MFI of CD8a in viable CD8⁺ T cells.* ***D****. Western Blot analysis of TCF1 and LEF1 in activated P14 cells. Grp94 protein levels were used as loading control.* ***E****. Representative FACS plots of TCF1⁺ CD8⁺ T cells.* ***F****. Representative FACS plots of CD62L⁺ CD8⁺ T cells.* ***G****. Representative FACS plots of Slamf6⁺ CD8⁺ T cells.* ***H****. Representative FACS plots of CD44⁺ CD8⁺ T cells.*

4.2.3 3-IPA treatment alters CD8⁺ T cell metabolism *in vitro*

The metabolism of CD8⁺ T cells is tightly linked to their phenotype. While naïve and memory T cells rather rely on OXPHOS, T_{eff} undergo metabolic reprogramming and engage aerobic glycolysis for ATP production [91]. Seahorse glycolytic and mitochondrial stress test was performed to investigate the effect of 3-IPA treatment on the metabolic capacity of CD8⁺ T cells. As described before, P14 cells were cultured for 3 days in the presence of GP33 and IL-2 and with or without 3-IPA (Figure 4.6A). The extracellular acidification rate (ECAR) and oxygen consumption rate (OCR) were measured using the Seahorse XFe96 analyzer.

For the glycolytic stress test, cells were cultured without glucose for 60 min prior the assay. Upon glucose injection, cells use this glucose for glycolysis leading to the production and extrusion of protons, which results in extracellular acidification. Surprisingly, 3-IPA-treated $CD8^+$ T cells displayed much higher glycolytic activity under basal conditions compared to untreated cells. Maximum glycolytic capacity can be determined after injection of the ATP synthase inhibitor Oligomycin [233]. While untreated P14 cells increased their glycolytic capacity upon ATP synthase inhibition, 3-IPA-treated cells maintained the same level of glycolysis indicating induction of maximal glycolysis under basal conditions. Even though glycolysis was not increased upon Oligomycin injection in 3-IPA-treated cells, their maximum glycolytic capacity was still higher compared to untreated cells. Injection of the glucose analogue 2-deoxy-glucose (2-DG), leads to inhibition of glycolysis [234] and the subsequent decrease in ECAR confirms a glycolysis-dependent measurement of ECAR (Figure 4.7A).

Basal respiration was determined by measuring the OCR of cells without injection of any drug. 3-IPA-treated cells displayed lower basal respiration compared to their untreated counterparts. Injection of Oligomycin lowered OCR of both treated and untreated cells, indicating the oxygen consumption which is used for ATP production. Carbonyl cyanide-4-(trifluoromethoxy)phenylhydrazone (FCCP) is un uncoupling agent that uncouples nutrient oxidation from ATP production by disrupting the mitochondrial membrane potential, which results in an uninhibited electron flow and maximal oxygen consumption [235]. Despite the great difference in basal respiration between 3-IPA-treated and untreated P14 cells, their maximal respiration was very similar (Figure 4.7B). Injection of rotenone, an inhibitor of complex I [236], shut down mitochondrial respiration.

The SRC is an indicator of the capacity of cells to respond to an increased energy demand and is therefore associated with longevity and function of cells [237]. Despite their low basal respiration, 3-IPA-treated cells were able to engage oxygen consumption after FCCP injection, leading to a significantly higher SRC compared to untreated cells (Figure 4.7C).

In summary, 3-IPA-treated cells rather rely on a glycolytic metabolism for ATP production under basal conditions. However, when required, they were able to engage OXPHOS leading to a higher SRC compared to their untreated counterparts, indicating an increased ability to respond to metabolic stressful conditions.

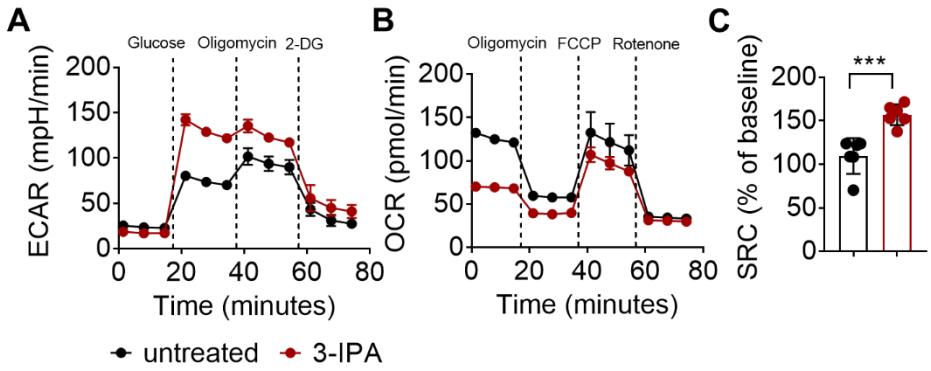

Figure 4.7. 3-IPA treatment alters CD8⁺ T cell metabolism in vitro. *P14 splenocytes were cultivated with or without 3-IPA in the presence of IL-2 and GP33 for 3 days.* ***A****. Seahorse glycolytic stress was performed to determine the extracellular acidification rate (ECAR).* ***B****. Seahorse mitochondrial stress test was performed to determine the oxygen consumption rate (OCR).* ***C****. Spare respiratory capacity (SRC) was calculated using the formula (Maximal Respiration) / (Basal Respiration) × 100. Data are means ± s.d of 5 measurements and were analyzed using two-tailed unpaired Student's t-test. Statistically significant changes are indicated by ***P ≤ 0.001.*

4.2.4 CD8⁺ T cell activation is required for 3-IPA-mediated effect

Stemness markers CD62L, TCF1 and Slamf6 were robustly upregulated in all treatment experiments conducted (exemplarily Figure 4.6D-G). To further explore the requirements of the 3-IPA-mediated effect, P14 cells were cultured with or without 3-IPA and in the presence of IL-2 for 3 days before determining surface markers by flow cytometry. Compared to the previous experiments, cells were not activated with their cognate antigen GP33 (Figure 4.8A).

Unlike in previous experiments, T cell stemness markers CD62L and Slamf6 were not altered upon 3-IPA treatment (Figure 4.8 B and C), indicating the requirement of T cell activation for the 3-IPA-induced effect.

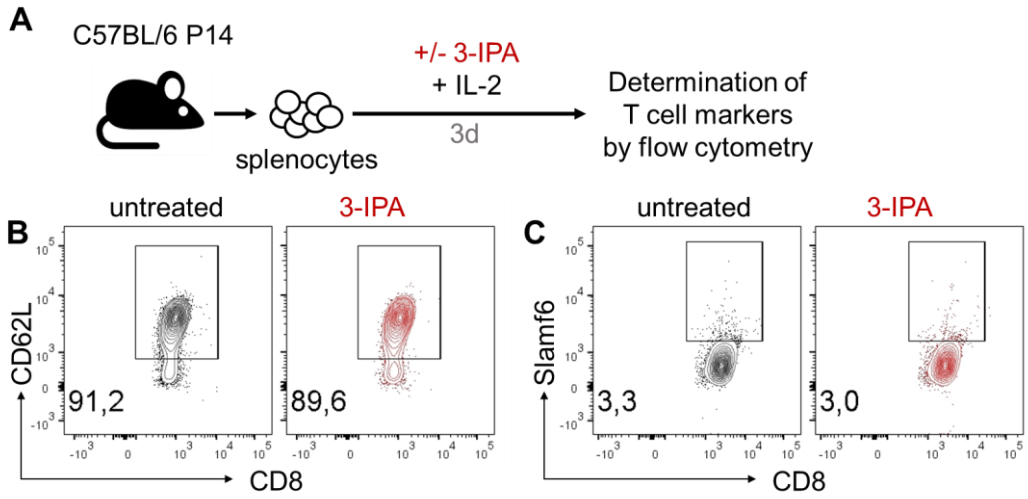

Figure 4.8. T cell activation is required for 3-IPA-mediated effect on CD8⁺ T cells. ***A****. Experimental setup. P14 splenocytes were cultivated with or without 3-IPA in the presence of IL-2, but without GP33 for 3 days. Surface markers of viable CD8⁺ T cells were analyzed by flow cytometry.* ***B****. Representative FACS plots of CD62L⁺ CD8⁺ T cells.* ***C****. Representative FACS plots of Slamf6⁺ CD8⁺ T cells.*

4.2.5 3-IPA reduces T cell exhaustion *in vitro*

Chronic antigen stimulation is the main driver of T cell exhaustion [95]. In the previous experiments, P14 cells were stimulated once with their cognate antigen, which resembles an acute infection. To mimic persistent antigen exposure as it is the case in chronic infection or cancer, the following experimental setup was used: P14 cells were cultured for 5 days with or without 3-IPA and in the presence of the homeostatic cytokines IL-7 and IL-15 (protocol adapted from [238]). Cells were repeatedly stimulated with their cognate antigen GP33 for five times in total and T cell markers were analyzed by flow cytometry a (Figure 4.9A).

After 5 days of repeated antigen stimulation, the survival rate of $CD8^+$ T cells was higher when treated with 3-IPA compared to untreated cells (Figure 4.9B). Chronic antigen stimulation of untreated cells resulted in equal percentages of stem-like TCF1-expressing and effector-like T-bet-expressing cells, while 3-IPA treatment shifted the ratio towards the side of stem-like TCF1-expressing $CD8^+$ T cells (Figure 4.9C). Co-expression of IRs is one of the main characteristics of T_{ex} [96]. Repeated GP33-treatment of untreated cells induced upregulation of the IRs PD-1 and TIGIT with a substantial proportion of $PD\text{-}1^+TIGIT^+$ co-expressing cells. Upon 3-IPA treatment, almost no $CD8^+$ T cells co-expressed PD-1 and TIGIT and the main proportion of cells lacked expression of any IRs (Figure 4.9D). Besides TCF1 as a stemness marker, expression of Slamf6 was investigated. While untreated chronically stimulated P14 cells lacked Slamf6 and upregulated TIGIT expression, 3-IPA-treated cells displayed a great proportion of $Slamf6^+$ $CD8^+$ T cells with very low TIGIT-expression (Figure 4.9E).

Terminally differentiated and exhausted $CD8^+$ T cells display superior cytotoxicity compared to progenitor stem cell-like T_{ex}, while progenitor T_{ex} exhibit cytokine polyfunctionality and long-term persistence [171]. Untreated P14 cells displayed a higher percentage of IFNγ- and TNFα-expressing cells compared to 3-IPA-treated cells, indicating a more cytotoxic phenotype. However, the proportion of IL-2-expressing cells among $IFN\gamma^+TNF\alpha^+$ $CD8^+$ T cells was significantly higher upon 3-IPA treatment, suggesting a more polyfunctional phenotype (Figure 4.9F).

Taken together, 3-IPA treatment increased $CD8^+$ T cell survival upon persistent antigen stimulation and viable $CD8^+$ T cells displayed higher expression of stemness markers TCF1 and Slamf6, while exhaustion markers PD-1 and TIGIT were decreased. Moreover, 3-IPA-treated cells exhibited lower cytotoxicity but higher cytokine polyfunctionality compared to untreated cells implying that 3-IPA treatment reduced T cell exhaustion *in vitro*.

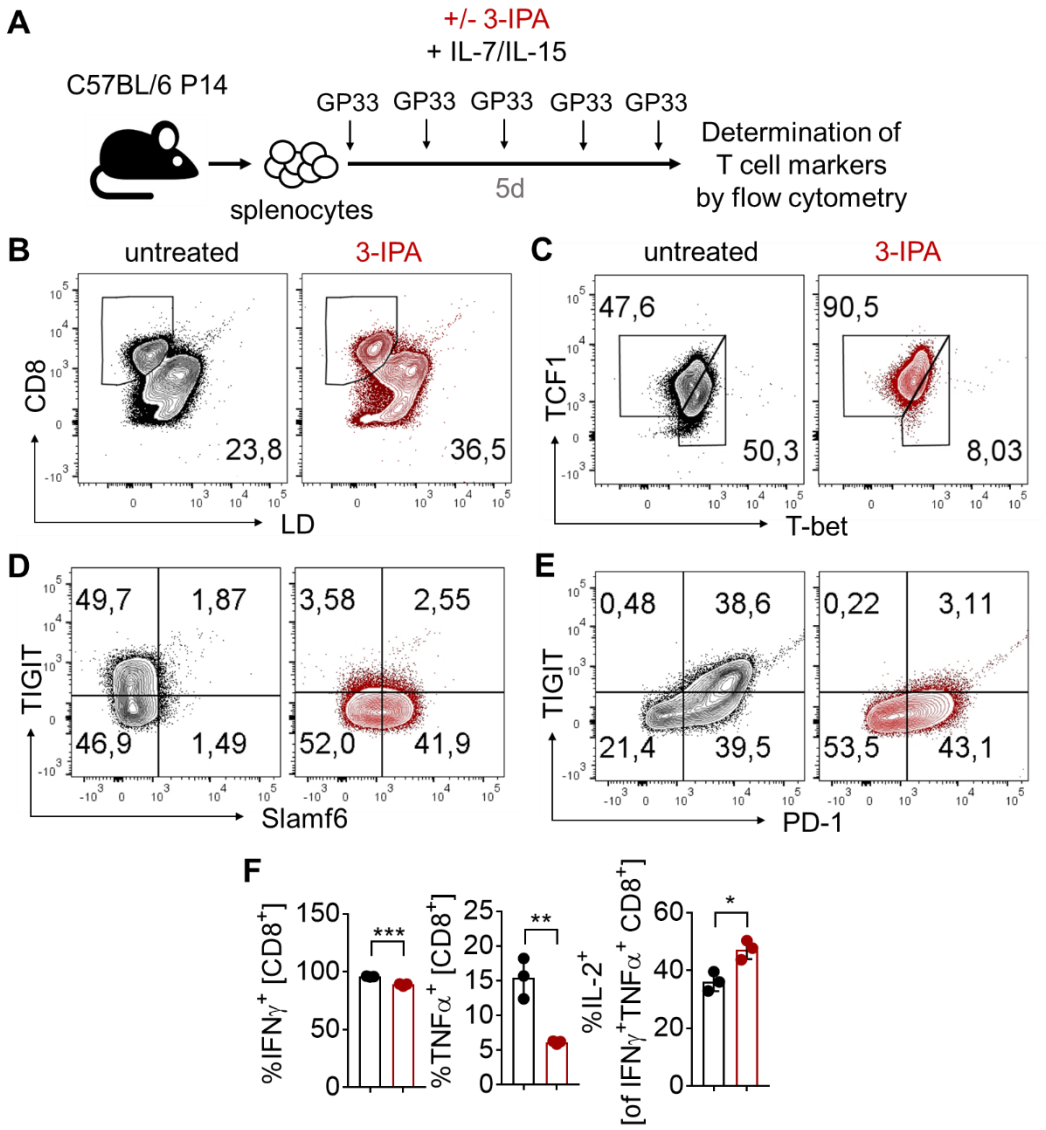

Figure 4.9. 3-IPA treatment prevents CD8⁺ T cells from exhaustion in vitro. A*. Experimental setup. P14 splenocytes were cultivated with or without 3-IPA in the presence of IL-7 and IL-15 for 5 days. Cells were repeatedly stimulated with GP33 every day. T cell markers were analyzed by flow cytometry.* ***B****. Representative FACS plots of viable CD8⁺ T cells (LD=live/dead).* ***C****. Representative FACS plots of TCF1⁺ and T-bet⁺ CD8⁺ T cells.* ***D****. Representative FACS plots of PD-1⁺ and TIGIT⁺ CD8⁺ T cells.* ***E****. Representative FACS plots of Slamf6⁺ and TIGIT⁺ CD8⁺ T cells.* ***F.*** *Quantification of cell ratios of cytokine-producing cells. Data are means ± s.d of 3 measurements and were analyzed using two-tailed unpaired Student's t-test. Statistically significant changes are indicated by *P ≤ 0.05, **P ≤ 0.01, ***P ≤ 0.001.*

4.3 3-IPA induces a stem-like CD8⁺ T cell phenotype of human PBMCs *in vitro*

All experiments shown so far were conducted using murine cells. Since the ultimate goal of translational biomedical research is to implement findings into clinical practice, it is crucial that observations made in animal experiments can be applied to the human situation.

To investigate if 3-IPA treatment is also effective on human CD8⁺ T cells, PBMCs were isolated from human buffy coat of nine different donors. Isolated PBMCs were cultured with or without 3-IPA for 4 days. Cells were activated using soluble anti-CD2/CD3/CD28 antibodies and re-stimulated after 2 days of culture. After 4 days, T cell markers were determined by flow cytometry (Figure 4.10A). Sex and age of the nine donors were identified after the experiment. Unfortunately, BMI of donors remained unknown.

As already observed in murine CD8⁺ T cells, MFI of CD8a of viable human CD8⁺ T cells was significantly increased upon 3-IPA treatment (Figure 4.10B). Furthermore, the percentages of both, TCF1- and CD62L-expressing CD8⁺ T cells were higher in PBMCs from most donors upon 3-IPA treatment compared to their untreated counterparts, resulting in a significant increase when taken all donors together (Figure 4.10C and D).

To conclude, similar to murine P14 cells, human CD8⁺ T cells significantly increased several stemness markers upon 3-IPA treatment.

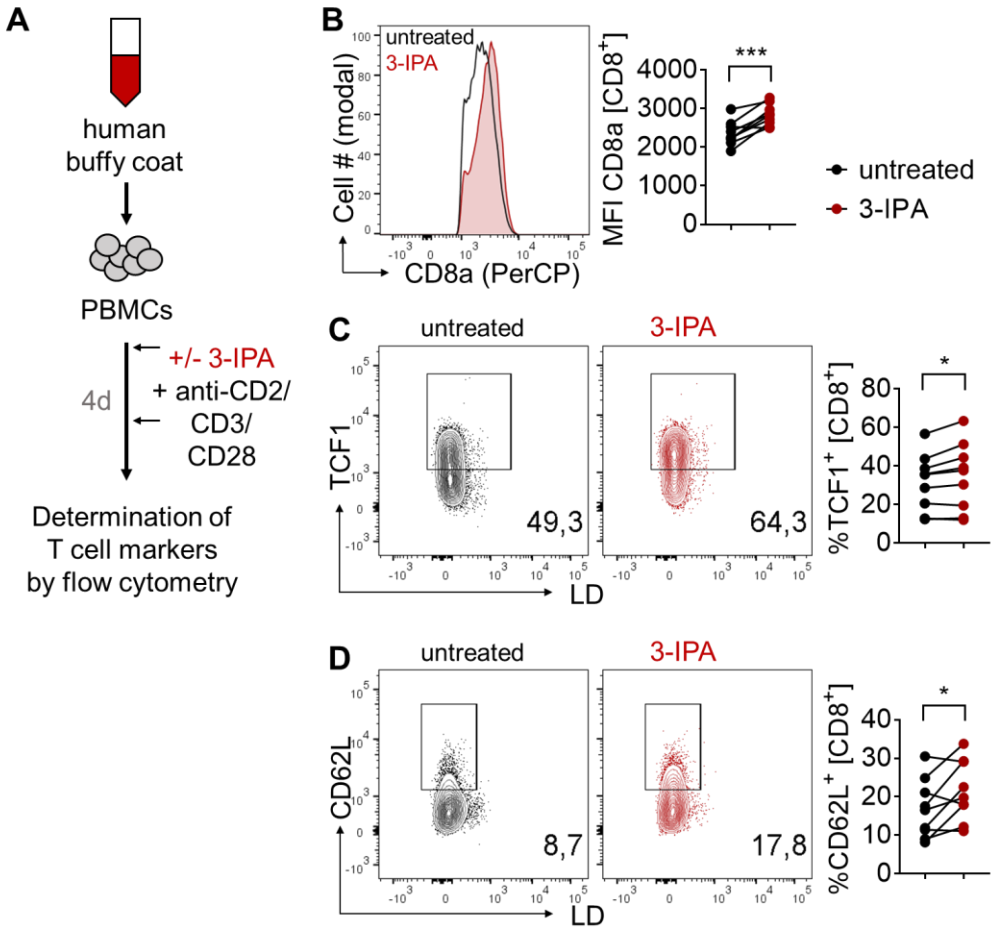

Figure 4.10. 3-IPA induces a stem-like CD8⁺ T cell phenotype of human PBMCs in vitro. ***A****. Experimental setup. PBMCs were isolated from human buffy coat and cultured with or without 3-IPA and in the presence of anti-CD2/3/28 for 4 days. Cells were restimulated at day 2.* ***B****. Representative MFI of CD8a in viable CD8⁺ T cells (left). Quantification of MFI values of CD8a without and with 3-IPA treatment (right).* ***C****. Representative FACS plots of TCF1⁺ CD8⁺ T cells (left). Quantification of cell ratios of TCF1⁺ CD8⁺ T cells without and with 3-IPA treatment (right).* ***D****. Representative FACS plots of CD62L⁺ CD8⁺ T cells (left). Quantification of cell ratios of CD62L⁺ CD8⁺ T cells without and with 3-IPA treatment (right). Data are means ± s.d of 9 measurements and were analyzed using two-tailed paired Student's t-test. Statistically significant changes are indicated by ns: not significant, *P ≤ 0.05, **P ≤ 0.01, ***P ≤ 0.001.*

4.4 3-IPA treatment doesn't improve anti-tumor immunity of CD8⁺ T cells

It has been shown by several groups that TCF1-expressing stem-like CD8⁺ T cells are the main players to sustain an immune response to chronic viral infections and are responsible for long-term tumor control and responsiveness towards ICB [165, 166, 168-172, 182, 239].

Having generated CD8⁺ T cells with a stem-like phenotype and increased TCF1 expression *in vitro*, their performance and the potential translational application of 3-IPA treatment was further investigated in the context of anti-tumor immunity.

Therefore, B16 melanoma cells, expressing the epitopes GP_{33-41} (referred to as B16-gp33) were implanted to CD90.2 (Thy1.2) congenically marked C57BL/6 mice. Six days after tumor implantation, CD90.1 (Thy1.1) congenically marked P14 splenocytes were isolated and cultured for 3 days with or without 3-IPA in the presence of GP33 and IL-2. Nine days after tumor implantation, *in vitro* activated 3-IPA-treated and control P14 cells were adoptively transferred to tumor-bearing mice and acceptor mice were vaccinated (GP33 peptide plus poly(I:C), [172]). Expression of GP33 on the surface of B16-gp33 tumor cells allows their recognition by P14 cells. Tumor growth was monitored regularly and 20 days after tumor implantation, tumor-bearing mice were sacrificed. Splenocytes and TILs were isolated and P14 donor cells (identified by Thy1.1) were analyzed by flow cytometry (experimental setup depicted in Figure 4.11A).

To ensure effectiveness of 3-IPA treatment, P14 donor cells were analyzed by flow cytometry after 3 days of activation and treatment shortly before adoptive transfer to tumor-bearing mice. As expected, 3-IPA-treated P14 cells displayed higher TCF1 and CD62L expression compared to untreated cells (Figure 4.11B). The same numbers of 3-IPA-treated and untreated donor cells were transferred to tumor-bearing mice and tumor growth was monitored. Despite higher TCF1 expression prior adoptive transfer, there was no significant difference in tumor growth in acceptor mice which received either 3-IPA-treated or untreated P14 cells (Figure 4.11C). Flow cytometry analysis of Thy1.1 P14 donor cells showed no

difference of the percentage of donor cells among other lymphocytes in spleen and tumor between 3-IPA-treated and untreated cells. When analyzing the donor cells further, there was no difference in CD44, CD62L, TCF1 and IFNγ expression between the two groups neither in spleen nor in tumors. The only marker that was significantly increased in 3-IPA-treated donor cells in the spleen was the proliferation marker Ki67 [240]. This increase, however, was lost in the tumor (Figure 4.11D).

In summary, despite an effective treatment of donor cells with 3-IPA and increased expression of TCF1 at the time point of adoptive transfer, they were not able to exert a superior anti-tumor immune response and T cell markers of recovered donor cells were not altered in 3-IPA-treated compared to untreated cells. Proliferation marker Ki67 was significantly increased in 3-IPA-treated P14 cells recovered from spleen, but not in donor TILs.

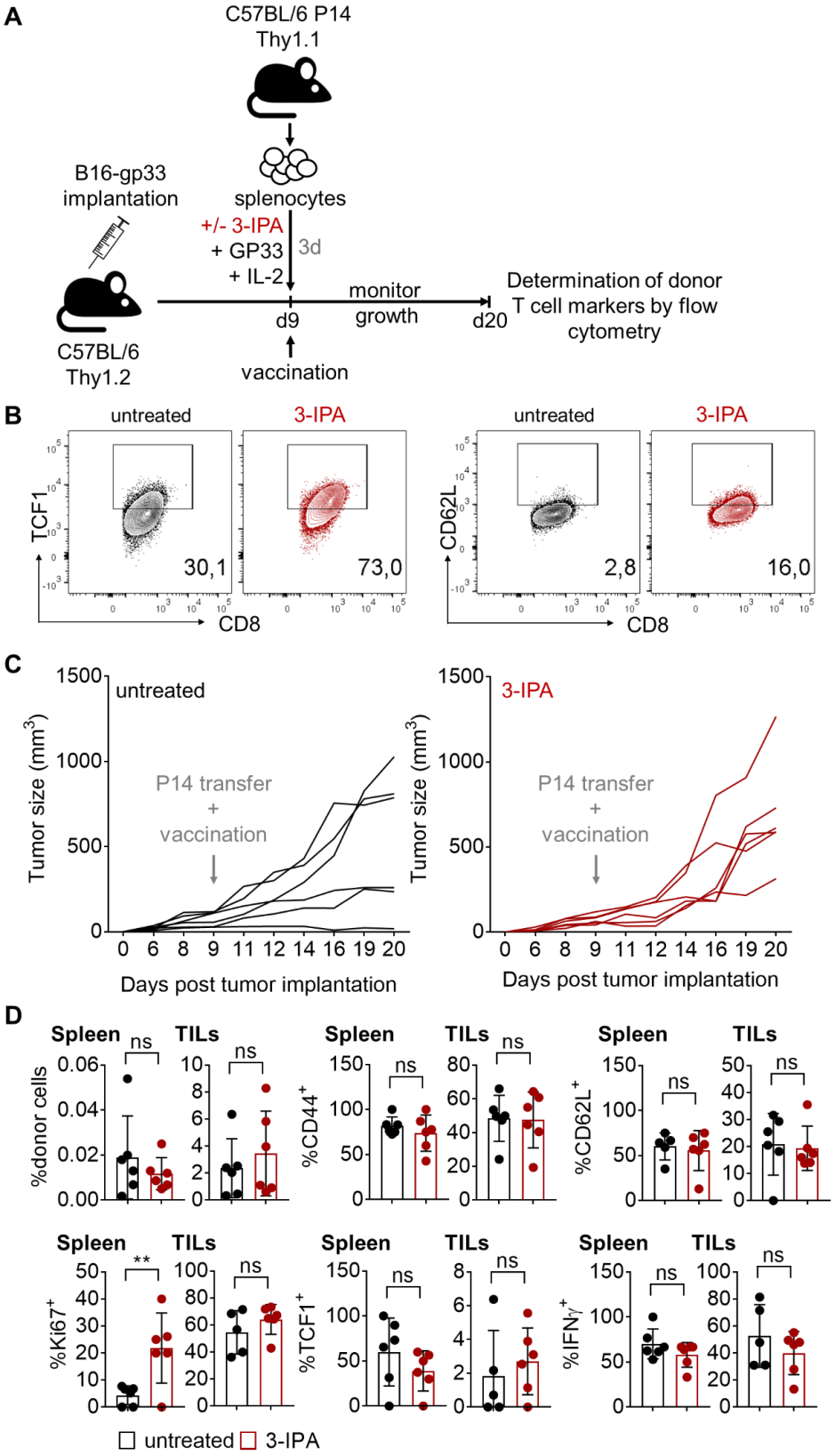

Figure 4.11. 3-IPA treatment of tumor-specific CD8⁺ T cells doesn't improve their anti-tumor function. A*. Schematic depiction of experimental approach of B16-gp33-tumor implantation, donor cell treatment and adoptive transfer.* ***B****. Representative FACS plots of TCF1⁺ (left) and CD62L⁺ (right) CD8⁺ donor T cells before adoptive transfer.* ***C****. Tumor growth of B16-gp33 melanoma cells of mice receiving untreated (black) or 3-IPA-treated (red) P14 cells.* ***D****. Quantification of cell ratios of selected T cell markers of recovered donor cells from spleen and tumor (TILs). Statistically significant changes are indicated by ns: not significant, **P ≤ 0.01.*

4.5 3-IPA treatment rescues anti-viral CD8$^+$ T cell functions

4.5.1 3-IPA treatment rescues mitochondrially impaired anti-viral CD8$^+$ T cell functions

Mitochondrial integrity of cells is essential to sustain metabolic fitness to further ensure cell functionality. Mitochondrial fusion and biogenesis take place to adapt to metabolic demands [241]. During this process, damaged mitochondria are removed by mitophagy. Impaired mitophagy leads to accumulation of dysfunctional mitochondria with high mitochondrial mass, but low mitochondrial membrane potential, a mitochondrial phenotype observed in aged cells [242].

Staining with MitoTracker Green (MG) allows examination of the mitochondrial mass while staining with MitoTracker Deep Red (MDR) can be used to investigate the membrane potential. The ratio of MDR to MG is an indicator of mitochondrial activity per mitochondrial mass [243]. By collective staining of MDR and MG, two distinct populations can be identified, namely MDR/MG^{high} and MDR/MG^{low} cells. MDR/MG^{high} cells are metabolically fit, while MDR/MG^{low} cells represent metabolically impaired CD8$^+$ T cells (Figure 4.12B) [114].

Having found that 3-IPA treatment of antigen-specific CD8$^+$ T cells increases SRC (Figure 4.7C), 3-IPA treatment was further investigated in its therapeutical application towards mitochondrially impaired CD8$^+$ T cells. Therefore, Thy1.1 congenically marked P14 cells were *in vitro* activated with GP33 and IL-2 and cultured with or without 3-IPA for 3 days. Subsequently, cells were treated with a combination of electron transport chain complex V inhibitor oligomycin and the mitophagy inhibitor Mdivi-1 for 6 h in order to induce MDR/MG^{low} , “exhausted” cells [114]. Cells were subsequently adoptively transferred to Thy1.2 congenically marked C57BL/6 acceptor mice and mice were infected with LCMV Arm the same day. Eight days after infection, acceptor mice were sacrificed and donor cells were analyzed by flow cytometry (experimental setup see Figure 4.12A).

Donor cells were analyzed after treatment with Mdivi-1/oligomycin prior adoptive transfer to acceptor mice. While “healthy” cells, which have not been treated with Mdivi-1/oligomycin, displayed almost no MDR/MG^{low} cells, “exhausted” Mdivi-1/oligomycin-treated donor cells showed a much higher percentage of mitochondrially impaired cells. Pre-treatment with 3-IPA (“exhausted”+3-IPA) could rescue a great proportion of cells from mitochondrial dysfunction (Figure 4.12C). Subsequently, equal numbers of viable cells were adoptively transferred to LCMV Arm infected acceptor mice

After 8 days, donor cells were recovered and analyzed by flow cytometry. The percentage and total number of *in vitro* exhausted donor cells among all lymphocytes was significantly

decreased compared to healthy, untreated cells, indicating decreased survival capacity. This phenotype was rescued by pre-treatment with 3-IPA (Figure 4.12D and E). Analyzing the recovered donor cells in more detail, *in vitro* exhausted P14 cells displayed a significantly higher proportion of PD-1 and TIGIT-expressing cells. This percentage was decreased to the level of untreated donor cells by 3-IPA pre-treatment (Figure 4.12F). Furthermore, the total number of recovered IFNγ- and TNFα-expressing donor cells was significantly lower in mice, which received the *in vitro* exhausted donor cells compared to the groups receiving untreated, healthy donor cells as well as 3-IPA-treated exhausted cells (Figure 4.12G).

To sum up, treatment with Mdivi-1/oligomycin *in vitro* induced an “exhausted” phenotype, represented by a substantial increase of MDR/MG^{low} cells. The percentage of *in vitro* exhausted CD8^{+} T cells could be lowered by pre-treatment with 3-IPA. Furthermore, 3-IPA pre-treatment of donor cells could rescue the survival capacity and anti-viral functions of mitochondrially impaired donor cells *in vivo*.

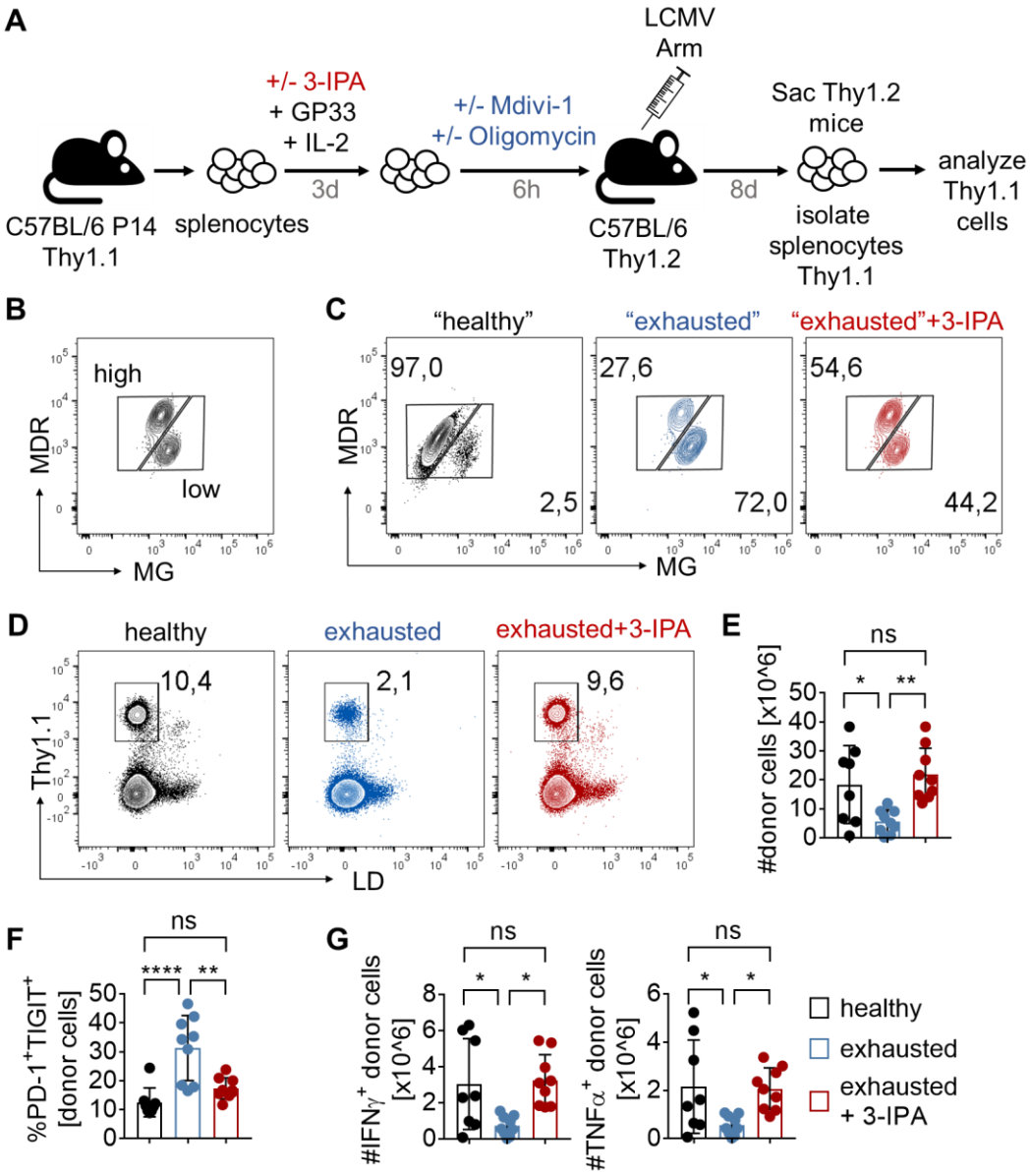

Figure 4.12. 3-IPA treatment rescues mitochondrially impaired anti-viral CD8⁺ T cell functions. ***A****. Schematic depiction of experimental approach of donor cell treatment and adoptive transfer to LCMV Arm-infected acceptor mice.* ***B****. Exemplary FACS plot of two distinct CD8⁺ T cells populations (high and low) based on the ratio of MDR to MG.* ***C****. Representative FACS plots of MDR/MG high and low CD8⁺ T cells before adoptive transfer. "healthy" = untreated cells, "exhausted" = cells which received only Mdivi-1/Oligomycin treatment, "exhausted"+3-IPA = cells which received 3-IPA + Mdivi-1/Oligomycin treatment* ***D****. Representative FACS plots of recovered donor cell percentages among total lymphocytes.* ***E****. Quantification of donor cell numbers.* ***F****. Quantification of cell ratios of recovered PD-1⁺TIGIT⁺ CD8⁺ donor T cells.* ***G****. Quantification of numbers of recovered cytokine-expressing donor cells. Data are means ± s.d. of 8 measurements and were analyzed by one-way ANOVA. Statistically significant changes are indicated by ns: not significant, *P ≤ 0.05, **P ≤ 0.01, ***P ≤ 0.001, ****P ≤ 0.0001.*

4.5.2 3-IPA treatment partially reinvigorates tumor-exhausted anti-viral CD8$^+$ T cell functions

Having shown that 3-IPA treatment could rescue an exhaustion phenotype generated *in vitro*, in a next step 3-IPA treatment was investigated in the context of *in vivo* exhaustion.

In order to generate antigen-specific T_{ex} *in vivo*, Thy1.2 acceptor mice were implanted with B16-gp33 melanoma cells. Thy1.1 congenically marked P14 donor cells were *in vitro* activated with GP33 and IL-2 for 3 days and adoptively transferred to tumor-bearing mice 15 days after tumor implantation. Nine days later, tumor-bearing mice were sacrificed and donor Thy1.1 TILs were sorted in stem cell-like TILs (T_{stem}) and T_{ex} according to the surface markers Slamf6 and Tim-3 [171] (Figure 4.13B). Sorted cells were cultivated for 3 days in the presence of GP33, IL-2 and with or without 3-IPA. Activated Thy1.1 P14 were then adoptively transferred to a new batch of Thy1.2 acceptor mice and mice were infected with LCMV Arm. Eight days after infection, acceptor mice were sacrificed and Thy1.1 donor splenocytes analyzed by flow cytometry (experimental setup see Figure 4.13A).

After culturing sorted donor TILs with or without 3-IPA for 3 days, T_{stem}, T_{ex} and T_{ex} treated with 3-IPA were analyzed by flow cytometry. T_{stem} displayed higher TCF1 expression compared to T_{ex} and 3-IPA-treated T_{ex} (T_{ex}+3-IPA). 3-IPA treatment did not increase TCF1 expression of T_{ex}. Furthermore, T_{ex} expressed highest levels of the exhaustion marker Tim-3, while T_{stem} displayed the lowest levels. T_{ex}+3-IPA showed higher levels of Tim-3 compared to T_{stem}, but decreased levels compared to untreated T_{ex} (Figure 4.13C).

Equal numbers of T_{stem}, T_{ex} and T_{ex}+3-IPA were adoptively transferred to LCMV Arm-infected Thy1.2 mice and donor cells were recovered 8 days after infection. The proportion of donor cells among all lymphocytes as well as total numbers were significantly lower in mice who received T_{ex} cells compared to T_{stem} cells, confirming the better survival capacity of T_{stem}. 3-IPA treatment increased the proportion of T_{ex} donor cells among other lymphocytes, however not total numbers. Numbers of stem cell-like CD62L$^+$TCF1$^+$ donor cells were decreased in the T_{ex} compared to the T_{stem} group and this phenotype could be reversed by 3-IPA treatment. Moreover, the number of cytokine-producing donor cells was lower in the T_{ex} compared to the T_{stem} group. This phenotype, however, was not rescued upon 3-IPA treatment (Figure 4.13D).

In summary, 3-IPA treatment of *in vivo* T_{ex} didn't increase their TCF1 expression, but slightly decreased expression of Tim-3. While adoptively transferred antigen-specific T_{stem} were recovered in highest numbers, this number was significantly lower in T_{ex} and could not be rescued by 3-IPA treatment. While the number of stem cell-like donor cells was significantly increased in T_{ex}+3-IPA compared to their untreated counterparts, cytokine production could

not be rescued upon treatment and therefore 3-IPA treatment of *in vivo* T_{ex} could only partially reinvigorate the T_{stem} phenotype.

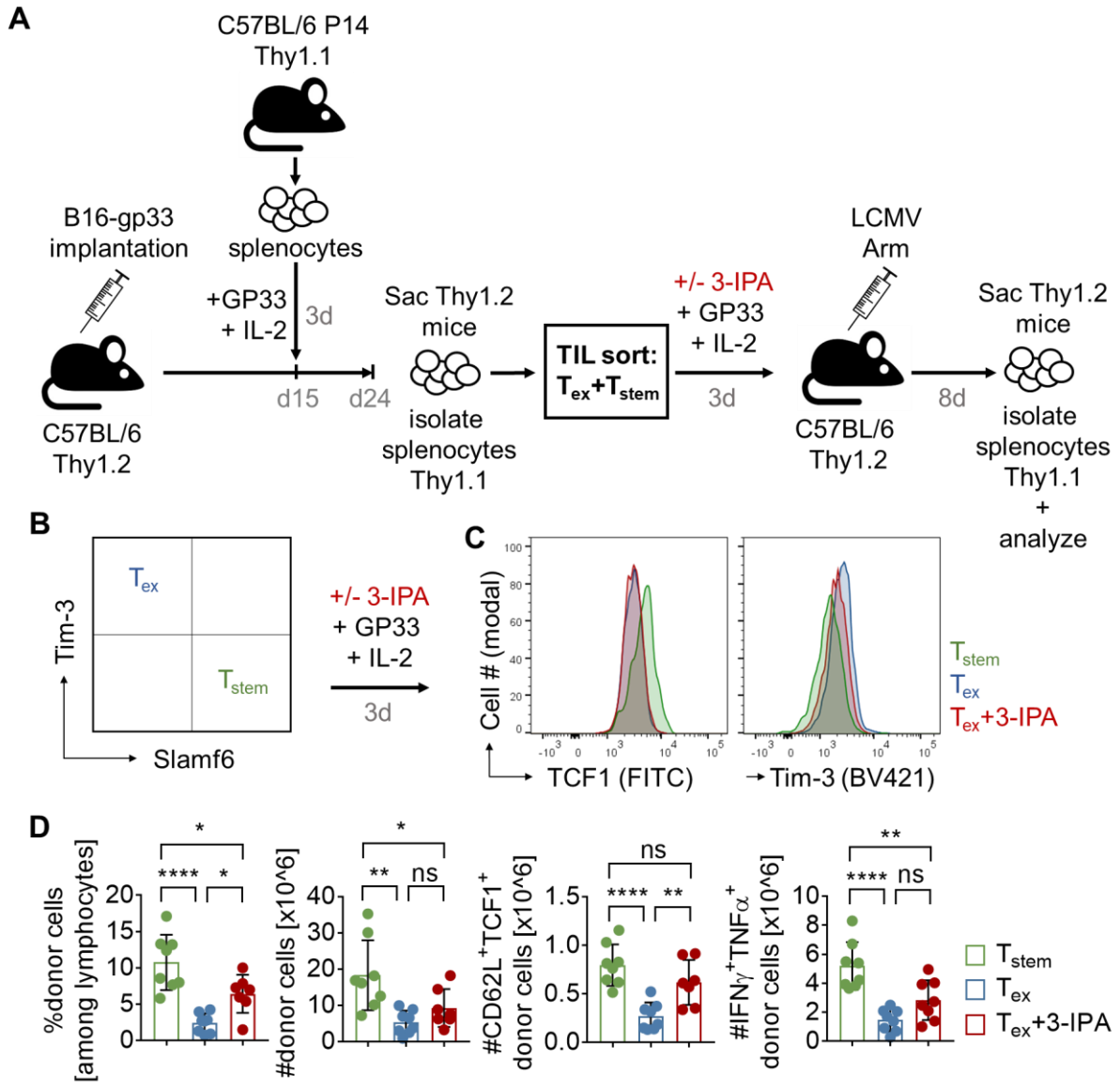

Figure 4.13. 3-IPA treatment partially reinvigorates tumor-exhausted anti-viral CD8⁺ T cell functions. ***A***. *Schematic depiction of experimental approach of adoptive transfer of P14 donor cells to B16-gp33-tumor-bearing mice followed by TIL isolation, donor cell sort, donor cell treatment and re-transfer to LCMV Arm-infected acceptor mice.* ***B***. *Exemplary FACS plot of sorting into T_{ex} and T_{stem} based on Slamf6 and Tim-3 expression.* ***C***. *Representative MFI of TCF1 (left) and Tim-3 (right) of sorted TILs before adoptive transfer.* ***D***. *Quantification of donor cell ratios and numbers, of CD62L⁺TCF1⁺ and cytokine-producing donor cells. Data are means ± s.d. of 8 measurements and were analyzed by one-way ANOVA. Statistically significant changes are indicated by ns: not significant, *P ≤ 0.05, **P ≤ 0.01, ***P ≤ 0.001, ****P ≤ 0.0001.*

4.5.3 3-IPA treatment rescues aging- and obesity-impaired anti-viral CD8$^+$ T cell functions

Aging and obesity are both well-known factors for increased susceptibility towards infectious diseases [9, 19] as well as decreased vaccination efficacy [201, 218]. To investigate the potential therapeutic effect of 3-IPA treatment to overcome those defects, the following experiment was set up: CD45.1 (Ly5.1) congenically marked splenocytes from YL and AO P14 mice were isolated and cultured for 3 days in the presence of GP33 and IL-2. Half of the AO cells were additionally treated with 3-IPA. Activated donor cells were adoptively transferred to CD45.2 (Ly5.2) acceptor mice, which were infected with LCMV Arm the same day. After 30 days, in the phase of memory formation, acceptor mice were sacrificed and Ly5.1 donor cells recovered from the spleen. Equal numbers of recovered Ly5.1 donor cells were adoptively transferred to a new batch of Ly5.2 acceptor mice, which were infected with LCMV cl13 the same day, in order to induce a recall response. Eight days after infection, acceptor mice were sacrificed and Ly5.1 donor cells analyzed by flow cytometry (experimental setup see Figure 4.14A).

Stemness markers TCF1 and CD62L of naïve YL and AO donor cells were analyzed directly after isolation. While almost all CD8$^+$ donor cells of YL mice were double-positive for CD62L and TCF1, this percentage was significantly decreased in donor cells of AO mice, confirming the reduction of stem cell-like CD8$^+$ T cells by aging and obesity (Figure 4.14B).

After *in vitro* activating and culturing the P14 donor cells with or without 3-IPA for 3 days, equal cell numbers were adoptively transferred to naïve Ly5.2 acceptor mice, which were infected with LCMV Arm the same day. After 30 days, acceptor mice were sacrificed and Ly5.1 cells were recovered from the spleen. There was no difference in ratio and cell numbers of recovered donor cells between the three groups (Figure 4.14C). However, MFI of CD8a of AO donor cells was significantly lower compared to YL cells and this was rescued by 3-IPA treatment (Figure 4.14D). Furthermore, analysis of CD62L and TCF1 expression of donor cells revealed decreased ratios of CD62L$^+$TCF1$^+$ double-positive stem-like cells in the AO donor cell group compared to YL donor cells, while this phenotype was also rescued by 3-IPA treatment (Figure 4.14E). Furthermore, the ratio of AO long-lived T_{cm} was lower compared to YL and 3-IPA-treated donor cells, while the percentage of more differentiated T_{em} cells was higher (Figure 4.14F).

Equal numbers of recovered donor cells from all three groups were transferred to a new batch of congenically marked Ly5.2 acceptor mice, which were infected with LCMV cl13 in order to induce a recall response. Acceptor mice were sacrificed 8 days after infection, the

time point of peak response, and Ly5.1 donor cells from the three different groups were analyzed by flow cytometry.

While there was no difference in donor cell ratio and numbers after primary infection (Figure 4.14C), upon recall infection, however, significantly reduced ratios and numbers of AO cells were recovered compared to the YL group. This could be rescued by 3-IPA pre-treatment (Figure 4.14G) and is in concordance with increased T_{cm} ratios in YL and 3-IPA-treated AO cells after primary infection (Figure 4.14F). As observed already after primary infection, MFI of CD8a of AO donor cells was significantly lower compared to YL and 3-IPA-treated AO cells after secondary infection (Figure 4.14H). Furthermore, the ratio of $TCF1^+$ donor cells, marking stem-like cells, was significantly lower in AO cells compared to YL and 3-IPA-treated AO cells, even at the effector time point (Figure 4.14I). At the same time, percentage and number of IFNγ- and TNFα-expressing effector cells were significantly lowered by aging and obesity and this could be rescued by pre-treatment with 3-IPA back to the level of YL cells (Figure 4.14J).

To sum up, the proportion of stem-like $CD8^+$ T cells in the spleen was higher in YL compared to AO mice. After *in vitro* activation and treatment, and adoptive transfer to LCMV Arm-infected mice, equal numbers of YL, AO and 3-IPA-treated AO donor cells were recovered in the memory phase. However, AO cells displayed reduced ratios of stem-like memory cells compared to YL donor and this phenotype was rescued by 3-IPA treatment. This is reflected by decreased AO cell numbers and functionality of AO compared to YL and 3-IPA-treated AO donor cells upon recall infection, indicating that 3-IPA treatment can rescue aging- and obesity-impaired anti-viral $CD8^+$ T cell functions and memory formation *in vivo*.

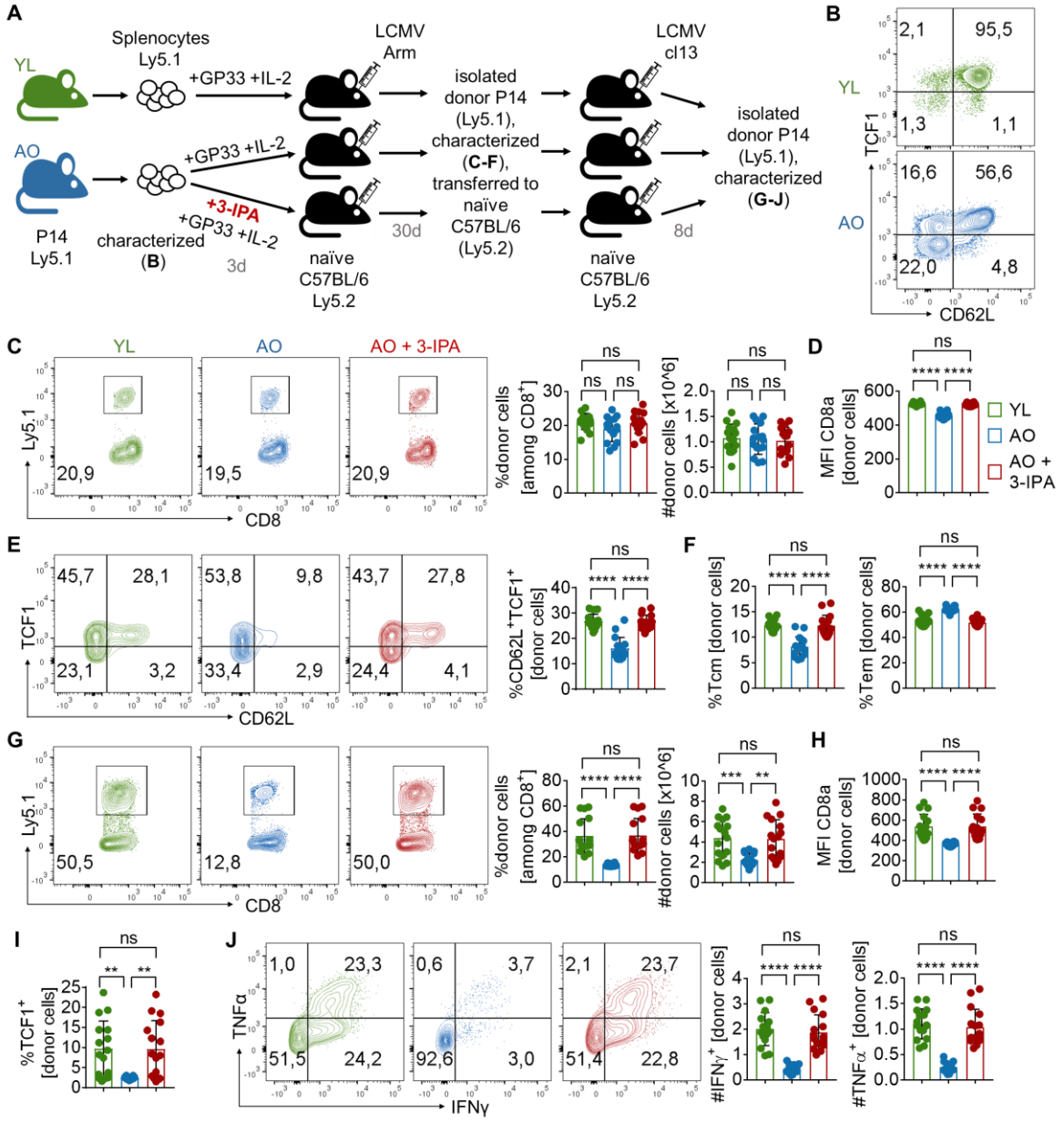

Figure 4.14. 3-IPA treatment rescues aging- and obesity-impaired anti-viral CD8⁺ T cell functions. ***A****. Schematic depiction of experimental approach of YL and AO donor cell treatment, two serial adoptive transfers and infections.* ***B****. Representative FACS plots of TCF1 and CD62L expression of YL (top) and AO (bottom) donor P14 cells directly after isolation.* ***C****. Representative FACS plots of recovered donor cells among viable CD8⁺ T cells (left), quantification of recovered donor cell ratios (middle) and numbers of total donor cell numbers (right) after first adoptive transfer and infection.* ***D****. Quantification of MFI values of CD8a of donor cells after first infection.* ***E****. Representative FACS plots of CD62L and TCF1 expression (left) and quantification of CD62L⁺TCF1⁺ donor cell ratios after first infection (right).* ***F****. Quantification of T_{cm} and T_{em} ratios after first infection.* ***G****. Representative FACS plots of recovered donor cells among viable CD8⁺ T cells (left), quantification of recovered donor cell ratios (middle) and numbers of total donor cell numbers (right) after second adoptive transfer and infection.* ***H****. Quantification of MFI values of CD8a of donor cells after second infection.* ***I****. Quantification of TCF1⁺ donor cell ratios after second infection.* ***J****. Representative FACS plots of IFNγ and TNFα expression (left) and quantification of IFNγ- (middle) and TNFα-expressing donor cell numbers (right) after second infection. Data are means ± s.d. of 16 measurements and were analyzed by one-way ANOVA. Statistically significant changes are indicated by ns: not significant, **P ≤ 0.01, ***P ≤ 0.001, ****P ≤ 0.0001.*

4.6 Elucidating the mechanism of 3-IPA in CD8$^+$ T cells

3-IPA treatment of CD8$^+$ T cells induced a stem cell-like phenotype *in vitro*, altered their metabolic profile and rescued aging- and obesity-impaired anti-viral CD8$^+$ T cell functions and memory formation *in vivo*. To elucidate the mechanism how 3-IPA acts on CD8$^+$ T cells, several approaches were chosen.

4.6.1 AhR or Foxo1 are dispensable for the 3-IPA-induced effect

Tryptophan can be metabolized by gut microbiota into several molecules, which are well known ligands of the aryl hydrocarbon receptor (AhR) [244]. The AhR is a cytosolic ligand-activated TF that has been reported to modulate both CD4$^+$ and CD8$^+$ T cell functions [245]. Therefore, AhR was investigated as a potential mediator for the 3-IPA-induced effects on CD8$^+$ T cells.

Another protein that was considered to be involved in mediating the effect of 3-IPA on CD8$^+$ T cells is the TF Foxo1. Foxo1 has been described to play a central role in CD8$^+$ T cell memory formation and *Tcf7* has been reported to be a target of Foxo1. Furthermore, lack of Foxo1 in activated CD8$^+$ T cells resulted in deficient recall, but not primary responses to infection [246], similar to the results reported in chapter 4.5.3.

Antigen-specific CD8$^+$ T cells lacking either AhR or Foxo1 (KO) and their wildtype (WT) counterpart were cultured for 3 days with or without 3-IPA and in the presence of their specific antigen peptide. 3-IPA-inducible markers TCF1 and CD62L were investigated by flow cytometry in order to test whether a lack of either protein abolishes the 3-IPA-induced effect.

Untreated AhR WT and KO CD8$^+$ T cells displayed similar percentages of CD62L- and TCF1-expressing CD8$^+$ T cells. 3-IPA treatment of both, AhR KO and WT CD8$^+$ T cells resulted in upregulation of CD62L and TCF1. The proportion of CD62L$^+$TCF1$^+$ double-positive cells was even higher in AhR KO than in WT cells, indicating that the 3-IPA-induced upregulation of stemness markers in CD8$^+$ T cells is not mediated by AhR (Figure 4.15A).

Untreated Foxo1 KO cells displayed lower proportions of CD62L- and especially TCF1-expressing cells compared to untreated WT cells. When treated with 3-IPA, both Foxo1 KO and WT cells upregulated CD62L and TCF1. While the proportion of CD62L$^+$TCF1$^+$ CD8$^+$ T cells was still much higher in WT compared to KO cells, upregulation of the two stemness markers in Foxo1 KO cells upon 3-IPA treatment was still very clear and therefore, also Foxo1 was determined to not be essential for the 3-IPA-induced effect on CD8$^+$ T cells (Figure 4.15B).

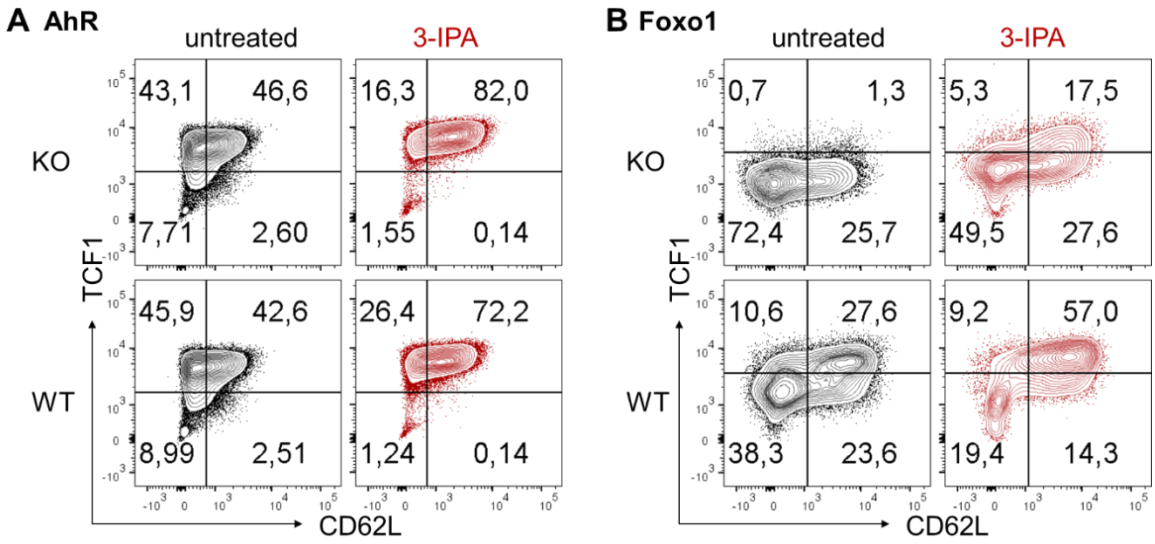

Figure 4.15. The effect of 3-IPA on CD8⁺ T cells is not mediated by AhR or Foxo1. A*. AhR KO and WT OT-I splenocytes were cultivated with or without 3-IPA in the presence of IL-2 and their cognate antigen peptide SIINFEKEL for 3 days. T cell markers were analyzed by flow cytometry. Representative FACS plots of TCF1 and CD62L expression of KO and WT cells with and without 3-IPA treatment.* ***B****. Foxo1 KO and WT P14 splenocytes were cultivated with or without 3-IPA in the presence of IL-2 and GP33 for 3 days. T cell markers were analyzed by flow cytometry. Representative FACS plots of TCF1 and CD62L expression of KO and WT cells with and without 3-IPA treatment.*

4.6.2 Identification of structural properties essential for biological activity of 3-IPA

3-IPA, but not the other tested metabolites from the mass spectrometry analysis induced changes in CD8⁺ T cell marker expression (Figure 4.4). Besides 3-IPA, the gut microbiome can metabolize dietary tryptophan into structurally similar metabolites such as trans-indole-3-acrylic acid or indole-3-acetic acid [247]. In addition to bacterial synthesized molecules, other structurally very similar molecules exist and some are even endogenously produced, such as the well-known molecules melatonin and serotonin. To test, whether the effect of 3-IPA treatment on CD8⁺ T cells is specific for this molecule, 11 additional structurally similar molecules were tested on CD8⁺ T cells (metabolite 1-11, chemical name and molecular structures depicted in Supplementary Figure 1).

Using the experimental setup described in Figure 4.4A, P14 cells were treated with 3-IPA and the 11 chosen molecules in five different concentrations ranging from 10-100 µM for 3 days and stemness markers CD62L and TCF1 were analyzed by flow cytometry. Results are summarized in heatmaps showing MFIs of the two analyzed markers as fold change compared to the untreated control (Figure 4.16A and B).

As observed before, 3-IPA treatment induced upregulation of the homing receptor CD62L in a dose-dependent manner from 50 µM on. A similar increase in CD62L expression was

observed after treatment with metabolites 3 and 11. Metabolite 8 slightly increased CD62L MFI only in the highest tested concentration of 100 µM (Figure 4.16A).

A similar pattern was observed for TCF1 expression after treatment. While 3-IPA and metabolite 11 induced TCF1 upregulation in concentrations from 50 µM on, metabolite 3 was even more potent in inducing TCF1 expression since upregulation was observed starting at concentrations of 25 µM and the fold change of MFI TCF1 at 100 µM was higher compared to 3-IPA and metabolite 11 (Figure 4.16B).

Therefore, besides 3-IPA, trans-indole-3-acrylic acid (metabolite 3) and the screening compound $C_{15}H_{20}N2_O$ (metabolite 11) were found to be potent modulators of $CD8^+$ T cell markers (Figure 4.16C).

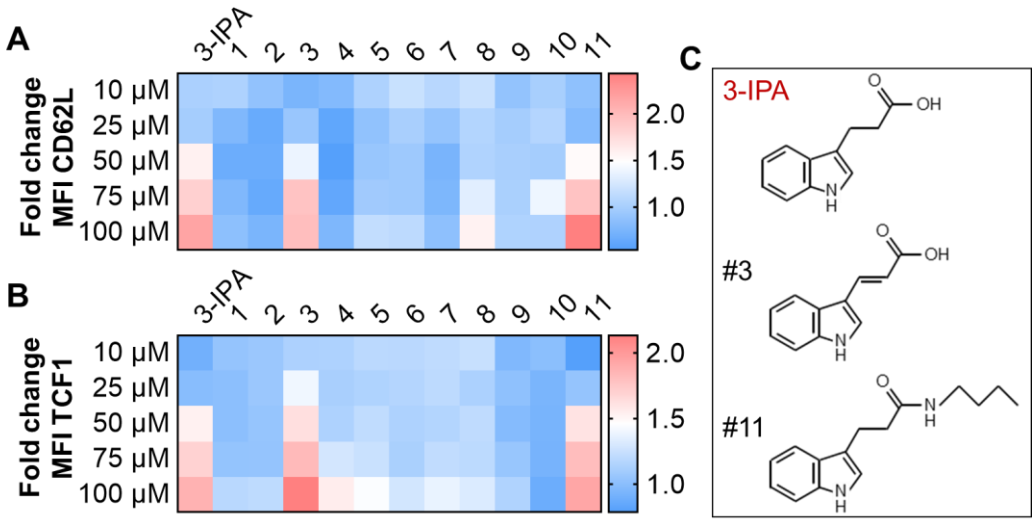

Figure 4.16. Identification of chemical properties essential for 3-IPA-mediated effect. *P14 splenocytes were activated in vitro with GP33 and IL-2 and treated with 3-IPA and structurally similar molecules (here named #1 - #11) in different concentrations. T cell markers were analyzed by flow cytometry.* ***A****. Heatmap displaying the fold change of MFI CD62L after treatment with different metabolites in various concentrations compared to the untreated control.* ***B****. Heatmap displaying the fold change of MFI TCF1 after treatment with different metabolites in various concentrations compared to the untreated control.* ***C****. Chemical structures of effective molecules 3-IPA, #3 (trans-indole-3-acrylic acid), #11 (Screening Compound ($C_{15}H_{20}N_2O$)).*

The chemical structures of the biological potent molecules 3-IPA, trans-indole-3-acrylic acid (metabolite 3) and the screening compound $C_{15}H_{20}N2_O$ (metabolite 11) (Figure 4.16C) were compared to the other tested, non-functional molecules (Supplementary Figure 1). For the biological potency to influence $CD8^+$ T cell marker expression, compounds seem to require an indole molecule that carries a rest at C3, but not on any other C atom. Furthermore, the rest on C3 consisting of two C atoms followed by either a carboxyl group (3-IPA, metabolite 3) or an amide bond (metabolite 11) seems to be necessary.

4.6.3 Identification of potential 3-IPA binding partners

Having identified structural properties essential for the biological activity of 3-IPA and similar compounds on $CD8^+$ T cells, in a next step, this knowledge was applied to identify potential 3-IPA binding partners. With the help of Dr Aubry Miller (Research Group Cancer Drug Development, DKFZ, Heidelberg), a new compound was designed and synthesized by linking 3-IPA to biotin-PEG3-Amine (Figure 4.17B, orange box).

The biological activity of this newly synthesized compound was confirmed by *in vitro* activating and treating P14 cells with either the newly synthesized 3-IPA-Biotin-PEG3-Amine, 3-IPA as a positive control or Biotin-PEG3-Amine and DMSO as negative controls. When treated in concentrations of 125 µM, both 3-IPA and 3-IPA-Biotin-PEG3-Amine treatment resulted in an increase of TCF1 expression, while Biotin-PEG3-Amine alone did not alter TCF1 expression compared to the DMSO control (Figure 4.17A). Therefore, the biological activity of the newly synthesized 3-IPA-Biotin-PEG3-Amine was confirmed and the compound was used for further experiments.

To identify proteins that interact with 3-IPA and are potentially responsible for mediation of its biological activity, the workflow depicted in Figure 4.17B was followed: P14 splenocytes were *in vitro* activated for 3 days as described before. Afterwards, cells were lysed and lysates incubated with 3-IPA-Biotin-PEG3-Amine or Biotin-PEG3-Amine for 2 h. Immunoprecipitation (IP) was performed using magnetic streptavidin beads and eluates sent to the EMBL Proteomics Core Facility for mass spectrometry and subsequent analysis (Figure 4.17B). Differential expression was analyzed using the Limma software package. A protein is considered a ‘hit’, if the false discovery rate is smaller 0.05 and a fold change of at least 2-fold is observed.

Out of 2486 investigated proteins, only six were identified as hits, which are encoded by the genes *Jup*, *Dsp*, *Lmna*, *Ide*, *Hal* and *Tgm1*. Out of the six hits, *Jup*, encoding the protein γ-catenin and *Dsp*, encoding desmoplakin, were the ones with the highest fold change and lowest p-value (Figure 4.17C).

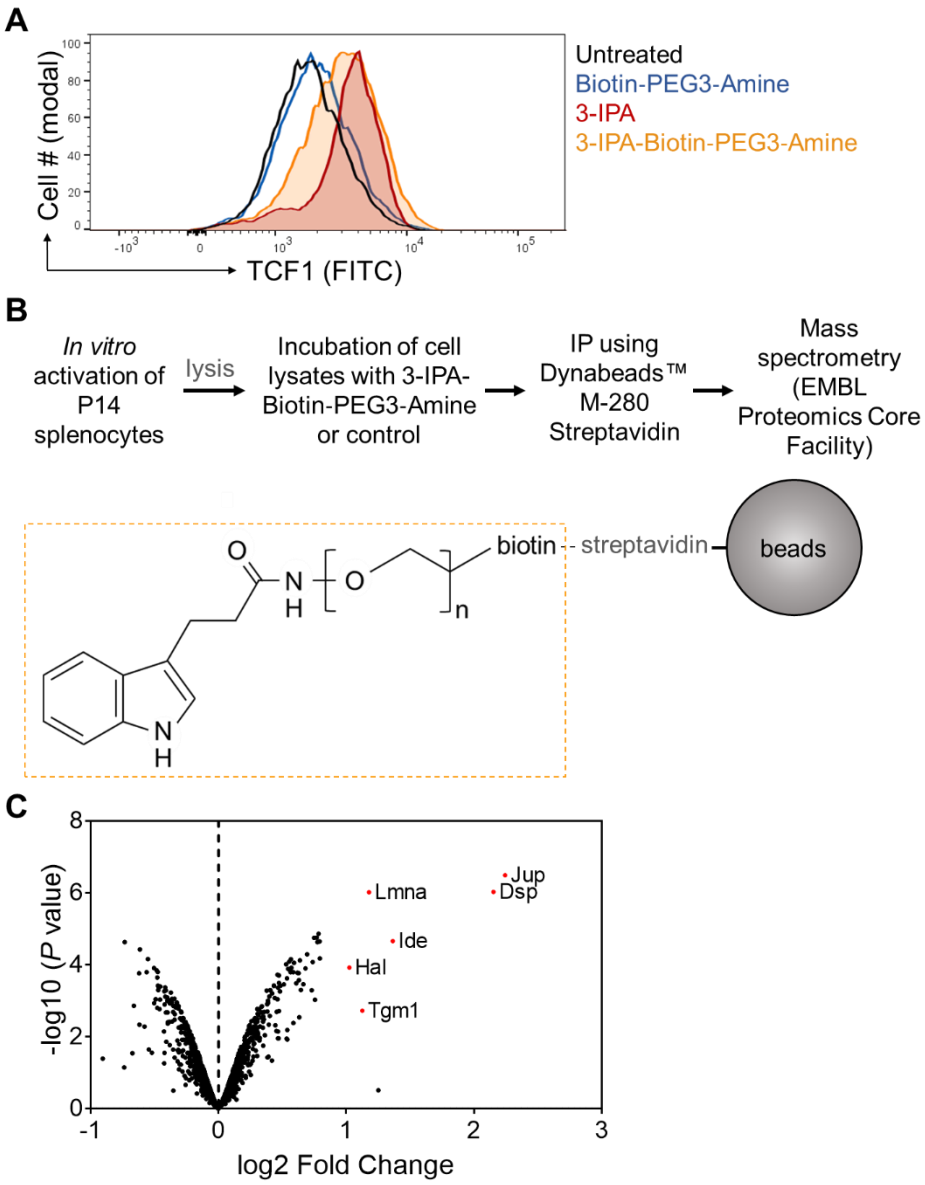

Figure 4.17. Identification of potential 3-IPA binding proteins. *3-IPA-Biotin-PEG3-Amine was designed and synthesized with the help of Dr. Aubry Miller (DKFZ, Heidelberg).* ***A****. Representative MFI of TCF1 of in vitro activated P14 cell treated with Biotin-PEG3-Amine, 3-IPA, 3-IPA-Biotin-PEG3-Amine in a concentration of 125 µM each and the respective DMSO control (untreated).* ***B****. Workflow of pulldown and mass spectrometry experiment (top). Chemical structure of 3-IPA-Biotin-PEG3-Amine (orange box) and schematic display of its binding to Dynabeads™ M-280 Streptavidin (bottom).* ***C****. Volcano plot showing gene names of hits identified by Limma analysis of mass spectrometry data from IP eluates of 3-IPA-Biotin-PEG3-Amine and control Biotin-PEG3-Amine incubated P14 cells lysates.*

Therefore, γ-catenin and desmoplakin were investigated in more detail. To do so, crRNAs targeting the *Jup* and the *Dsp* genes were designed and annealed to a fluorescently coupled tracrRNA to form a functional gRNA duplex. Splenocytes from a P14-Cas9 mouse, which endogenously express Cas9, were isolated and nucleofected with the respective complex. After nucleofection, cells were cultured for 24 h in the presence of IL-7. Subsequently, newly generated KO and control nucleofected cells were *in vitro* activated and cultured with or without

3-IPA for 3 days. Stemness markers CD62L and TCF1 were assessed by flow cytometry (Figure 4.18A)

Transfection efficacy was determined 24 h after nucleofection. Annealed tracrRNAs were coupled to the fluorescent dye ATTO™ 550 and therefore transfection efficacy could be determined by flow cytometry. Endogenously expressed Cas9 protein was further co-expressed with EGFP and therefore genetically modified cells could be identified by gating on $GFP^+ATTO^{TM}550^+$ double-positive cells. Control cells were nucleofected with unconjugated crRNA only and therefore they were negative for ATTO™. Almost all cells nucleofected with a functional gRNA duplex were ATTO™550-positive. Since also almost all cells were positive for GFP, indicating Cas9 expression, nucleofection was successful (Figure 4.18B).

ATTO™550 signal was lost after 3 days of culture (data not shown) and intracellular EGFP is sensitive towards necessary fixation. However, since the majority of cells was double-positive for EGFP and ATTO™550 24 h after nucleofection, marker expression upon *in vitro* activation and 3-IPA treatment was determined by gating on all viable cells. While control cells increased CD62L expression upon treatment, both, *Jup* and *Dsp* KO cells, expressed CD62L in very high levels already without 3-IPA treatment and those levels were not further increased upon treatment. *Dsp* KO cells displayed even higher CD62L expression levels when untreated (Figure 4.18C). TCF1 levels were slightly increased by 3-IPA treatment in all tested cells. *Jup* and *Dsp* KO cells seem to have slightly higher basal levels of TCF1 compared to the control cells (Figure 4.18D). However, due to low experimental replicate numbers, no statistical analysis was performed.

In conclusion, nucleofection of P14 Cas9 cells with gRNAs for *Jup* and *Dsp* was successful. Cells lacking γ-catenin and desmoplakin displayed increased expression of CD62L and potentially also TCF1 without 3-IPA treatment. Due to low replicate numbers, no statistical analysis was possible. Therefore, their role in mediating 3-IPA-induced effects was not ruled out but remains inconclusive.

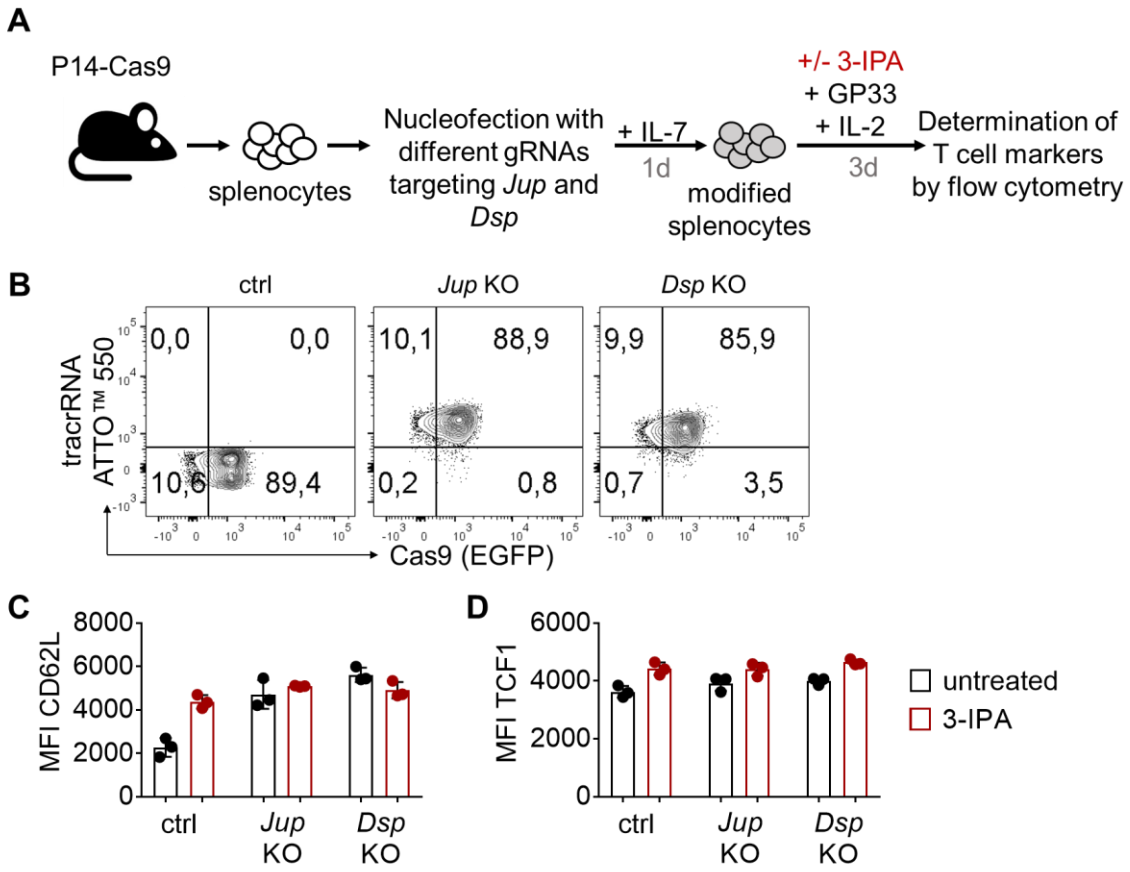

Figure 4.18. Investigating γ-catenin and desmoplakin as potential mediators of 3-IPA. ***A****. Experimental setup. P14-Cas9 splenocytes were nucleofected with gRNAs targeting the genes encoding γ-catenin (Jup) or desmoplakin (Dsp). Nucleofected cells were cultivated for 24 h in the presence of IL-7. Modified cells were cultivated with or without 3-IPA in the presence of IL-2 and GP33 for 3 days. T cell markers were analyzed by flow cytometry.* ***B****. Quantification of MFI CD62L and TCF1 after in vitro culture and treatment are shown for cells nucleofected with crRNA alone (control = ctrl), gRNA targeting Jup and gRNA targeting Dsp.*

4.6.4 3-IPA treatment decelerates β- and γ-catenin degradation

γ-Catenin is a close homologue of β-catenin, whose role in $CD8^+$ T cell differentiation in the context of stemness and memory formation has been intensively and controversially discussed [194-198]. Therefore, γ-catenin identified as a potential 3-IPA-binding protein was of special interest for further mechanistical studies.

To investigate if β- and γ-catenin levels are changed by 3-IPA treatment, several experiments trying to detect both proteins in Western Blot analysis were performed. However, none of them were successful due to the lack of protein detection in activated P14 cells (data not shown). Since antibodies were selected based on a publication in which the authors detected both, β- and γ-catenin [197], in naïve T cells, expression of both proteins under the influence of 3-IPA treatment was investigated at different time points after activation by Western Blot analysis.

While naïve P14 cells displayed high levels of β- and γ-catenin, levels were reduced over time. Already 6 h after activation a decrease of β- and γ-catenin was observed, while the decrease in γ-catenin expression was much stronger. Higher β- and γ-catenin levels were observed in 3-IPA-treated compared to untreated cells 12 h after activation. For γ-catenin this effect was not visible anymore 24 h after activation. From 48 h on, there was almost no γ-catenin detectable. Increased β-catenin levels upon 3-IPA treatment were observable until the latest time point (Figure 4.19), indicating that 3-IPA treatment decelerates catenin degradation after T cell activation with a stronger effect on β-catenin.

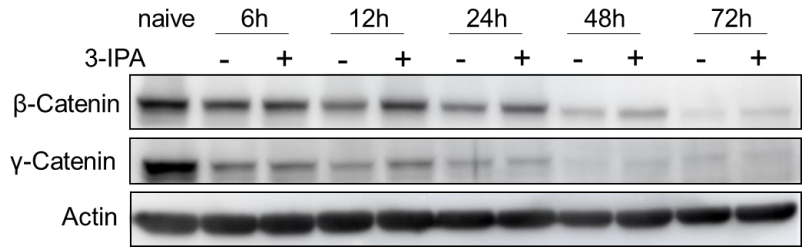

Figure 4.19. 3-IPA treatment decelerates β- and γ-catenin degradation after T cell activation. *Western Blot analysis of β- and γ-catenin in activated P14 cells at different time points after in vitro activation (IL-2, GP33) and 3-IPA treatment. Protein levels were normalized and 50 µg total protein loaded per lane. Actin protein levels were used as loading control.*

4.6.5 3-IPA influences *Tcf7* promoter activity

One of the most robust and major effects of 3-IPA treatment on $CD8^+$ T cells is upregulation of the key TF TCF1. Having identified γ-catenin as a potential 3-IPA-binding protein, its role and in addition the role of its homologue β-catenin on TCF1 transcription were investigated using the Dual-Glo® Luciferase Assay System. This assay allows examination of the promoter activity of a gene of interest and alterations of its activity in the presence of potential transcriptional activators or repressors.

The *Tcf7* pGL3 luciferase reporter vector was kindly provided by Ken Oestreich, PhD [219]. The overexpression plasmid for β-catenin (pcDNA6-N-3XFLAG-Ctnnb1) was purchased from Addgene and the respective control vector was generated by removal of the *Ctnnb1* gene via restriction digest. The overexpression plasmid for γ-catenin was generated by cloning the *Jup* gene into the MigR1-SARM backbone vector.

The human epithelial-like cell line HEK293T and murine T lymphoblast cell line EL4 were transfected with the two different overexpressing vectors alone or in combination and the respective control vectors. Cells were cultured with or without 3-IPA for 3 days. The assay was performed according to manufacturer's instructions.

In HEK293T cells, overexpression of *Ctnnb1* (β-catenin) significantly increased *Tcf7* promoter activity, while overexpression of *Jup* (γ-catenin) as well as their combination did not change activity (Figure 4.20A). 3-IPA treatment of the same cell line significantly increased

promoter activity in in all conditions, except for the combinatorial overexpression of *Ctnnb1* and *Jup* (Figure 4.20B). In contrast to the activating effect of β-catenin on *Tcf7* promoter activity in HEK293T cells, in EL4 cells overexpression of both genes and their combination decreased *Tcf7* promoter activity compared to the control (Figure 4.20C). 3-IPA treatment significantly increased *Tcf7* promoter activity in control cells and in *Ctnnb1* overexpressing, but not in *Jup* overexpressing EL4 cells (Figure 4.20D).

In both cell lines, 3-IPA treatment increased *Tcf7* promoter activity in almost all conditions, whereas the roles of γ- and β-catenin remain inconclusive in this context. Interestingly, when *Jup* was overexpressed, the activating effect of 3-IPA was decreased (HEK293T) or even abolished (EL4). Due to the contradicting results upon *Ctnnb1* overexpression in the two different cell lines, the role of β-catenin as a potential TF for *Tcf7* expression needs to be further investigated.

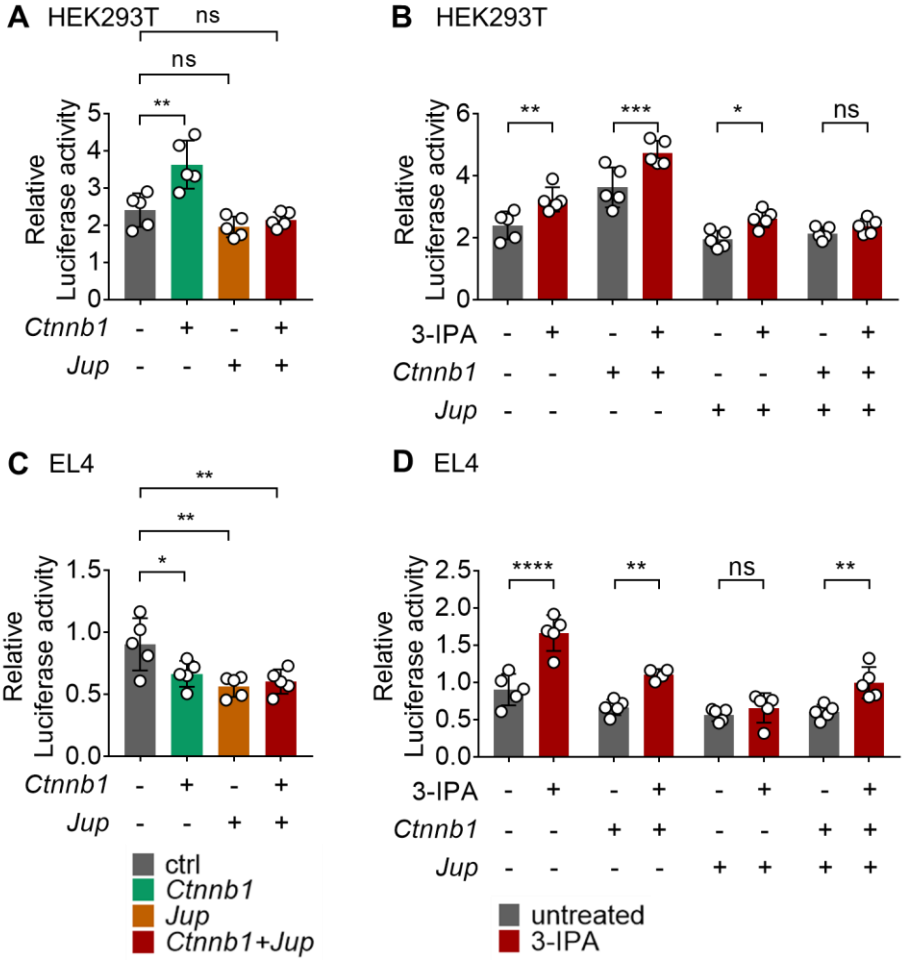

Figure 4.20. Modification of Tcf7 promoter activity by β-catenin, γ-catenin and 3-IPA. ***A****. Modification of Tcf7 promoter activity by overexpression of Ctnnb1 (β-catenin), Jup (γ-catenin) or their combination in HEK293T cells.* ***B****. Modification of Tcf7 promoter activity by 3-IPA in combination with Ctnnb1 and Jup overexpression in HEK293T cells.* ***C****. Modification of Tcf7 promoter activity by overexpression of Ctnnb1, Jup or their combination in EL4 cells.* ***D****. Modification of Tcf7 promoter activity by 3-IPA in combination with Ctnnb1 and Jup overexpression in EL4 cells. Data are means ± s.d. of 5 measurements and were analyzed by one-way ANOVA. Statistically significant changes are indicated by ns: not significant, *P ≤ 0.05, **P ≤ 0.01, ***P ≤ 0.001, ****P ≤ 0.0001.*

4.6.6 Different β-catenin levels in combination with 3-IPA modify TCF1 and CD62L expression

To finally determine the role of β- and γ-catenin in 3-IPA-induced upregulation of TCF1, $CD8^+$ T cells deficient in β- or/and γ-catenin are required. Mice harboring such $CD8^+$ T cells are currently in breeding but not yet ready to use. For that reason, in a next experiment, P14 cells were treated with the specific β-catenin inhibitor FzM1 in two concentrations and cultured with or without 3-IPA for 3 days. In addition to FzM1, the GSK3 inhibitor CHIR-99021 was included in the experiment (Figure 4.21A). GSK3 inhibition prevents phosphorylation and subsequent ubiquitination and proteasomal degradation of β-catenin, thereby leading to higher levels of cytosolic β-catenin. To date there are no specific γ-catenin inhibitors available.

3-IPA treatment of P14 cells made them more sensitive towards FzM1 treatment. While there was no difference in the percentage of viable cells between the DMSO control and FzM1 (2 µM)-treated cells when untreated, this percentage was lowered in the combination with 3-IPA treatment. The higher concentration of FzM1 (5 µM) led to slightly reduced percentages of viable cells when untreated but was completely cytotoxic when combined with 3-IPA. This effect was not only observed for FzM1, but also other tested β-catenin inhibitors (data not shown). The GSK3 inhibitor CHIR-99021 slightly reduced the percentage of viable $CD8^+$ T cells compared to the DMSO control, and this percentage was only slightly lower in the presence of 3-IPA (Figure 4.21B).

In cells cultured without 3-IPA, only treatment with the β-catenin inhibitor FzM1 in the higher concentration increased TCF1 expression, while there was no difference upon treatment with the other inhibitors. 3-IPA treatment increased TCF1 expression both in the DMSO control and the inhibitor treatments compared to the untreated counterparts. This increase, however, was slightly lower upon FzM1 treatment (2 µM) and even more decreased upon CHIR-99021 treatment. Due to high cytotoxicity upon combinatorial treatment of FzM1 (5 µM) and 3-IPA, no analysis was possible for this condition (Figure 4.21C).

P14 cells displayed higher expression levels of CD62L when treated with the β-catenin inhibitor FzM1, while showing decreased levels upon treatment with CHIR-99021. 3-IPA treatment increased CD62L expression in all conditions. However, the decrease compared to the DMSO control was lower, in the presence of both, FzM1 (2 µM) and CHIR-99021 (Figure 4.21D).

In summary, 3-IPA treatment made cells more sensitive towards reduced β-catenin levels due to FzM1 treatment. Furthermore, reduced β-catenin levels upon FzM1 treatment increased TCF1 and CD62L expression levels, while increased levels of β-catenin due to CHIR-99021 treatment decreased expression of both markers. 3-IPA treatment increased TCF1 and CD62L

marker expression in all combinations, but the increase itself was lower compared to the DMSO control.

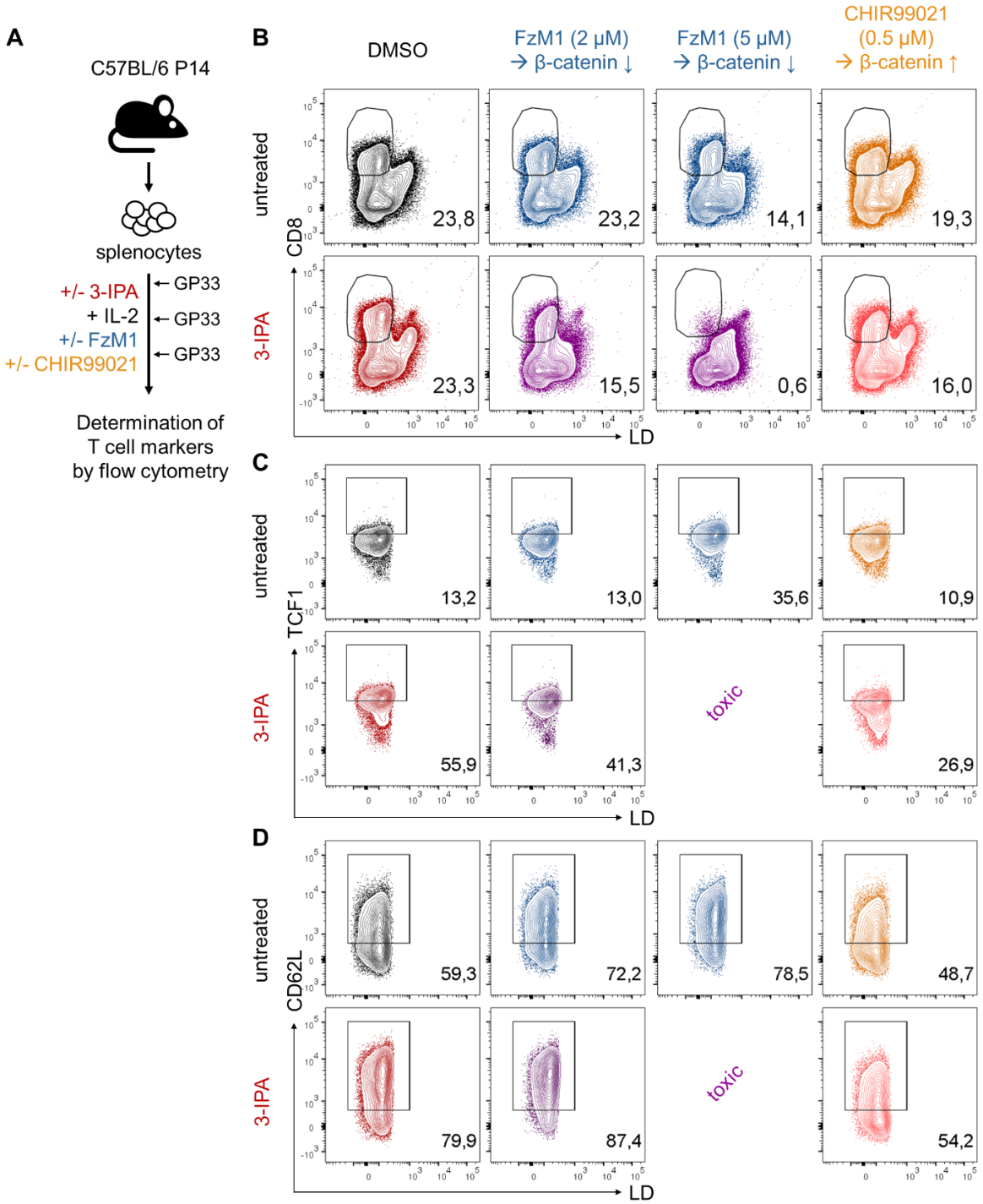

Figure 4.21. Effect of β-catenin and GSK3 inhibitors in combination with 3-IPA on CD8⁺ T cell markers. A*. Experimental setup. P14 splenocytes were cultivated with β-catenin inhibitor FzM1 (2 and 5 µM) or GSK3 inhibitor CHIR-99021 (0.5 µM) and the respective DMSO concentration (1:1000). Cells were cultivated with or without 3-IPA in the presence of IL-2 for 3 days and repeatedly stimulated with GP33 every day. T cell markers were analyzed by flow cytometry.* ***B****. Representative FACS plots of viable CD8⁺ T cells.* ***C****. Representative FACS plots of TCF1 expression of viable CD8⁺ T cells.* ***D****. Representative FACS plots of CD62L expression of viable CD8⁺ T cells.*

5 Discussion

Aging and obesity are growing global health issues, since both conditions are accompanied by increased cancer risk, higher susceptibility to infectious diseases as well as decreased vaccination efficacy. Both aging and obesity have been described to be associated with metabolic changes as well as compromised adaptive immunity. $CD8^+$ T cells are the main effectors of cell-mediated adaptive immunity to fight viral infections and cancer. Upon specific antigen encounter, naïve $CD8^+$ T cells undergo clonal expansion and differentiation to effector cells. After antigen clearance, a small proportion of T_{eff} differentiates into memory cells to be able to rapidly respond to recurrent antigen. In the case of chronic infection and cancer, however, antigen persists, leading to T cell exhaustion. T_{ex} can be identified by surface expression of IRs as well as their TF profile. The pool of T_{ex}, however, is heterogenous and can be mainly divided into T_{pex} and terminally differentiated T_{ex}. $CD8^+$ T cells displaying signs of exhaustion have been reported to be increased in aged and obese individuals compared to their young and lean counterparts [248, 249]. There are studies focusing on either aging or obesity in the context of $CD8^+$ T cell immunity in anti-viral infections or cancer. However, there are no studies so far including both factors, even though obesity and aging often coincide [250].

The aim of this thesis was to find a potential link between aging- and obesity-induced alterations of immune cells with a specific focus on $CD8^+$ T cells as well as changes of the plasma metabolite profile. The combination of aging and obesity induced a terminally differentiated phenotype of naïve $CD8^+$ T cells. Moreover, several metabolites were found to be altered by the combination of aging and obesity, and the tryptophan metabolite 3-IPA was identified to be decreased. Treatment of $CD8^+$ T cells with 3-IPA *in vitro*, induced a stem cell-like phenotype, reversed T cell exhaustion and lead to significant modification of their metabolism. Pre-treatment of antigen-specific $CD8^+$ T cells did not enhance their anti-tumor function but could rescue pre-exhausted as well as aging- and obesity-impaired anti-viral $CD8^+$ T cell functions *in vivo*. Mechanistically, γ-catenin was found to directly interact with 3-IPA and therefore the role of γ-catenin and its close homologue β-catenin were investigated in the context of 3-IPA-mediated TCF1 upregulation. 3-IPA treatment was found to decelerate degradation of β- and γ-catenin after activation of $CD8^+$ T cells. Furthermore, 3-IPA increased *Tcf7* promoter activity. Intracellular β- and γ-catenin were found to modify the same set of markers as 3-IPA treatment does, indicating a potential link between 3-IPA and β- and γ-catenin in $CD8^+$ T cell stemness control.

5.1 Aging and obesity promote terminal differentiation of CD8$^+$ T cells and alter the metabolic profile in mice

To identify changes on immune cells and the metabolic profile that are synergistically induced by the combination of aging and obesity, young and lean mice were fed a HFD or chow diet in order to generate four groups of mice (YL, YO, AL and AO) for further investigation. These groups allowed the study of alterations induced by either aging or obesity alone or by the combination of the two conditions.

Blood glucose levels of all four groups were determined after a fasting period of 12 h. While YL mice displayed the lowest blood glucose levels, YO mice showed the highest (Figure 4.1C). It has been reported before that obesity increases blood glucose levels both in humans and in mice [251, 252]. Abnormal high blood glucose levels, also termed hyperglycemia, is a symptom of diabetes mellitus, an illness resulting from insufficient insulin secretion (type 1 diabetes) or insulin resistance (type 2 diabetes). Obesity is the main risk factor for type 2 diabetes [253]. Due to nutritional excess, insulin secretion is enhanced, while its biological action to mediate uptake of glucose in fat, muscle and liver cells is reduced. The mechanisms responsible for insulin resistance, especially as a result of obesity, are heavily investigated, but not fully elucidated yet [254].

Surprisingly, there was no significant difference in blood glucose levels between AL and AO mice and levels were significantly lower in AO compared to YO mice, while slightly increased in AO compared to YL mice (Figure 4.1C). At first sight, it seems that aging reduces hyperglycemia, even in the obese condition. Diabetes, however, is highly prevalent in aged individuals and therefore aging is considered one of the main risk factors. There are several criteria to diagnose diabetes, such as fasting plasma glucose or post-prandial glucose, to name only two. Blood glucose in this experiment was measured after a fasting period of 12 h. There are studies showing that determining hyperglycemia and thereby diagnosing diabetes at this time point, misses a great proportion of diabetic individuals, especially older adults [255, 256]. This could partly explain normal blood glucose levels in aged mice in this experiment. More importantly, in contrast to humans, in mice, fasting blood glucose levels decrease with age [257]. Therefore, one must be cautious when translating age-related metabolic changes from mice to humans.

To identify changes on immune cells, with a specific focus on T cells, immune characterization of splenocytes from mice of all four groups was performed (Figure 4.2). Interestingly, the percentage of splenic CD4$^+$ T cells was mainly dependent on age and less on obesity, since the proportion was lowered in aged mice compared to their lean counterparts. In contrast, the proportion of CD8$^+$ T cells among lymphocytes from the spleen was lowered

by obesity, but not by aging (Figure 4.2A and B). The decline of $CD4^+$ T cells in aged mice has been reported before [258]. The results regarding splenic $CD4^+$ and $CD8^+$ T cell alterations are contradictory to a previous publication, in which the authors found proportions of both, $CD8^+$ and $CD4^+$, to be increased in the spleens of obese mice [259]. Duration of HFD, sex and age (of young mice) are similar between the two studies, while compositions of the HFD are slightly different. If and how different HFD compositions alter the immune cell profile of obese mice, should be further investigated in order to ensure comparability between different studies. In conclusion, in this experiment, either aging or obesity led to decrease in the proportion of either $CD4^+$ or $CD8^+$ T cells, resulting in synergistically reduced proportions of both T cell subsets in AO compared to YL mice.

The percentage of immunosuppressive T_{reg} in the spleen has been described to be elevated by aging [260] and obesity [214]. This is in concordance with data of this experiment, since the proportion of splenic T_{reg} among $CD4^+$ T cells was significantly increased by aging and even higher by the combination of aging and obesity (Figure 4.2C and D).

Life-long exposure to antigen as well as thymic involution result in a decline of naïve T cells and accumulation of T_{mem} in the elderly [206, 261]. Based on the well-defined surface markers CD62L and CD44, T cells can be divided into naïve ($CD62L^{high}CD44^{low}$), T_{cm} ($CD62L^{high}CD44^{high}$) and T_{em} cells ($CD62L^{low}CD44^{high}$) [84] (Figure 4.2E (left)). Both, T_{cm} and T_{em} are known to increase with aging. A similar decline in naïve T cells with a concomitant increase in T_{cm} and T_{em} cells has been observed in mice receiving a HFD due to diminished thymopoiesis induced by obesity [262]. In concordance with literature, YL mice displayed the highest percentage of naïve $CD8^+$ T cells, while AO showed the lowest. Furthermore, T_{em} cells, which are the most differentiated one among the three subsets, were significantly increased by the combination of aging and obesity (Figure 4.2E). As mentioned before, memory cells in aged humans accumulate partly due to life-long antigen exposure. Since the mice used for this experiment were housed in a pathogen-free facility, they should not have been exposed to peripheral antigen. Chiu *et al.* reported, however, that most of T_{cm} cells are antigen-inexperienced virtual T_{mem} that accumulate over time [263], which explains the presence of T_{mem} despite the lack of antigen.

$CD8^+$ T cells from aged mice displayed a much more activated and cytotoxic phenotype compared to young cells, which was accompanied by increased IR expression and decreased expression of the stemness marker TCF1, regardless of the diet (Figure 4.2F). These results are in line with a report from Decman *et al.*, in which the authors found increased CD44 and IR receptor expression during the course of aging without immune challenge [264]. The phenotype of aged $CD8^+$ T cells is intensively investigated. While some reports show reduced effector functions of aged $CD8^+$ T cells [248] others report increased cytotoxicity [265, 266].

However, setups for these investigations, differ among the studies. Similar to this study, increased activation and cytotoxicity was observed in studies which examined aged $CD8^+$ T cells without immune challenge, while reduced effector functions were reported in response to infections or cancer [84, 267]. Since cells already display a terminally differentiated, cytotoxic phenotype with reduced stemness (Figure 4.2F) without immune challenge, these cells are prone to fail when exposed to infection or cancer. Obesity has been reported to accelerate T cell aging [249]. This is confirmed by findings of this study, since obesity potentiated the terminally differentiated phenotype induced by aging, making AO $CD8^+$ T cells the most differentiated and least stem cell-like phenotypic group.

Aging is the time-dependent progressive decline of physiological functions and is associated with alterations in body composition and metabolism [268]. These changes are pictured by alterations of the metabolome [269]. Besides aging, also obesity is considered a systemic condition. To determine metabolic changes induced by the combination of aging and obesity, plasma concentrations of 630 different metabolites from 26 biochemical classes were determined in all four mouse groups. In total, 29 metabolites were significantly decreased, while 142 were found to be significantly increased in AO compared to YL mice (Figure 4.3A). Most of the significantly altered compound classes were lipid- and amino acid-related. Significantly altered lipid-related metabolites were mainly increased in AO compared to YL mice, similar to amino acid-related compounds. However, 75 % of the significantly altered amino acids were synergistically decreased by the combination of aging and obesity. An increase in lipid-associated metabolites has been described for humans, both in aging and obesity [270, 271].

The aim of this study was to link metabolic changes induced by the combination of aging and obesity and T cell immunity. Therefore, in a first screening experiment, several metabolites were chosen and their effect on $CD8^+$ T cell surface marker expression investigated *in vitro* (Figure 4.3B and Figure 4.4). Out of all tested metabolites, 3-IPA emerged to strongly alter $CD8^+$ T cell surface molecules and was therefore further investigated.

5.2 3-IPA induces a stem-like $CD8^+$ T cell phenotype with effector properties in murine and human cells *in vitro*

3-IPA is a tryptophan metabolite that is produced by commensal gut microbes exclusively. For a decade, the gut bacterium *Clostridium sporogenes* was thought to be the only bacterium capable of producing 3-IPA [226]. Dodd *et al.*, however, identified four more 3-IPA-producing gut bacteria: *Peptostreptococcus anaerobius* CC14N as well as three strains of *Clostridium cadaveris* [227]. Aging is accompanied by alterations of the gut microbiota and beneficial

bacteria, including Clostridium strains were found to be decreased [272]. Also obesity induces alterations of the microbiome [273], however, no studies specifically mention alteration of 3-IPA producing bacteria.

3-IPA has been described to have anti-oxidative and anti-inflammatory properties [274, 275]. Furthermore, 3-IPA was identified to have potential as a biomarker for several metabolic diseases such as type 2 diabetes [229], atherosclerosis [230] as well as non-alcoholic fatty liver disease [231] and high levels are associated with good patient prognosis in all aforementioned illnesses.

Plasma levels of 3-IPA are known to be reduced in obese individuals [276], while no reports so far mention a decrease of 3-IPA by aging. Aging alone did not significantly decrease 3-IPA plasma levels in lean mice. In obese mice however, both age groups displayed significantly lower 3-IPA plasma levels. Compared to YO mice, plasma concentrations were significantly decreased in AO mice, indicating that aging in combination with obesity further reduces 3-IPA levels (Figure 4.3B).

In humans, physiological concentrations range from 0,5 to 10 µM [277, 278], while similar plasma concentrations have been reported for mice [279]. Measured plasma concentrations of 3-IPA in this study ranged from 0.1 to 1.7 µM (Figure 4.3B), which is comparable with reported concentrations from other studies. However, treatment of $CD8^+$ T cells in physiological concentrations didn't alter $CD8^+$ T cell markers, but only concentrations starting from 50 µM on appeared to be effective. A treatment concentration of 75 µM was determined to be optimal for further investigations (Figure 4.5A and B). Even though this concentration is roughly 100-fold higher than the physiological one, due to the strong and reproducible effect on T cell marker expression, the therapeutic potential of this metabolite was further explored.

3-IPA treatment in combination with activation *in vitro* significantly altered $CD8^+$ T cell marker expression in murine cells. Markers associated with T cell stemness, such as TCF1 [73], CD62L [72] and Slamf6 [166] were increased while activation marker CD44 was decreased upon treatment (Figure 4.6D-H). Furthermore, the MFI of CD8a of $CD8^+$ T cells was increased despite similar percentages, indicating higher CD8a expression per cell (Figures 4.6B and D). Madi *et al.* recently reported selective upregulation of CD8 on T cells with stem cell-like features [232]. Western Blot analysis showed that 3-IPA treatment specifically induced TCF1, but not is homologue LEF1 (Figure 4.6D), indicating a specific effect on TCF1.

The ultimate goal of translational biomedical research is to implement findings into clinical practice This is why it is crucial that conclusions drawn from experiments performed in animals or animal tissues are applicable to the human situation. Therefore, PBMCs were isolated from human buffy coat and marker expression determined upon treatment with 3-IPA. PBMCs from nine different donors of different age and sex were used. Except for one donor, $CD8^+$ T cells

from all other donors upregulated CD8a expression upon 3-IPA treatment as observed in murine $CD8^+$ T cells. Not all PBMCs from different donors were responsive towards 3-IPA treatment regarding TCF1 and CD62L expression. In summary, however, increase of both markers was significant, therefore confirming the effectiveness of 3-IPA also on human $CD8^+$ T cells (Figure 4.10). Background information regarding sex and age were obtained retrospectively for all donors (data not shown). Unfortunately, data on BMI was not available. There was no obvious correlation between responsiveness towards 3-IPA and sex or age of donors. To draw a clear conclusion regarding factors influencing $CD8^+$ T cells' responsiveness towards 3-IPA, however, a much bigger sample size is required. Interestingly, increase of one marker was not necessarily associated with increase of the other one, indicating the possibility that TCF1 and CD62L upregulation might be independent from one another.

Chronic antigen stimulation is the main driver of T cell exhaustion [95]. To mimic this condition *in vitro*, antigen-specific murine $CD8^+$ T cells were repeatedly stimulated with their cognate antigen five times in total. Treatment with 3-IPA resulted in increased survival capacity, maintained high levels of stemness markers TCF1 and Slamf6 and reduced IR surface expression (Figure 4.9B-E). Terminally exhausted T cells display superior cytotoxicity but reduced survival capacity, while T_{pex} show higher polyfunctionality and the ability for long-term survival in the absence of antigen [171]. 3-IPA-treated, chronically stimulated $CD8^+$ T cells displayed lower expression of IFNγ and TNFα alone. However, the proportion of $CD8^+$ T cells co-expressing IFNγ, TNFα and IL-2 were increased compared to untreated cells (Figure 4.9F). Overall, 3-IPA treatment in a chronically stimulating environment skewed $CD8^+$ T cells towards a T_{pex} phenotype with enhanced survival capacity and increased polyfunctionality.

The $CD8^+$ T cell differentiation status is tightly linked to the metabolic phenotype. While quiescent naïve T cells rely on OXPHOS for energy production, activated $CD8^+$ T cells engage glycolysis, glutaminolysis as well as OXPHOS to meet their energetic and anabolic demands [280]. T_{mem} subpopulations are heterogenous and so is their metabolic profile. While T_{cm} display higher SRC, T_{em} cells maintain reliance on glycolytic metabolism [281]. Similar to T_{mem} populations, T_{ex} subsets are phenotypically and functionally diverse. TCF1-expressing T_{pex} are able to sustain high SRC, while terminally exhausted T_{ex} lose this ability [282].

Surprisingly, despite high levels of TCF1 and CD62L, thereby representing a naïve or T_{cm} $CD8^+$ T cell phenotype, 3-IPA-treated cells displayed an increased glycolytic metabolism while showing decreased basal OXPHOS. Induction of maximal respiration upon FCCP injection, however, showed similar oxidative capacity and resulted in higher SRC of 3-IPA-treated compared to untreated cells, indicating greater metabolic flexibility of cells upon 3-IPA treatment (Figure 4.7).

In conclusion, 3-IPA treatment resulted in generation of $CD8^+$ T cells with a stem-cell like phenotype that displayed superior survival capacity in response to chronic antigen stimulation and decreased markers of exhaustion *in vitro*. At the same time, 3-IPA-treated cells displayed metabolic features of effector cells with high metabolic flexibility.

5.3 3-IPA doesn't improve anti-tumor immunity of $CD8^+$ T cells

$CD8^+$ T cells are the most important immune cell type in the context of anti-tumor immunity [283]. Once a tumor has established, however, $CD8^+$ T cells within the tumor display an exhausted phenotype [95]. Tumor-associated T_{ex} have been mainly divided in the two subsets T_{pex} and terminally differentiated T_{ex}, which are distinguished by TCF1 expression [284], even though the differentiation and organization of T_{ex} is much more complex and several subsets exist.

Having generated $CD8^+$ T cells with high TCF1 expression and a general stem-like phenotype by treating them with 3-IPA *in vitro*, the anti-tumor functionality of those cells was investigated in the B16 melanoma model. Even though increased TCF1 expression compared to untreated control $CD8^+$ T cells was confirmed prior adoptive transfer, 3-IPA-treated cells were not able to perform better regarding tumor control (Figure 4.11C). Furthermore, flow cytometry analysis of antigen-specific donor cells recovered from spleen and tumors showed no differential marker expression in 3-IPA pre-treated compared to untreated donor cells. Not even the before-analyzed molecules TCF1 and CD62L were altered between the two groups. The only difference among all analyzed molecules, was the increase of proliferation marker Ki67 in 3-IPA-treated donor cells recovered from the spleen. This difference, however, was lost in cells recovered from the tumor (Figure 4.11D).

$CD8^+$ T cells entering the tumor are exposed to a highly immunosuppressive TME consisting of cancer cells, stromal cells, inflammatory cells and cytokines with decreased nutrient availability and increased concentrations of metabolic by-products. Furthermore, the TME provides a milieu with increased pH and decreased oxygen levels [285]. Besides these general immunosuppressive factors, also specific T-cell suppressive mechanisms exist. DC, for example, release the enzyme indoleamine 2,3-dioxygenase (IDO), which deprives the TME of tryptophan, an amino acid required for T cell effector functions [286]. Furthermore, IDO induces T_{reg} differentiation, which accumulate in tumor tissues and secrete IL-10 and TGFβ leading to T_{eff} suppression as well as upregulation of PD-L1 on DCs [287]. Chronic antigen stimulation induces upregulation of inhibitory receptors on $CD8^+$ TILs. Cancer cells and proinflammatory

cells within the tumor overexpress ligands for those receptors, resulting in further inhibition of effector functions [288, 289].

The versatile immunosuppressive mechanisms of the TME have most likely been too strong to sustain the stem-like phenotype and function induced upon 3-IPA treatment. This assumption is supported by the fact, that the only detected difference between pre- and untreated cells (Ki67 expression) was only observed in the spleen, but not in the tumor. Which factors of the TME in particular are responsible for this abrogation need to be further explored.

Furthermore, Philip *et al.* have shown that over the course of tumorigenesis, chromatin states of T_{ex} within the tumor change. More specifically, two distinct chromatin states of PD-1^{high} T_{ex} have been described. T_{ex} in the first state are therapeutically reprogrammable and so is their chromatin state. Upon progressing tumorigenesis, however, those cells transition to a fixed dysfunctional chromatin state, that can't be remodelled by therapeutic interventions. Interestingly, the authors found that memory cells which already gained a specific epigenetic program, altered their chromatin state to the one of T_{ex}, indicating the tumoral environment is able to overwrite pre-existing epigenetic imprints [290]. Therefore, potential alterations of 3-IPA treatment on an epigenetic level might have been overwritten by the strong influence of the TME.

3-IPA treatment was able to prevent an exhausted-like phenotype *in vitro* (Figure 4.9). This exhaustion-like phenotype, however, was solely induced by repeated stimulation with the cognate antigen peptide. 3-IPA treatment of "real" T_{ex} isolated from the tumor did not increase TCF1 expression in those cells, while expression of the exhaustion marker Tim-3 was slightly reduced (Figure 4.13C). Furthermore, in the LCMV Arm infection model, 3-IPA was able to restore anti-viral functions of tumor-exhausted T_{ex} partially, but insufficiently (Figure 4.13D). These results are in line with the previously observed ineffectiveness of 3-IPA in the tumor model (Figure 4.11).

The exhaustion-like phenotype of the *in vitro* study was induced by repeated stimulation of antigen-specific $CD8^+$ T cells for five times in total (Figure 4.9A). Philip *et al.* showed that chromatin remodeling towards a T_{ex} phenotype started at day 5 after tamoxifen administration to induce autochthonous liver cancer and this first state of T_{ex} differentiation was reversible. A second wave of remodeling took place between day 7 and 14 and the fixed, irreversible T_{ex} state was established from day 12 on [290]. Therefore, the *in vitro* exhaustion model used in the present study, most likely reproduces only the first, reversible T_{ex} state but not the fixed one. Furthermore, the mentioned studies identifying reversible vs fixed T_{ex} states have been performed in tumor models. The cell culture system is highly artificial and the great impact of the highly immunosuppressive TME on T_{ex} differentiation is not considered in this model.

Beltra *et al.* reported terminal T_{ex} subset commitment once TCF1 expression was lost [167]. TCF1 expression of tumor-exhausted T_{ex} could not be restored by 3-IPA treatment (Figure 4.13C), indicating that once T_{ex} have differentiated into the terminally exhausted, fixed state, this state can't be remodeled by 3-IPA treatment.

5.4 3-IPA rescues aging- and obesity- impaired anti-viral CD8$^+$ T cell functions *in vivo*

Besides in cancer, CD8$^+$ T cells are also the main players in anti-viral immunity. LCMV is a model system of viral infection that has contributed a great portion to the current understanding of anti-viral CD8$^+$ T cells. There are several well-characterized strains of LCMV, such as LCMV Arm and LCMV cl13. LCMV Arm infection of mice induces an acute infection that is cleared within 8 dpi and subsequently leads to memory formation [111]. LCMV cl13 differs to LCMV Arm by only two amino acids, which leads to better infectivity of DCs and macrophages as well as increased viral replication within infected cells [291, 292]. Therefore, infection of LCMV cl13 leads to establishment of a chronic infection that can last up to three months [111].

Mitochondrial functionality is crucial for anti-viral CD8$^+$ T cell immunity [136]. Exhausted TILs display reduced mitochondrial fitness and accumulation of depolarized mitochondria due to impaired mitophagy. Metabolically compromised CD8$^+$ T cells can be identified by a low MDR/MG ratio [114]. Having shown that 3-IPA treatment of CD8$^+$ T cells *in vitro* significantly increased their SRC, the therapeutic potential of 3-IPA to rescue mitochondrially impaired virus-specific CD8$^+$ T cells was investigated. 3-IPA pre-treatment prevented mitochondrial impairment of a great portion of CD8$^+$ T cells, shown by reduced MDR/MG^{low} cells compared to untreated control cells *in vitro* (Figure 4.12C).

In vivo anti-viral functions of 3-IPA pre-treated and untreated virus-specific CD8$^+$ T cells, with and without mitochondrial impairment, were investigated using the LCMV Arm model. Mitochondrial impairment decreased donor cell survival after LCMV Arm infection *in vivo*. This was rescued by 3-IPA pre-treatment (Figure 4.12D and E). Not only cell numbers, but also exhaustion markers and effector functions of cells were restored (Figure 4.12F and G), implicating that 3-IPA treatment is able to rescue mitochondrially compromised CD8$^+$ T cells not only *in vitro*, but also *in vivo*.

The aim of this project was to investigate the synergistic effect of aging and obesity on CD8$^+$ T cell phenotype and function. Both aging and obesity are both well-known factors for increased susceptibility towards infectious diseases [9, 19] as well as decreased vaccination efficacy [201, 218]. Naïve CD8$^+$ T cells from AO mice displayed a terminally differentiated

phenotype marked by high cytotoxicity and IR expression and low stemness marker expression (Figure 4.2).

Anti-viral $CD8^+$ T cell functions in aging and obesity are a hot topic in immunological research. Kapasi *et al.* found that uninfected aged $CD8^+$ T cells displayed higher CD44 expression prior infection, as observed for AO mice in this study. However, after LCMV Arm infection, primary $CD8^+$ T cells responses of aged mice were decreased compared to young mice and $CD8^+$ memory formation was impaired [293]. These results were confirmed and further specified by a study from Decman *et al.*, in which the authors found poor viral responsiveness of $CD44^{high}$ $CD8^+$ T cells, especially the ones from aged mice. The significantly higher number of $CD44^{high}$ $CD8^+$ T cells in aged mice prior infection, partially explains their reduced anti-viral response [264]. Moreover, proliferative capacity upon secondary infection was reported to be compromised in aged compared to young virus-specific $CD8^+$ T cells [267].

Karlsson *et al.* found that in obese mice $CD8^+$ T cell responses towards influenza virus after secondary challenge were reduced [217]. Impaired $CD8^+$ T_{eff} functions towards influenza virus infection could be partially explained by metabolic reprogramming and transcriptional changes of $CD8^+$ T cells in obesity [294]. In contrast, Khan *et al.* found that obesity did not impair $CD8^+$ memory formation, maintenance, or function in LMCV infection [295].

None of the above-mentioned studies consider aging and obesity in combination, even though both conditions often coincide and similar phenotypes of $CD8^+$ T cells have been described. In this study, anti-viral primary and recall functions of virus-specific $CD8^+$ T cells from YL and AO donor mice were compared. Furthermore, the effect of 3-IPA treatment on AO cells was investigated.

While there was no difference in cell ratio and number of recovered donor cells from YL, AO and 3-IPA-treated AO donor cells, AO cells displayed decreased expression of stemness markers such as MFI CD8a, CD62L and TCF1 compared to their YL counterparts. This phenotype could be reversed by pre-treatment of AO cells with 3-IPA. Moreover, recovered AO donor cells displayed lower ratios of long-lived T_{cm} and increased percentages of more differentiated T_{em} cells compared to the other donor cell groups (Figure 4.14C-F). Due to the chosen time point of 30 dpi, no conclusions can be drawn regarding differences in immune response towards primary infection, but rather differences in memory formation potential. Aging- and obesity-induced decrease in stemness and memory marker expression after primary infection was reflected by decreased donor cell ratios and numbers after recall infection compared to YL donor cells and this effect was rescued by 3-IPA treatment. Not only proliferative recall capacity, but also effector functionality could be recovered back to the level of YL cells by 3-IPA treatment of AO cells (Figure 4.14G-J).

This experiment indicates that aging and obesity impair memory formation and therefore recall capacity of $CD8^+$ T cells, which is in line with reported vaccination deficiencies in both conditions [200, 201, 218]. 3-IPA pre-treatment of AO cells could rescue these deficiencies in memory formation capacity and is therefore a promising therapeutic candidate to overcome aging- and obesity induced impairment of $CD8^+$ T cells.

In resting T_{cm} cells, TCF1 is required to rapidly induce glycolytic enzymes to fuel secondary effector $CD8^+$ T cell generation and functionality [296]. In accordance with this, YL and 3-IPA-treated AO cells displayed significantly higher TCF1 expression compared to untreated AO cells prior second infection and appeared superior regarding numbers, stemness and functionality after recovery from infected mice.

YL and AO donor cells preserved functional differences, despite they were removed from their original YL or AO environment and transferred to mice with the same sex, age and BW. This indicates that changes that occur during the course of aging and obesity are manifested internally at some point and are not maintained by external factors. Epigenetic alterations of immune cells have been described for both aging and obesity [297, 298] and could account for persisting differences.

Furthermore, reduced mitochondrial functions as well as reduced mitochondrial mass and activation have been described for aged T cells [299, 300]. In addition, cells of obese mice show morphological and functional alterations of mitochondria [301] and $CD8^+$ T cells from obese mice display decreased SRC [302]. 3-IPA treatment increased SRC of $CD8^+$ T cells (Figure 4.7) and was able to rescue mitochondrially impaired $CD8^+$ T cells *in vitro* and *in vivo* (Figure 4.12). Metabolic analysis of AO and YL $CD8^+$ T cells need to be performed in order to elucidate if AO cells are metabolically compromised and if 3-IPA is able to rescue this phenotype.

5.5 Elucidating the mechanism of 3-IPA in $CD8^+$ T cells

3-IPA is a small molecule that is able to alter phenotype and functions of $CD8^+$ T cells. Small molecules with biological activity interact with proteins to mediate their effects. To unravel the mechanism how 3-IPA influences marker expression in $CD8^+$ T cells, identification of 3-IPA interacting proteins is essential.

Tryptophan can be metabolised by gut microbiota into several molecules, 3-IPA being one of them. These metabolites are well known ligands of the AhR [244] The AhR is a cytosolic ligand-activated TF that has been reported to modulate $CD4^+$ and $CD8^+$ T cell functions [245]. AhR deficiency of $CD8^+$ T cells didn't abolish upregulation of TCF1 and CD62L upon 3-IPA

treatment suggesting that the 3-IPA-induced effect on $CD8^+$ T cells is not mediated by AhR (Figure 4.15A).

Upregulation of TCF1 is one of the strongest and most significant alterations induced by 3-IPA treatment of $CD8^+$ T cells. The TF Foxo1 has been described to play a central role in $CD8^+$ T cell memory formation and *Tcf7* has been reported to be a target of Foxo1. Furthermore, lack of Foxo1 in activated $CD8^+$ T cells resulted in diminished recall, but not primary responses to infection [246]. Since 3-IPA treatment of AO $CD8^+$ T cells increased TCF1 expression and rescued their recall capacity, Foxo1 was another protein suspected to mediate the effect induced by 3-IPA treatment. However, also Foxo1-deficient cells upregulated CD62L and TCF1 upon 3-IPA treatment and therefore, also Foxo1 was excluded as a potential mediator of 3-IPA-induced effects on $CD8^+$ T cells (Figure 4.15B).

After two promising candidates were ruled out to be responsible for the 3-IPA-induced effect, another approach was chosen to identify mediators of 3-IPA in $CD8^+$ T cells. Instead of selecting proteins based on their reported function, a pulldown experiment was performed to identify potential 3-IPA interacting proteins and their biological function in $CD8^+$ T cells was investigated afterwards.

For the pulldown experiment, a biologically active but modified 3-IPA molecule was required. 3-IPA is an indole metabolite produced from the amino acid tryptophan. Almost all naturally occurring indoles are tryptophan-derived, however their occurrence as well as their synthesis are versatile. Besides, 3-IPA, 11 more indole-containing molecules with similar chemical structures were selected and their effect on $CD8^+$ T cells investigated in order to identify structural properties necessary for the biological activity (Supplementary Figure 1). Among the selected molecules were several other microbiota-derived tryptophan metabolites (#2, #3), auxins, which are a class of plant hormones (/#1, #4) or chemically derived molecules (#5, #6, #7, #11). Two prominent metabolites, serotonin (#8) and melatonin (#10), were included in the list. In addition to their well-known functions as neurotransmitter and hormone, both molecules have been reported to modulate T cell activation [303, 304].

Surprisingly, besides 3-IPA, only two other metabolites exerted the same biological effect on $CD8^+$ T cells (defined by upregulation of CD62L and TCF1 expression), namely trans-indole-3-acrylic acid (#3) and the screening compound $C_{15}H_{20}N2_O$ (#11) (Figure 4.16C). These results demonstrate that biological activity on $CD8^+$ T cells is structure-specific and not induced by unspecific factors, such as anti-oxidative properties, which have been described for several tryptophan metabolites [305]. Besides this finding, structural properties required for biological activity of compounds were identified and this knowledge was used to design a molecule that allowed pull-down experiments with subsequent mass spectrometry analysis to identify 3-IPA interacting proteins.

Out of the six identified hits, *Jup*, encoding the protein γ-catenin and *Dsp*, encoding desmoplakin, were the ones with the highest fold change and lowest p-value (Figure 4.17C). Both desmoplakin and γ-catenin (also known as plakoglobin), are components of desmosomes, intracellular junctions which provide strong adhesion between cells [306]. Besides its role in cell-cell adhesion, γ-catenin has been described to have TCF/LEF family-dependent transcriptional activity [307]. Furthermore, ectopic expression of desmoplakin was found to upregulate γ-catenin, thereby suppressing Wnt/β-catenin signaling pathway activity in a non-small cell lung cancer (NSCLC) cell line [308]. Interestingly, both identified proteins were found to be involved or modify the Wnt/β-catenin signaling pathway, a pathway that has been intensively studied and controversially discussed in the context of T cell differentiation.

γ-Catenin is a close homologue of β-catenin and both proteins share common intracellular interacting partners, such as AdPC, Axin and TCF/LEF [309]. β-Catenin plays a key role in the canonical Wnt signaling pathway. In β-catenin deficient cells, γ-catenin is able to robustly activate Wnt target genes therefore suggesting a partial functional overlap [310]. The role of β-catenin in the context of TCF1-dependent T cell development and function is controversially discussed. While some groups describe the Wnt-β-catenin pathway to be crucial for the generation of $CD8^+$ stem-like T_{mem} [194, 195], other groups report β-catenin as well as γ-catenin to be dispensable for $CD8^+$ T cell development and memory formation [196, 197]. Besides its crucial role in Wnt signaling, β-catenin has been described to be a negative regulator of peripheral T cell activation by inhibiting pathways downstream of the TCR [311].

Since γ-catenin was identified as a potential 3-IPA interacting protein (Figure 4.17C) and both γ- and β-catenin have been reported to potentially be involved in $CD8^+$ memory stem cell formation [194], the effect of 3-IPA on β- and γ-catenin levels in $CD8^+$ T cell at different time points after activation was determined. Both proteins were degraded shortly after activation and declined over time. Especially degradation of β-catenin was by decelerated upon 3-IPA treatment (Figure 4.19). The rapid decline of β-catenin after activation is contradictory to a publication in which the authors detected no β-catenin in naïve T cells, but found high levels upon TCR stimulation in human T cells [312]. A study from Driessens *et al.*, however, showed constitutive degradation of β-catenin in primary mouse T cells and introduction of a stabilized β-catenin in those cells resulted in reduced T cell activation and effector functions [311]. This is in line with the experiment of this study, confirming degradation of β-catenin in primary mouse T cells. One striking difference between the studies is the species of T cell origin. While increased β-catenin levels after T cell activation were observed in human T cells, decreased levels upon T cell activation were observed in mouse T cells. If there is a species-specific difference regarding intracellular β- and γ-catenin levels in $CD8^+$ T cells, remains to be tested using the similar experimental setup and the same antibodies for primary human and mouse T cells.

One of the most robust and major effects of 3-IPA treatment on CD8$^+$ T cells is upregulation of the TF TCF1. Several TFs are known to regulate *Tcf7* expression, such as NOTCH, RUNX or GATA3 [313]. A recent study found that the androgen receptor directly binds to the *Tcf7* promoter thereby regulating CD8$^+$ T cell exhaustion [314]. Furthermore, TCF1 itself might also be involved in regulation of *Tcf7* expression [183]. However, no publications so far mention β- and γ-catenin in the context of *Tcf7* regulation.

Having shown that cellular β- and γ-catenin levels are influenced by 3-IPA treatment and 3-IPA leads to increased TCF1 expression in CD8$^+$ T cells, a potential connection was investigated. In different cell lines, β- and γ-catenin overexpression had contradictory effect on *Tcf7* promoter activity. Overexpression of β-catenin in HEK293T cells significantly increased *Tcf7* promoter activity, while activity was decreased in EL4 cells. γ-Catenin overexpression did not alter *Tcf7* promoter activity in HEK293 T cells but decreased activity in EL4 cells (Figure 4.20A and C). Differences in *Tcf7* promoter activity upon overexpression between the two cell lines might be due to different endogenous levels of β- and γ-catenin. In EL4 cells no internal levels of β- and γ-catenin were detected by Western Blot analysis, while HEK293T cells did express both proteins already without overexpression (data not shown), thereby confounding the results. Furthermore, while HEK293T is a cell line isolated from human embryonic kidney, the EL4 cell line was established from mouse lymphoma. Therefore, cell lines differ in specie, tissue and malignancy origin, which suggests a whole different proteome. In the canonical Wnt signaling pathway, β- and γ-catenin associate with TCF proteins to activate target genes. β- And γ-catenin have several binding partners [309] and the presence of different proteins as interaction partners might change their transcriptional activity.

Independent of β- and γ-catenin overexpression, 3-IPA treatment increased *Tcf7* promoter activity in almost all conditions (Figure 4.20B and D). From this experiment, however, the role of β- and γ-catenin on *Tcf7* promoter activity remains elusive and the mechanism how 3-IPA modifies *Tcf7* promoter activity remains to be clarified.

To ultimately unravel the role of β- and γ-catenin in 3-IPA-mediated alterations of the CD8$^+$ T cell phenotype, CD8$^+$ T cells deficient in β- or/and γ-catenin are required. Mice harboring a specific KO for those proteins in CD8$^+$ T cells are currently in breeding, but not yet ready to use. Therefore, a specific inhibitor for Wnt-β-catenin signaling, FzM1 [315], was used to determine the role of this signaling pathway in 3-IPA-induced alterations of CD8$^+$ T cells. In addition to FzM1, the GSK3 inhibitor CHIR-99021 was used. GSK3 inhibition prevents phosphorylation and subsequent ubiquitination and proteasomal degradation of β-catenin, thereby leading to higher levels of cytosolic β-catenin [316]. Specific inhibitors for γ-catenin are not available and therefore, only the role of varying β-catenin levels could be investigated.

Interestingly, inhibition of Wnt-β-catenin signaling appeared to be toxic for $CD8^+$ T cells, but only in combination with 3-IPA indicating a potential involvement of 3-IPA in this signaling pathway (Figure 4.21B). FzM1 was tested in two different concentration and the higher concentration in combination with 3-IPA was too toxic to allow further analysis for this condition. The high toxicity of the combination of 3-IPA treatment and β-catenin inhibition was not only observed for FzM1, but also for other β-catenin inhibitors (data not shown), indicating that 3-IPA treatment sensitizes $CD8^+$ T cells towards the absence of β-catenin or the other way around. The exact mechanism, however, remains elusive and requires further investigation.

Decreased β-catenin levels increased CD62L, while increased β-catenin levels decreased CD62L on $CD8^+$ T cells, both in untreated and 3-IPA-treated cells (Figure 4.21D). The clear correlation between β-catenin levels observed for CD62L was not seen for TCF1 expression (Figure 4.21C), indicating that expression regulation of both markers might be independent. This observation was already made when treating human PBMCs with 3-IPA (Figure 4.10), therefore indicating a different mechanism for CD62L and TCF1 regulation by 3-IPA. Tsui *et al.* recently reported the presence of two distinct T_{pex} subsets, which both express TCF1, but can be distinguished by CD62L expression and are regulated by the TF MYB. $CD62L^+$ T_{pex} were identified as a stem-like population that is exclusively responsive towards PD-1 ICB therapy [317]. To investigate if increased CD62L expression upon 3-IPA treatment is a result of increased TCF1 expression or is upregulated independently, potentially via MYB, requires further investigations.

Rather an overall shift upon Wnt-β-catenin or GSK3 inhibitor treatment with subsequent altered β-catenin levels than the abrogation of the 3-IPA-mediated effects was observed for the analyzed markers. Moreover, increased levels of CD62L in the absence of β-catenin coincide with data from the CRISPR/Cas9 induced KO of γ-catenin, where CD62L expression levels were increased in the absence of γ-catenin to levels of 3-IPA treatment (Figure 4.18C). These results imply overlapping functions for β- and γ-catenin in the context of CD62L expression in $CD8^+$ T cells.

Drawing first conclusions from these results, β- and γ-catenin might act as negative regulators of $CD8^+$ T cells stemness based on TCF1 and CD62L expression. 3-IPA treatment of $CD8^+$ T cells exerts similar effects as FzM1, indicating that 3-IPA might interfere with the Wnt-β-catenin signaling pathway. The sensitivity towards Wnt-β-catenin signaling inhibition in 3-IPA treated cells support this hypothesis. Increased levels of β- and γ-catenin in 3-IPA-treated cells (Figure 4.19) might be a compensatory effect as a response to β- and γ-catenin inhibition upon 3-IPA treatment. However, these assumptions are purely hypothetical, since inhibitor treatment might not fully inhibit the protein of interest or might have off-target effects, as GSK3 for example regulates multiple downstream signaling molecules and not only

cytosolic β-catenin levels. Furthermore, lack of β-catenin could have been compensated by γ-catenin in this experiment. Mouse strains harboring T cells deficient in either β- or γ-catenin as well as a mouse strain with T cells lacking both catenin isoforms are currently in breeding and will ultimately clarify the role of β- and/or γ-catenin in 3-IPA-mediated T cell marker modification.

Taken all mechanistical studies together, 3-IPA was identified to directly interact with γ-catenin, a close homolog of β-catenin and 3-IPA treatment of cells decelerated degradation of both, β- and γ-catenin in activated $CD8^+$ T cells. Furthermore, 3-IPA treatment increased *Tcf7* promoter activity, while the role of β- and γ-catenin in this context remains elusive. Moreover, increased levels of β-catenin decreased CD62L and TCF1 expression, while these markers were increased in the absence of Wnt-β-catenin signals, irrespectively of 3-IPA. Therefore, 3-IPA most likely plays a role in TCF1 regulation and was shown to influence internal β- and γ-catenin levels of activated $CD8^+$ T cells. However, the link between β- and γ-catenin and TCF1 expression in the context of 3-IPA treatment remains speculative and requires further investigations. Furthermore, if increased CD62L expression upon 3-IPA treatment is a result of increased TCF1 expression or is upregulated independently should also be addressed.

5.6 Conclusion and outlook

In this thesis, alterations induced by the combination of aging and obesity on the $CD8^+$ T cell phenotype as well as on the overall metabolism were investigated. The T cell department displayed significant changes with the main finding that naïve $CD8^+$ T cells from AO mice showed a terminally differentiated phenotype with reduced TCF1 expression compared to cells from YL mice.

Several metabolites were synergistically altered by aging and obesity and 3-IPA was identified to be decreased in the plasma of AO compared to YL mice. 3-IPA treatment of murine and human $CD8^+$ T cells *in vitro* induced upregulation of stemness markers, such as TCF1, while decreasing exhaustion markers. Furthermore, 3-IPA treatment increased SRC and rescued mitochondrially compromised $CD8^+$ T cells. Effective treatment concentration was roughly 100 times higher than the physiological one and therefore 3-IPA was rather exploited in a therapeutic context than in a physiological one.

In vivo, pre-treatment of antigen-specific $CD8^+$ T cells didn't increase their anti-tumor effector functions and 3-IPA treatment was not able to rescue terminally exhausted $CD8^+$ TILs. However, 3-IPA pre-treatment of aging- and obesity-impaired virus-specific $CD8^+$ T cells rescued their recall capacity, indicating a therapeutic potential for 3-IPA in aging- and obesity-compromised anti-viral immunity.

Mechanistically, γ-catenin, a close homologue of β-catenin, was identified as a 3-IPA binding protein. Further investigations revealed decelerated degradation of both, β- and γ-catenin upon 3-IPA treatment of activated CD8$^+$ T cells. 3-IPA treatment increased *Tcf7* promoter activity, while the role of β- and γ-catenin in this context remains elusive. Modulation of intracellular β-catenin levels affected TCF1 and CD62L expression to different extents. However, the link between β- and γ-catenin and TCF1 expression in the context of 3-IPA treatment remains speculative and requires further investigations.

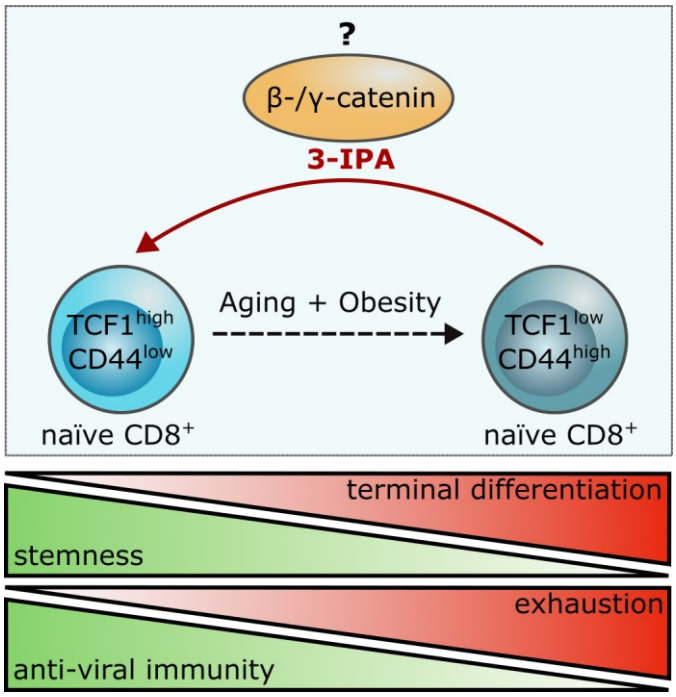

Figure 5.1. 3-IPA treatment of CD8$^+$ T cells reverses aging- and obesity-induced impairment. *During the course of aging and obesity in combination, naïve CD8$^+$ T cells lose their stem-like phenotype (TCF1^{high}CD44^{low}) and gain a terminally differentiated phenotype (TCF1^{low}CD44^{high}). Moreover, anti-viral immunity is lost while a dysfunctional, exhausted state develops. 3-IPA treatment of CD8$^+$ T cells induces a stem-like phenotype and reverses aging- and obesity impaired anti-viral functions. β- And γ-catenin are currently investigated as potential mediators of 3-IPA-induced effects.*

Findings of this thesis show that aging and obesity synergistically potentiate each other's adverse effect on CD8$^+$ T cells, making them a detrimental combination. Since the numbers of aged as well as obese people have dramatically risen over the past years and the two conditions often coincide, therapeutical interventions are inevitable. Even though the mechanism is not fully elucidated yet, 3-IPA is a promising candidate to overcome aging- and obesity-mediated impairment of CD8$^+$ T cells in order to improve anti-viral immune response.

Wikoff *et al.* showed that after intraperitoneal injection of 3-IPA and subsequent serum measurements in mice, 3-IPA is rapidly cleared from the blood indicating that it needs to be continuously produced in order to be detectable in serum [226]. This indicates that modification of the gut microbiome would be necessary to permanently increase 3-IPA plasma levels.

Diet is a key factor influencing the gut microbiota composition [318] and there are studies implicating a potential role of milk and fiber intake in modulation of 3-IPA levels [319]. However, the effect of nutrition on 3-IPA serum levels needs further exploration in order to determine if dietary interventions are a potential approach to increase 3-IPA levels in the plasma.

Furthermore, Wikoff *et al.* showed that colonization of germ-free mice with *Clostridium sporogenes* increased 3-IPA serum levels to the ones of normal mice 5 days after colonization [226]. Another study reported serum concentrations of 3-IPA of 80 µM four weeks after colonization, which would represent the effective treatment concentration [227]. Therefore, microbial replacement therapy could be another potential approach to modify the microbiome in order to accomplish permanent increase of 3-IPA plasma levels without the necessity of daily medication.

Final elucidation of the mechanism of 3-IPA in $CD8^+$ T cells might provide new insights in $CD8^+$ T cell stemness control and will further allow target-specific application of 3-IPA to ameliorate aging- and obesity-associated comorbidities, thereby preventing new aging- and obesity-associated pandemics to arise.

Literature

1. Telenti, A., et al., *After the pandemic: perspectives on the future trajectory of COVID-19.* Nature, 2021. **596**(7873): p. 495-504.
2. Fermini, B. and D.C. Bell, *On the perspective of an aging population and its potential impact on drug attrition and pre-clinical cardiovascular safety assessment.* J Pharmacol Toxicol Methods, 2022: p. 107184.
3. Berry, E.M., *The Obesity Pandemic-Whose Responsibility? No Blame, No Shame, Not More of the Same.* Front Nutr, 2020. **7**: p. 2.
4. Cantini, L., et al., *Evaluation of COVID-19 impact on DELAYing diagnostic-therapeutic pathways of lung cancer patients in Italy (COVID-DELAY study): fewer cases and higher stages from a real-world scenario.* ESMO Open, 2022. **7**(2): p. 100406.
5. United Nations, D.o.E.a.S.A., Population Division, *World Population Ageing 2015*. 2015.
6. United Nations, D.o.E.a.S.A., Population Division, *World Population Ageing 2019. Highlights*. 2019.
7. Niccoli, T. and L. Partridge, *Ageing as a risk factor for disease.* Curr Biol, 2012. **22**(17): p. R741-52.
8. Gavazzi, G. and K.H. Krause, *Ageing and infection.* Lancet Infect Dis, 2002. **2**(11): p. 659-66.
9. Santesmasses, D., et al., *COVID-19 is an emergent disease of aging.* Aging Cell, 2020. **19**(10): p. e13230.
10. Hayflick, L., *The Limited in Vitro Lifetime of Human Diploid Cell Strains.* Exp Cell Res, 1965. **37**: p. 614-36.
11. Campisi, J. and F. d'Adda di Fagagna, *Cellular senescence: when bad things happen to good cells.* Nat Rev Mol Cell Biol, 2007. **8**(9): p. 729-40.
12. Balistreri, C.R., et al., *NF-kappaB pathway activators as potential ageing biomarkers: targets for new therapeutic strategies.* Immun Ageing, 2013. **10**(1): p. 24.
13. Franceschi, C., et al., *Inflamm-aging. An evolutionary perspective on immunosenescence.* Ann N Y Acad Sci, 2000. **908**: p. 244-54.
14. Franceschi, C. and J. Campisi, *Chronic inflammation (inflammaging) and its potential contribution to age-associated diseases.* J Gerontol A Biol Sci Med Sci, 2014. **69 Suppl 1**: p. S4-9.
15. Divo, M.J., C.H. Martinez, and D.M. Mannino, *Ageing and the epidemiology of multimorbidity.* Eur Respir J, 2014. **44**(4): p. 1055-68.
16. Bluher, M., *Obesity: global epidemiology and pathogenesis.* Nat Rev Endocrinol, 2019. **15**(5): p. 288-298.
17. WHO, *Obesity and Overweight, https://www.who.int/news-room/fact-sheets/detail/obesity-and-overweight*. 2021, World Health Organization.
18. Bhaskaran, K., et al., *Body-mass index and risk of 22 specific cancers: a population-based cohort study of 5.24 million UK adults.* Lancet, 2014. **384**(9945): p. 755-65.
19. Karlsson, E.A. and M.A. Beck, *The burden of obesity on infectious disease.* Exp Biol Med (Maywood), 2010. **235**(12): p. 1412-24.
20. Gao, M., et al., *Associations between body-mass index and COVID-19 severity in 6.9 million people in England: a prospective, community-based, cohort study.* Lancet Diabetes Endocrinol, 2021. **9**(6): p. 350-359.
21. Ahima, R.S. and M.A. Lazar, *Adipokines and the peripheral and neural control of energy balance.* Mol Endocrinol, 2008. **22**(5): p. 1023-31.
22. Kawai, T., M.V. Autieri, and R. Scalia, *Adipose tissue inflammation and metabolic dysfunction in obesity.* Am J Physiol Cell Physiol, 2021. **320**(3): p. C375-C391.

23. Hotamisligil, G.S., *Inflammation and metabolic disorders.* Nature, 2006. **444**(7121): p. 860-7.
24. Murphy, K. and C. Weaver, *Janeway's Immunobiology, 9th Edition*. Vol. 9. 2017. 928.
25. Marcus, A., et al., *Recognition of tumors by the innate immune system and natural killer cells.* Adv Immunol, 2014. **122**: p. 91-128.
26. Bernheim, A. and R. Sorek, *The pan-immune system of bacteria: antiviral defence as a community resource.* Nat Rev Microbiol, 2020. **18**(2): p. 113-119.
27. Jones, J.D. and J.L. Dangl, *The plant immune system.* Nature, 2006. **444**(7117): p. 323-9.
28. Boehm, T., *Evolution of vertebrate immunity.* Curr Biol, 2012. **22**(17): p. R722-32.
29. Iwasaki, A. and R. Medzhitov, *Control of adaptive immunity by the innate immune system.* Nat Immunol, 2015. **16**(4): p. 343-53.
30. Janeway, C.A., Jr., *Approaching the asymptote? Evolution and revolution in immunology.* Cold Spring Harb Symp Quant Biol, 1989. **54 Pt 1**: p. 1-13.
31. Janeway, C.A., Jr. and R. Medzhitov, *Innate immune recognition.* Annu Rev Immunol, 2002. **20**: p. 197-216.
32. Iwasaki, A. and R. Medzhitov, *Toll-like receptor control of the adaptive immune responses.* Nat Immunol, 2004. **5**(10): p. 987-95.
33. Moretta, A., et al., *NK cells at the interface between innate and adaptive immunity.* Cell Death Differ, 2008. **15**(2): p. 226-33.
34. Marshall, J.S., et al., *An introduction to immunology and immunopathology.* Allergy Asthma Clin Immunol, 2018. **14**(Suppl 2): p. 49.
35. Miller, J.F., *Immunological function of the thymus.* Lancet, 1961. **2**(7205): p. 748-9.
36. Osmond, D.G., *B cell development in the bone marrow.* Semin Immunol, 1990. **2**(3): p. 173-80.
37. Akira, S., S. Uematsu, and O. Takeuchi, *Pathogen recognition and innate immunity.* Cell, 2006. **124**(4): p. 783-801.
38. Wieczorek, M., et al., *Major Histocompatibility Complex (MHC) Class I and MHC Class II Proteins: Conformational Plasticity in Antigen Presentation.* Front Immunol, 2017. **8**: p. 292.
39. Hozumi, N. and S. Tonegawa, *Evidence for somatic rearrangement of immunoglobulin genes coding for variable and constant regions.* Proc Natl Acad Sci U S A, 1976. **73**(10): p. 3628-32.
40. Cooper, M.D. and M.N. Alder, *The evolution of adaptive immune systems.* Cell, 2006. **124**(4): p. 815-22.
41. LeBien, T.W. and T.F. Tedder, *B lymphocytes: how they develop and function.* Blood, 2008. **112**(5): p. 1570-80.
42. Starr, T.K., S.C. Jameson, and K.A. Hogquist, *Positive and negative selection of T cells.* Annu Rev Immunol, 2003. **21**: p. 139-76.
43. Cyster, J.G., *Chemokines and cell migration in secondary lymphoid organs.* Science, 1999. **286**(5447): p. 2098-102.
44. Ngo, V.N., R.J. Cornall, and J.G. Cyster, *Splenic T zone development is B cell dependent.* J Exp Med, 2001. **194**(11): p. 1649-60.
45. Janeway, C.A., Jr., *The T cell receptor as a multicomponent signalling machine: CD4/CD8 coreceptors and CD45 in T cell activation.* Annu Rev Immunol, 1992. **10**: p. 645-74.
46. Zamoyska, R., *CD4 and CD8: modulators of T-cell receptor recognition of antigen and of immune responses?* Curr Opin Immunol, 1998. **10**(1): p. 82-7.
47. Singer, A. and R. Bosselut, *CD4/CD8 coreceptors in thymocyte development, selection, and lineage commitment: analysis of the CD4/CD8 lineage decision.* Adv Immunol, 2004. **83**: p. 91-131.
48. Holler, P.D. and D.M. Kranz, *Quantitative analysis of the contribution of TCR/pepMHC affinity and CD8 to T cell activation.* Immunity, 2003. **18**(2): p. 255-64.
49. Irvine, D.J., et al., *Direct observation of ligand recognition by T cells.* Nature, 2002. **419**(6909): p. 845-9.

50. Hampl, J., Y.H. Chien, and M.M. Davis, *CD4 augments the response of a T cell to agonist but not to antagonist ligands.* Immunity, 1997. **7**(3): p. 379-85.
51. Luescher, I.F., et al., *CD8 modulation of T-cell antigen receptor-ligand interactions on living cytotoxic T lymphocytes.* Nature, 1995. **373**(6512): p. 353-6.
52. Zhou, L., M.M. Chong, and D.R. Littman, *Plasticity of CD4+ T cell lineage differentiation.* Immunity, 2009. **30**(5): p. 646-55.
53. Swain, S.L., K.K. McKinstry, and T.M. Strutt, *Expanding roles for CD4(+) T cells in immunity to viruses.* Nat Rev Immunol, 2012. **12**(2): p. 136-48.
54. Lu, L., J. Barbi, and F. Pan, *The regulation of immune tolerance by FOXP3.* Nat Rev Immunol, 2017. **17**(11): p. 703-717.
55. Lalvani, A., et al., *Rapid effector function in CD8+ memory T cells.* J Exp Med, 1997. **186**(6): p. 859-65.
56. Veiga-Fernandes, H., et al., *Response of naive and memory CD8+ T cells to antigen stimulation in vivo.* Nat Immunol, 2000. **1**(1): p. 47-53.
57. McLane, L.M., M.S. Abdel-Hakeem, and E.J. Wherry, *CD8 T Cell Exhaustion During Chronic Viral Infection and Cancer.* Annu Rev Immunol, 2019. **37**: p. 457-495.
58. Russ, B.E., et al., *T cell immunity as a tool for studying epigenetic regulation of cellular differentiation.* Front Genet, 2013. **4**: p. 218.
59. Osinska, I., K. Popko, and U. Demkow, *Perforin: an important player in immune response.* Cent Eur J Immunol, 2014. **39**(1): p. 109-15.
60. Afonina, I.S., S.P. Cullen, and S.J. Martin, *Cytotoxic and non-cytotoxic roles of the CTL/NK protease granzyme B.* Immunol Rev, 2010. **235**(1): p. 105-16.
61. Badovinac, V.P. and J.T. Harty, *Intracellular staining for TNF and IFN-gamma detects different frequencies of antigen-specific CD8(+) T cells.* J Immunol Methods, 2000. **238**(1-2): p. 107-17.
62. Pipkin, M.E. and J. Lieberman, *Delivering the kiss of death: progress on understanding how perforin works.* Curr Opin Immunol, 2007. **19**(3): p. 301-8.
63. Karupiah, G., et al., *Inhibition of viral replication by interferon-gamma-induced nitric oxide synthase.* Science, 1993. **261**(5127): p. 1445-8.
64. Zhou, F., *Molecular mechanisms of IFN-gamma to up-regulate MHC class I antigen processing and presentation.* Int Rev Immunol, 2009. **28**(3-4): p. 239-60.
65. Carneiro, M.B., et al., *IFN-gamma-Dependent Recruitment of CD4(+) T Cells and Macrophages Contributes to Pathogenesis During Leishmania amazonensis Infection.* J Interferon Cytokine Res, 2015. **35**(12): p. 935-47.
66. Sethi, J.K. and G.S. Hotamisligil, *Metabolic Messengers: tumour necrosis factor.* Nat Metab, 2021. **3**(10): p. 1302-1312.
67. Sultana, D.A., et al., *Eliciting the T cell fate with Notch.* Semin Immunol, 2010. **22**(5): p. 254-60.
68. Germar, K., et al., *T-cell factor 1 is a gatekeeper for T-cell specification in response to Notch signaling.* Proc Natl Acad Sci U S A, 2011. **108**(50): p. 20060-5.
69. Van de Walle, I., et al., *GATA3 induces human T-cell commitment by restraining Notch activity and repressing NK-cell fate.* Nat Commun, 2016. **7**: p. 11171.
70. Li, L., M. Leid, and E.V. Rothenberg, *An early T cell lineage commitment checkpoint dependent on the transcription factor Bcl11b.* Science, 2010. **329**(5987): p. 89-93.
71. Taniuchi, I., *CD4 Helper and CD8 Cytotoxic T Cell Differentiation.* Annu Rev Immunol, 2018. **36**: p. 579-601.
72. Wills, M.R., et al., *Identification of naive or antigen-experienced human CD8(+) T cells by expression of costimulation and chemokine receptors: analysis of the human cytomegalovirus-specific CD8(+) T cell response.* J Immunol, 2002. **168**(11): p. 5455-64.
73. Danilo, M., et al., *Suppression of Tcf1 by Inflammatory Cytokines Facilitates Effector CD8 T Cell Differentiation.* Cell Rep, 2018. **22**(8): p. 2107-2117.
74. Seo, W., C. Jerin, and H. Nishikawa, *Transcriptional regulatory network for the establishment of CD8(+) T cell exhaustion.* Exp Mol Med, 2021. **53**(2): p. 202-209.

75. Schumann, J., et al., *Differences in CD44 Surface Expression Levels and Function Discriminates IL-17 and IFN-gamma Producing Helper T Cells.* PLoS One, 2015. **10**(7): p. e0132479.
76. Chakraborty, A.K. and A. Weiss, *Insights into the initiation of TCR signaling.* Nat Immunol, 2014. **15**(9): p. 798-807.
77. Riha, P. and C.E. Rudd, *CD28 co-signaling in the adaptive immune response.* Self Nonself, 2010. **1**(3): p. 231-240.
78. Curtsinger, J.M. and M.F. Mescher, *Inflammatory cytokines as a third signal for T cell activation.* Curr Opin Immunol, 2010. **22**(3): p. 333-40.
79. Robbins, S.H., et al., *Differential regulation of killer cell lectin-like receptor G1 expression on T cells.* J Immunol, 2003. **170**(12): p. 5876-85.
80. Schoenborn, J.R. and C.B. Wilson, *Regulation of interferon-gamma during innate and adaptive immune responses.* Adv Immunol, 2007. **96**: p. 41-101.
81. Intlekofer, A.M., et al., *Anomalous type 17 response to viral infection by CD8+ T cells lacking T-bet and eomesodermin.* Science, 2008. **321**(5887): p. 408-11.
82. Pearce, E.L., et al., *Control of effector CD8+ T cell function by the transcription factor Eomesodermin.* Science, 2003. **302**(5647): p. 1041-3.
83. Joshi, N.S., et al., *Inflammation directs memory precursor and short-lived effector CD8(+) T cell fates via the graded expression of T-bet transcription factor.* Immunity, 2007. **27**(2): p. 281-95.
84. Nakajima, Y., et al., *Critical role of the CD44(low)CD62L(low) CD8(+) T cell subset in restoring antitumor immunity in aged mice.* Proc Natl Acad Sci U S A, 2021. **118**(23).
85. Sallusto, F., et al., *Two subsets of memory T lymphocytes with distinct homing potentials and effector functions.* Nature, 1999. **401**(6754): p. 708-12.
86. Wherry, E.J., et al., *Lineage relationship and protective immunity of memory CD8 T cell subsets.* Nat Immunol, 2003. **4**(3): p. 225-34.
87. Martin, M.D. and V.P. Badovinac, *Defining Memory CD8 T Cell.* Front Immunol, 2018. **9**: p. 2692.
88. Mackay, L.K., et al., *The developmental pathway for CD103(+)CD8+ tissue-resident memory T cells of skin.* Nat Immunol, 2013. **14**(12): p. 1294-301.
89. Wu, J., et al., *T Cell Factor 1 Suppresses CD103+ Lung Tissue-Resident Memory T Cell Development.* Cell Rep, 2020. **31**(1): p. 107484.
90. Williams, M.A. and M.J. Bevan, *Effector and memory CTL differentiation.* Annu Rev Immunol, 2007. **25**: p. 171-92.
91. Buck, M.D., D. O'Sullivan, and E.L. Pearce, *T cell metabolism drives immunity.* J Exp Med, 2015. **212**(9): p. 1345-60.
92. Vander Heiden, M.G., L.C. Cantley, and C.B. Thompson, *Understanding the Warburg effect: the metabolic requirements of cell proliferation.* Science, 2009. **324**(5930): p. 1029-33.
93. van der Windt, G.J., et al., *Mitochondrial respiratory capacity is a critical regulator of CD8+ T cell memory development.* Immunity, 2012. **36**(1): p. 68-78.
94. O'Sullivan, D., et al., *Memory CD8(+) T cells use cell-intrinsic lipolysis to support the metabolic programming necessary for development.* Immunity, 2014. **41**(1): p. 75-88.
95. Wherry, E.J., *T cell exhaustion.* Nat Immunol, 2011. **12**(6): p. 492-9.
96. Blank, C.U., et al., *Defining 'T cell exhaustion'.* Nat Rev Immunol, 2019. **19**(11): p. 665-674.
97. Gallimore, A., et al., *Induction and exhaustion of lymphocytic choriomeningitis virus-specific cytotoxic T lymphocytes visualized using soluble tetrameric major histocompatibility complex class I-peptide complexes.* J Exp Med, 1998. **187**(9): p. 1383-93.
98. Zajac, A.J., et al., *Viral immune evasion due to persistence of activated T cells without effector function.* J Exp Med, 1998. **188**(12): p. 2205-13.
99. Gruener, N.H., et al., *Sustained dysfunction of antiviral CD8+ T lymphocytes after infection with hepatitis C virus.* J Virol, 2001. **75**(12): p. 5550-8.
100. Ye, B., et al., *T-cell exhaustion in chronic hepatitis B infection: current knowledge and clinical significance.* Cell Death Dis, 2015. **6**: p. e1694.

101. Shankar, P., et al., *Impaired function of circulating HIV-specific CD8(+) T cells in chronic human immunodeficiency virus infection.* Blood, 2000. **96**(9): p. 3094-101.
102. Mumprecht, S., et al., *Programmed death 1 signaling on chronic myeloid leukemia-specific T cells results in T-cell exhaustion and disease progression.* Blood, 2009. **114**(8): p. 1528-36.
103. Schietinger, A., et al., *Tumor-Specific T Cell Dysfunction Is a Dynamic Antigen-Driven Differentiation Program Initiated Early during Tumorigenesis.* Immunity, 2016. **45**(2): p. 389-401.
104. Ahmadzadeh, M., et al., *Tumor antigen-specific CD8 T cells infiltrating the tumor express high levels of PD-1 and are functionally impaired.* Blood, 2009. **114**(8): p. 1537-44.
105. Gandhi, M.K., et al., *Expression of LAG-3 by tumor-infiltrating lymphocytes is coincident with the suppression of latent membrane antigen-specific CD8+ T-cell function in Hodgkin lymphoma patients.* Blood, 2006. **108**(7): p. 2280-9.
106. Thommen, D.S., et al., *A transcriptionally and functionally distinct PD-1(+) CD8(+) T cell pool with predictive potential in non-small-cell lung cancer treated with PD-1 blockade.* Nat Med, 2018. **24**(7): p. 994-1004.
107. Wherry, E.J. and M. Kurachi, *Molecular and cellular insights into T cell exhaustion.* Nat Rev Immunol, 2015. **15**(8): p. 486-99.
108. Brooks, D.G., et al., *Interleukin-10 determines viral clearance or persistence in vivo.* Nat Med, 2006. **12**(11): p. 1301-9.
109. Fahey, L.M., et al., *Viral persistence redirects CD4 T cell differentiation toward T follicular helper cells.* J Exp Med, 2011. **208**(5): p. 987-99.
110. Crawford, A., et al., *Molecular and transcriptional basis of CD4(+) T cell dysfunction during chronic infection.* Immunity, 2014. **40**(2): p. 289-302.
111. Wherry, E.J., et al., *Viral persistence alters CD8 T-cell immunodominance and tissue distribution and results in distinct stages of functional impairment.* J Virol, 2003. **77**(8): p. 4911-27.
112. Moskophidis, D., et al., *Virus persistence in acutely infected immunocompetent mice by exhaustion of antiviral cytotoxic effector T cells.* Nature, 1993. **362**(6422): p. 758-61.
113. Li, W. and L. Zhang, *Rewiring Mitochondrial Metabolism for CD8(+) T Cell Memory Formation and Effective Cancer Immunotherapy.* Front Immunol, 2020. **11**: p. 1834.
114. Yu, Y.R., et al., *Disturbed mitochondrial dynamics in CD8(+) TILs reinforce T cell exhaustion.* Nat Immunol, 2020. **21**(12): p. 1540-1551.
115. Shin, H. and E.J. Wherry, *CD8 T cell dysfunction during chronic viral infection.* Curr Opin Immunol, 2007. **19**(4): p. 408-15.
116. Yamazaki, T., et al., *Expression of programmed death 1 ligands by murine T cells and APC.* J Immunol, 2002. **169**(10): p. 5538-45.
117. Lin, Y.M., et al., *High PD-L1 Expression Correlates with Metastasis and Poor Prognosis in Oral Squamous Cell Carcinoma.* PLoS One, 2015. **10**(11): p. e0142656.
118. Moon, J., Y.M. Oh, and S.J. Ha, *Perspectives on immune checkpoint ligands: expression, regulation, and clinical implications.* BMB Rep, 2021. **54**(8): p. 403-412.
119. Ishida, Y., et al., *Induced expression of PD-1, a novel member of the immunoglobulin gene superfamily, upon programmed cell death.* EMBO J, 1992. **11**(11): p. 3887-95.
120. Freeman, G.J., et al., *Engagement of the PD-1 immunoinhibitory receptor by a novel B7 family member leads to negative regulation of lymphocyte activation.* J Exp Med, 2000. **192**(7): p. 1027-34.
121. Latchman, Y., et al., *PD-L2 is a second ligand for PD-1 and inhibits T cell activation.* Nat Immunol, 2001. **2**(3): p. 261-8.
122. Nishimura, H., et al., *Development of lupus-like autoimmune diseases by disruption of the PD-1 gene encoding an ITIM motif-carrying immunoreceptor.* Immunity, 1999. **11**(2): p. 141-51.
123. Nishimura, H., et al., *Autoimmune dilated cardiomyopathy in PD-1 receptor-deficient mice.* Science, 2001. **291**(5502): p. 319-22.

124. Ahn, E., et al., *Role of PD-1 during effector CD8 T cell differentiation.* Proc Natl Acad Sci U S A, 2018. **115**(18): p. 4749-4754.
125. Hui, E., et al., *T cell costimulatory receptor CD28 is a primary target for PD-1-mediated inhibition.* Science, 2017. **355**(6332): p. 1428-1433.
126. Staron, M.M., et al., *The transcription factor FoxO1 sustains expression of the inhibitory receptor PD-1 and survival of antiviral CD8(+) T cells during chronic infection.* Immunity, 2014. **41**(5): p. 802-14.
127. Tivol, E.A., et al., *Loss of CTLA-4 leads to massive lymphoproliferation and fatal multiorgan tissue destruction, revealing a critical negative regulatory role of CTLA-4.* Immunity, 1995. **3**(5): p. 541-7.
128. Waterhouse, P., et al., *Lymphoproliferative disorders with early lethality in mice deficient in Ctla-4.* Science, 1995. **270**(5238): p. 985-8.
129. Brunet, J.F., et al., *A new member of the immunoglobulin superfamily--CTLA-4.* Nature, 1987. **328**(6127): p. 267-70.
130. Goldberg, M.V. and C.G. Drake, *LAG-3 in Cancer Immunotherapy.* Curr Top Microbiol Immunol, 2011. **344**: p. 269-78.
131. Agresta, L., K.H.N. Hoebe, and E.M. Janssen, *The Emerging Role of CD244 Signaling in Immune Cells of the Tumor Microenvironment.* Front Immunol, 2018. **9**: p. 2809.
132. Vigano, S., et al., *CD160-associated CD8 T-cell functional impairment is independent of PD-1 expression.* PLoS Pathog, 2014. **10**(9): p. e1004380.
133. Das, M., C. Zhu, and V.K. Kuchroo, *Tim-3 and its role in regulating anti-tumor immunity.* Immunol Rev, 2017. **276**(1): p. 97-111.
134. Harjunpaa, H. and C. Guillerey, *TIGIT as an emerging immune checkpoint.* Clin Exp Immunol, 2020. **200**(2): p. 108-119.
135. Blackburn, S.D., et al., *Coregulation of CD8+ T cell exhaustion by multiple inhibitory receptors during chronic viral infection.* Nat Immunol, 2009. **10**(1): p. 29-37.
136. Bengsch, B., et al., *Bioenergetic Insufficiencies Due to Metabolic Alterations Regulated by the Inhibitory Receptor PD-1 Are an Early Driver of CD8(+) T Cell Exhaustion.* Immunity, 2016. **45**(2): p. 358-73.
137. Xu, S., et al., *Uptake of oxidized lipids by the scavenger receptor CD36 promotes lipid peroxidation and dysfunction in CD8(+) T cells in tumors.* Immunity, 2021. **54**(7): p. 1561-1577 e7.
138. Ng, C.T. and M.B. Oldstone, *Infected CD8alpha- dendritic cells are the predominant source of IL-10 during establishment of persistent viral infection.* Proc Natl Acad Sci U S A, 2012. **109**(35): p. 14116-21.
139. Said, E.A., et al., *Programmed death-1-induced interleukin-10 production by monocytes impairs CD4+ T cell activation during HIV infection.* Nat Med, 2010. **16**(4): p. 452-9.
140. Richter, K., et al., *Macrophage and T cell produced IL-10 promotes viral chronicity.* PLoS Pathog, 2013. **9**(11): p. e1003735.
141. Ejrnaes, M., et al., *Resolution of a chronic viral infection after interleukin-10 receptor blockade.* J Exp Med, 2006. **203**(11): p. 2461-72.
142. Thomas, D.A. and J. Massague, *TGF-beta directly targets cytotoxic T cell functions during tumor evasion of immune surveillance.* Cancer Cell, 2005. **8**(5): p. 369-80.
143. Gunderson, A.J., et al., *TGFbeta suppresses CD8(+) T cell expression of CXCR3 and tumor trafficking.* Nat Commun, 2020. **11**(1): p. 1749.
144. Veiga-Parga, T., S. Sehrawat, and B.T. Rouse, *Role of regulatory T cells during virus infection.* Immunol Rev, 2013. **255**(1): p. 182-96.
145. Ng, C.T., et al., *Networking at the level of host immunity: immune cell interactions during persistent viral infections.* Cell Host Microbe, 2013. **13**(6): p. 652-64.
146. Goh, C., S. Narayanan, and Y.S. Hahn, *Myeloid-derived suppressor cells: the dark knight or the joker in viral infections?* Immunol Rev, 2013. **255**(1): p. 210-21.
147. Waggoner, S.N., et al., *Natural killer cells act as rheostats modulating antiviral T cells.* Nature, 2011. **481**(7381): p. 394-8.
148. Holderried, T.A., et al., *Genetic disruption of CD8+ Treg activity enhances the immune response to viral infection.* Proc Natl Acad Sci U S A, 2013. **110**(52): p. 21089-94.

149. Lim, A.R., W.K. Rathmell, and J.C. Rathmell, *The tumor microenvironment as a metabolic barrier to effector T cells and immunotherapy.* Elife, 2020. **9**.
150. Pauken, K.E., et al., *Epigenetic stability of exhausted T cells limits durability of reinvigoration by PD-1 blockade.* Science, 2016. **354**(6316): p. 1160-1165.
151. Sen, D.R., et al., *The epigenetic landscape of T cell exhaustion.* Science, 2016. **354**(6316): p. 1165-1169.
152. Intlekofer, A.M., et al., *Effector and memory CD8+ T cell fate coupled by T-bet and eomesodermin.* Nat Immunol, 2005. **6**(12): p. 1236-44.
153. Paley, M.A., et al., *Progenitor and terminal subsets of CD8+ T cells cooperate to contain chronic viral infection.* Science, 2012. **338**(6111): p. 1220-5.
154. Khan, O., et al., *TOX transcriptionally and epigenetically programs CD8(+) T cell exhaustion.* Nature, 2019. **571**(7764): p. 211-218.
155. Scott, A.C., et al., *TOX is a critical regulator of tumour-specific T cell differentiation.* Nature, 2019. **571**(7764): p. 270-274.
156. Yao, C., et al., *Single-cell RNA-seq reveals TOX as a key regulator of CD8(+) T cell persistence in chronic infection.* Nat Immunol, 2019. **20**(7): p. 890-901.
157. Alfei, F., et al., *TOX reinforces the phenotype and longevity of exhausted T cells in chronic viral infection.* Nature, 2019. **571**(7764): p. 265-269.
158. Stephen, T.L., et al., *Transforming growth factor beta-mediated suppression of antitumor T cells requires FoxP1 transcription factor expression.* Immunity, 2014. **41**(3): p. 427-439.
159. Shin, H., et al., *A role for the transcriptional repressor Blimp-1 in CD8(+) T cell exhaustion during chronic viral infection.* Immunity, 2009. **31**(2): p. 309-20.
160. Agnellini, P., et al., *Impaired NFAT nuclear translocation results in split exhaustion of virus-specific CD8+ T cell functions during chronic viral infection.* Proc Natl Acad Sci U S A, 2007. **104**(11): p. 4565-70.
161. Quigley, M., et al., *Transcriptional analysis of HIV-specific CD8+ T cells shows that PD-1 inhibits T cell function by upregulating BATF.* Nat Med, 2010. **16**(10): p. 1147-51.
162. Im, S.J., et al., *Defining CD8+ T cells that provide the proliferative burst after PD-1 therapy.* Nature, 2016. **537**(7620): p. 417-421.
163. Jadhav, R.R., et al., *Epigenetic signature of PD-1+ TCF1+ CD8 T cells that act as resource cells during chronic viral infection and respond to PD-1 blockade.* Proceedings of the National Academy of Sciences, 2019. **116**(28): p. 14113-14118.
164. Jansen, C.S., et al., *An intra-tumoral niche maintains and differentiates stem-like CD8 T cells.* Nature, 2019. **576**(7787): p. 465-470.
165. Utzschneider, D.T., et al., *T Cell Factor 1-Expressing Memory-like CD8(+) T Cells Sustain the Immune Response to Chronic Viral Infections.* Immunity, 2016. **45**(2): p. 415-27.
166. Martinez-Usatorre, A., et al., *Enhanced Phenotype Definition for Precision Isolation of Precursor Exhausted Tumor-Infiltrating CD8 T Cells.* Front Immunol, 2020. **11**: p. 340.
167. Beltra, J.C., et al., *Developmental Relationships of Four Exhausted CD8(+) T Cell Subsets Reveals Underlying Transcriptional and Epigenetic Landscape Control Mechanisms.* Immunity, 2020. **52**(5): p. 825-841 e8.
168. Wieland, D., et al., *TCF1(+) hepatitis C virus-specific CD8(+) T cells are maintained after cessation of chronic antigen stimulation.* Nat Commun, 2017. **8**: p. 15050.
169. Kefalakes, H., et al., *Hepatitis D Virus-Specific CD8(+) T Cells Have a Memory-Like Phenotype Associated With Viral Immune Escape in Patients With Chronic Hepatitis D Virus Infection.* Gastroenterology, 2019. **156**(6): p. 1805-1819 e9.
170. Leong, Y.A., et al., *CXCR5(+) follicular cytotoxic T cells control viral infection in B cell follicles.* Nat Immunol, 2016. **17**(10): p. 1187-96.
171. Miller, B.C., et al., *Subsets of exhausted CD8(+) T cells differentially mediate tumor control and respond to checkpoint blockade.* Nat Immunol, 2019. **20**(3): p. 326-336.
172. Siddiqui, I., et al., *Intratumoral Tcf1(+)PD-1(+)CD8(+) T Cells with Stem-like Properties Promote Tumor Control in Response to Vaccination and Checkpoint Blockade Immunotherapy.* Immunity, 2019. **50**(1): p. 195-211 e10.

173. Weisshaar, N., et al., *Rgs16 promotes antitumor CD8(+) T cell exhaustion.* Sci Immunol, 2022. **7**(71): p. eabh1873.
174. Hudson, W.H., et al., *Proliferating Transitory T Cells with an Effector-like Transcriptional Signature Emerge from PD-1(+) Stem-like CD8(+) T Cells during Chronic Infection.* Immunity, 2019. **51**(6): p. 1043-1058 e4.
175. Leach, D.R., M.F. Krummel, and J.P. Allison, *Enhancement of antitumor immunity by CTLA-4 blockade.* Science, 1996. **271**(5256): p. 1734-6.
176. Huang, A.C., et al., *T-cell invigoration to tumour burden ratio associated with anti-PD-1 response.* Nature, 2017. **545**(7652): p. 60-65.
177. Zahavi, D. and L. Weiner, *Monoclonal Antibodies in Cancer Therapy.* Antibodies (Basel), 2020. **9**(3).
178. Hargadon, K.M., C.E. Johnson, and C.J. Williams, *Immune checkpoint blockade therapy for cancer: An overview of FDA-approved immune checkpoint inhibitors.* Int Immunopharmacol, 2018. **62**: p. 29-39.
179. Shi, H., J. Lan, and J. Yang, *Mechanisms of Resistance to Checkpoint Blockade Therapy.* Adv Exp Med Biol, 2020. **1248**: p. 83-117.
180. Tumeh, P.C., et al., *PD-1 blockade induces responses by inhibiting adaptive immune resistance.* Nature, 2014. **515**(7528): p. 568-71.
181. Martens, A., et al., *Increases in Absolute Lymphocytes and Circulating CD4+ and CD8+ T Cells Are Associated with Positive Clinical Outcome of Melanoma Patients Treated with Ipilimumab.* Clin Cancer Res, 2016. **22**(19): p. 4848-4858.
182. Sade-Feldman, M., et al., *Defining T Cell States Associated with Response to Checkpoint Immunotherapy in Melanoma.* Cell, 2018. **175**(4): p. 998-1013 e20.
183. Weber, B.N., et al., *A critical role for TCF-1 in T-lineage specification and differentiation.* Nature, 2011. **476**(7358): p. 63-8.
184. Xing, S., et al., *Tcf1 and Lef1 transcription factors establish CD8(+) T cell identity through intrinsic HDAC activity.* Nat Immunol, 2016. **17**(6): p. 695-703.
185. Lin, W.W., et al., *CD8(+) T Lymphocyte Self-Renewal during Effector Cell Determination.* Cell Rep, 2016. **17**(7): p. 1773-1782.
186. Pais Ferreira, D., et al., *Central memory CD8(+) T cells derive from stem-like Tcf7(hi) effector cells in the absence of cytotoxic differentiation.* Immunity, 2020. **53**(5): p. 985-1000 e11.
187. Jeannet, G., et al., *Essential role of the Wnt pathway effector Tcf-1 for the establishment of functional CD8 T cell memory.* Proc Natl Acad Sci U S A, 2010. **107**(21): p. 9777-82.
188. Charmoy, M., et al., *PD-1(+) Tcf1(+) CD8(+) T cells from established chronic infection can form memory while retaining a stable imprint of persistent antigen exposure.* Cell Rep, 2021. **37**(6): p. 110010.
189. He, X., et al., *LDL receptor-related proteins 5 and 6 in Wnt/beta-catenin signaling: arrows point the way.* Development, 2004. **131**(8): p. 1663-77.
190. MacDonald, B.T., K. Tamai, and X. He, *Wnt/beta-catenin signaling: components, mechanisms, and diseases.* Dev Cell, 2009. **17**(1): p. 9-26.
191. Cadigan, K.M. and M.L. Waterman, *TCF/LEFs and Wnt signaling in the nucleus.* Cold Spring Harb Perspect Biol, 2012. **4**(11).
192. van Kappel, E.C. and M.M. Maurice, *Molecular regulation and pharmacological targeting of the beta-catenin destruction complex.* Br J Pharmacol, 2017. **174**(24): p. 4575-4588.
193. Steinke, F.C., et al., *TCF-1 and LEF-1 act upstream of Th-POK to promote the CD4(+) T cell fate and interact with Runx3 to silence Cd4 in CD8(+) T cells.* Nat Immunol, 2014. **15**(7): p. 646-656.
194. Gattinoni, L., et al., *Wnt signaling arrests effector T cell differentiation and generates CD8+ memory stem cells.* Nat Med, 2009. **15**(7): p. 808-13.
195. Zhao, D.M., et al., *Constitutive activation of Wnt signaling favors generation of memory CD8 T cells.* J Immunol, 2010. **184**(3): p. 1191-9.
196. Driessens, G., Y. Zheng, and T.F. Gajewski, *Beta-catenin does not regulate memory T cell phenotype.* Nat Med, 2010. **16**(5): p. 513-4; author reply 514-5.

197. Zhao, X., et al., *beta-catenin and gamma-catenin are dispensable for T lymphocytes and AML leukemic stem cells.* Elife, 2020. **9**.
198. Xu, Z., et al., *Cutting Edge: beta-Catenin-Interacting Tcf1 Isoforms Are Essential for Thymocyte Survival but Dispensable for Thymic Maturation Transitions.* J Immunol, 2017. **198**(9): p. 3404-3409.
199. Goronzy, J.J. and C.M. Weyand, *Aging, autoimmunity and arthritis: T-cell senescence and contraction of T-cell repertoire diversity - catalysts of autoimmunity and chronic inflammation.* Arthritis Res Ther, 2003. **5**(5): p. 225-34.
200. Denis, F., et al., *Hepatitis-B vaccination in the elderly.* J Infect Dis, 1984. **149**(6): p. 1019.
201. Weston, W.M., et al., *Vaccination of adults 65 years of age and older with tetanus toxoid, reduced diphtheria toxoid and acellular pertussis vaccine (Boostrix((R))): results of two randomized trials.* Vaccine, 2012. **30**(9): p. 1721-8.
202. Gagliardi, A.M., et al., *Vaccines for preventing herpes zoster in older adults.* Cochrane Database Syst Rev, 2012. **10**: p. CD008858.
203. Weyand, C.M. and J.J. Goronzy, *Aging of the Immune System. Mechanisms and Therapeutic Targets.* Ann Am Thorac Soc, 2016. **13 Suppl 5**: p. S422-S428.
204. Pang, W.W., et al., *Human bone marrow hematopoietic stem cells are increased in frequency and myeloid-biased with age.* Proc Natl Acad Sci U S A, 2011. **108**(50): p. 20012-7.
205. Beerman, I., et al., *Functionally distinct hematopoietic stem cells modulate hematopoietic lineage potential during aging by a mechanism of clonal expansion.* Proc Natl Acad Sci U S A, 2010. **107**(12): p. 5465-70.
206. Palmer, D.B., *The effect of age on thymic function.* Front Immunol, 2013. **4**: p. 316.
207. Linton, P.J. and K. Dorshkind, *Age-related changes in lymphocyte development and function.* Nat Immunol, 2004. **5**(2): p. 133-9.
208. Ouyang, Q., et al., *Age-associated accumulation of CMV-specific CD8+ T cells expressing the inhibitory killer cell lectin-like receptor G1 (KLRG1).* Exp Gerontol, 2003. **38**(8): p. 911-20.
209. Haslam, D.W. and W.P. James, *Obesity.* Lancet, 2005. **366**(9492): p. 1197-209.
210. Kane, H. and L. Lynch, *Innate Immune Control of Adipose Tissue Homeostasis.* Trends Immunol, 2019. **40**(9): p. 857-872.
211. Howard, J.K., et al., *Leptin protects mice from starvation-induced lymphoid atrophy and increases thymic cellularity in ob/ob mice.* J Clin Invest, 1999. **104**(8): p. 1051-9.
212. Martin-Romero, C., et al., *Human leptin enhances activation and proliferation of human circulating T lymphocytes.* Cell Immunol, 2000. **199**(1): p. 15-24.
213. Farooqi, I.S., et al., *Beneficial effects of leptin on obesity, T cell hyporesponsiveness, and neuroendocrine/metabolic dysfunction of human congenital leptin deficiency.* J Clin Invest, 2002. **110**(8): p. 1093-103.
214. De Rosa, V., et al., *A key role of leptin in the control of regulatory T cell proliferation.* Immunity, 2007. **26**(2): p. 241-55.
215. Miyara, M. and S. Sakaguchi, *Natural regulatory T cells: mechanisms of suppression.* Trends Mol Med, 2007. **13**(3): p. 108-16.
216. Karlsson, E.A., P.A. Sheridan, and M.A. Beck, *Diet-induced obesity in mice reduces the maintenance of influenza-specific CD8+ memory T cells.* J Nutr, 2010. **140**(9): p. 1691-7.
217. Karlsson, E.A., P.A. Sheridan, and M.A. Beck, *Diet-induced obesity impairs the T cell memory response to influenza virus infection.* J Immunol, 2010. **184**(6): p. 3127-33.
218. Sheridan, P.A., et al., *Obesity is associated with impaired immune response to influenza vaccination in humans.* Int J Obes (Lond), 2012. **36**(8): p. 1072-7.
219. Oestreich, K.J., A.C. Huang, and A.S. Weinmann, *The lineage-defining factors T-bet and Bcl-6 collaborate to regulate Th1 gene expression patterns.* J Exp Med, 2011. **208**(5): p. 1001-13.
220. Dutko, F.J. and M.B.A. Oldstone, *Genomic and Biological Variation among Commonly Used Lymphocytic Choriomeningitis Virus-Strains.* Journal of General Virology, 1983. **64**(Aug): p. 1689-1698.

221. Ahmed, R., et al., *Selection of genetic variants of lymphocytic choriomeningitis virus in spleens of persistently infected mice. Role in suppression of cytotoxic T lymphocyte response and viral persistence.* J Exp Med, 1984. **160**(2): p. 521-40.
222. Pircher, H., et al., *Tolerance induction in double specific T-cell receptor transgenic mice varies with antigen.* Nature, 1989. **342**(6249): p. 559-61.
223. Rakhra, V., et al., *Obesity and the Western Diet: How We Got Here.* Mo Med, 2020. **117**(6): p. 536-538.
224. Fontenot, J.D., M.A. Gavin, and A.Y. Rudensky, *Foxp3 programs the development and function of CD4+CD25+ regulatory T cells.* Nat Immunol, 2003. **4**(4): p. 330-6.
225. Mombaerts, P., et al., *Mutations in T-cell antigen receptor genes alpha and beta block thymocyte development at different stages.* Nature, 1992. **360**(6401): p. 225-31.
226. Wikoff, W.R., et al., *Metabolomics analysis reveals large effects of gut microflora on mammalian blood metabolites.* Proc Natl Acad Sci U S A, 2009. **106**(10): p. 3698-703.
227. Dodd, D., et al., *A gut bacterial pathway metabolizes aromatic amino acids into nine circulating metabolites.* Nature, 2017. **551**(7682): p. 648-652.
228. Bendheim, P.E., et al., *Development of indole-3-propionic acid (OXIGON) for Alzheimer's disease.* J Mol Neurosci, 2002. **19**(1-2): p. 213-7.
229. de Mello, V.D., et al., *Indolepropionic acid and novel lipid metabolites are associated with a lower risk of type 2 diabetes in the Finnish Diabetes Prevention Study.* Sci Rep, 2017. **7**: p. 46337.
230. Cason, C.A., et al., *Plasma microbiome-modulated indole- and phenyl-derived metabolites associate with advanced atherosclerosis and postoperative outcomes.* J Vasc Surg, 2018. **68**(5): p. 1552-1562 e7.
231. Sehgal, R., et al., *Indole-3-Propionic Acid, a Gut-Derived Tryptophan Metabolite, Associates with Hepatic Fibrosis.* Nutrients, 2021. **13**(10).
232. Madi, A., et al., *CD8 agonism functionally activates memory T cells and enhances antitumor immunity.* Int J Cancer, 2022. **151**(5): p. 797-808.
233. Lardy, H.A., D. Johnson, and M.W. Mc, *Antibiotics as tools for metabolic studies. I. A survey of toxic antibiotics in respiratory, phosphorylative and glycolytic systems.* Arch Biochem Biophys, 1958. **78**(2): p. 587-97.
234. Jain, V.K., et al., *Effects of 2-deoxy-D-glucose on glycolysis, proliferation kinetics and radiation response of human cancer cells.* Int J Radiat Oncol Biol Phys, 1985. **11**(5): p. 943-50.
235. Underwood, E., et al., *A method for assessing tissue respiration in anatomically defined brain regions.* Sci Rep, 2020. **10**(1): p. 13179.
236. Barrientos, A. and C.T. Moraes, *Titrating the effects of mitochondrial complex I impairment in the cell physiology.* J Biol Chem, 1999. **274**(23): p. 16188-97.
237. Choi, S.W., A.A. Gerencser, and D.G. Nicholls, *Bioenergetic analysis of isolated cerebrocortical nerve terminals on a microgram scale: spare respiratory capacity and stochastic mitochondrial failure.* J Neurochem, 2009. **109**(4): p. 1179-91.
238. Zhao, M., et al., *Rapid in vitro generation of bona fide exhausted CD8+ T cells is accompanied by Tcf7 promotor methylation.* PLoS Pathog, 2020. **16**(6): p. e1008555.
239. Sade-Feldman, M., et al., *Defining T Cell States Associated with Response to Checkpoint Immunotherapy in Melanoma.* Cell, 2019. **176**(1-2): p. 404.
240. Soares, A., et al., *Novel application of Ki67 to quantify antigen-specific in vitro lymphoproliferation.* J Immunol Methods, 2010. **362**(1-2): p. 43-50.
241. Rambold, A.S., et al., *Tubular network formation protects mitochondria from autophagosomal degradation during nutrient starvation.* Proc Natl Acad Sci U S A, 2011. **108**(25): p. 10190-5.
242. Sun, N., R.J. Youle, and T. Finkel, *The Mitochondrial Basis of Aging.* Mol Cell, 2016. **61**(5): p. 654-666.
243. Pendergrass, W., N. Wolf, and M. Poot, *Efficacy of MitoTracker Green and CMXrosamine to measure changes in mitochondrial membrane potentials in living cells and tissues.* Cytometry A, 2004. **61**(2): p. 162-9.

244. Zelante, T., et al., *Tryptophan catabolites from microbiota engage aryl hydrocarbon receptor and balance mucosal reactivity via interleukin-22.* Immunity, 2013. **39**(2): p. 372-85.
245. Gutierrez-Vazquez, C. and F.J. Quintana, *Regulation of the Immune Response by the Aryl Hydrocarbon Receptor.* Immunity, 2018. **48**(1): p. 19-33.
246. Kim, M.V., et al., *The transcription factor Foxo1 controls central-memory CD8+ T cell responses to infection.* Immunity, 2013. **39**(2): p. 286-97.
247. Gao, J., et al., *Impact of the Gut Microbiota on Intestinal Immunity Mediated by Tryptophan Metabolism.* Front Cell Infect Microbiol, 2018. **8**: p. 13.
248. Lee, K.A., et al., *Characterization of age-associated exhausted CD8(+) T cells defined by increased expression of Tim-3 and PD-1.* Aging Cell, 2016. **15**(2): p. 291-300.
249. Wang, Z., et al., *Paradoxical effects of obesity on T cell function during tumor progression and PD-1 checkpoint blockade.* Nat Med, 2019. **25**(1): p. 141-151.
250. Jura, M. and L.P. Kozak, *Obesity and related consequences to ageing.* Age (Dordr), 2016. **38**(1): p. 23.
251. Akter, R., et al., *Effect of Obesity on Fasting Blood Sugar.* Mymensingh Med J, 2017. **26**(1): p. 7-11.
252. Chang, R.C., et al., *High-Fat Diet-Induced Retinal Dysfunction.* Invest Ophthalmol Vis Sci, 2015. **56**(4): p. 2367-80.
253. Barnes, A.S., *The epidemic of obesity and diabetes: trends and treatments.* Tex Heart Inst J, 2011. **38**(2): p. 142-4.
254. Wondmkun, Y.T., *Obesity, Insulin Resistance, and Type 2 Diabetes: Associations and Therapeutic Implications.* Diabetes Metab Syndr Obes, 2020. **13**: p. 3611-3616.
255. *Consequences of the new diagnostic criteria for diabetes in older men and women. DECODE Study (Diabetes Epidemiology: Collaborative Analysis of Diagnostic Criteria in Europe).* Diabetes Care, 1999. **22**(10): p. 1667-71.
256. Chia, C.W., J.M. Egan, and L. Ferrucci, *Age-Related Changes in Glucose Metabolism, Hyperglycemia, and Cardiovascular Risk.* Circ Res, 2018. **123**(7): p. 886-904.
257. Palliyaguru, D.L., et al., *Fasting blood glucose as a predictor of mortality: Lost in translation.* Cell Metab, 2021. **33**(11): p. 2189-2200 e3.
258. Menees, K.B., et al., *Sex- and age-dependent alterations of splenic immune cell profile and NK cell phenotypes and function in C57BL/6J mice.* Immun Ageing, 2021. **18**(1): p. 3.
259. Kiran, S., et al., *High Fat Diet-Induced CD8(+) T Cells in Adipose Tissue Mediate Macrophages to Sustain Low-Grade Chronic Inflammation.* Front Immunol, 2021. **12**: p. 680944.
260. Jagger, A., et al., *Regulatory T cells and the immune aging process: a mini-review.* Gerontology, 2014. **60**(2): p. 130-7.
261. Nikolich-Zugich, J., *Ageing and life-long maintenance of T-cell subsets in the face of latent persistent infections.* Nat Rev Immunol, 2008. **8**(7): p. 512-22.
262. Yang, H., et al., *Obesity accelerates thymic aging.* Blood, 2009. **114**(18): p. 3803-12.
263. Chiu, B.C., et al., *Cutting edge: Central memory CD8 T cells in aged mice are virtual memory cells.* J Immunol, 2013. **191**(12): p. 5793-6.
264. Decman, V., et al., *Defective CD8 T cell responses in aged mice are due to quantitative and qualitative changes in virus-specific precursors.* J Immunol, 2012. **188**(4): p. 1933-41.
265. Zophel, D., et al., *Faster cytotoxicity with age: Increased perforin and granzyme levels in cytotoxic CD8(+) T cells boost cancer cell elimination.* Aging Cell, 2022. **21**(8): p. e13668.
266. Saxena, R.K., Q.B. Saxena, and W.H. Adler, *Lectin-induced cytotoxic activity in spleen cells from young and old mice. Age-related changes in types of effector cells, lymphokine production and response.* Immunology, 1988. **64**(3): p. 457-61.
267. Decman, V., et al., *Cell-intrinsic defects in the proliferative response of antiviral memory CD8 T cells in aged mice upon secondary infection.* J Immunol, 2010. **184**(9): p. 5151-9.

268. St-Onge, M.P. and D. Gallagher, *Body composition changes with aging: the cause or the result of alterations in metabolic rate and macronutrient oxidation?* Nutrition, 2010. **26**(2): p. 152-5.
269. Johnson, L.C., et al., *The plasma metabolome as a predictor of biological aging in humans.* Geroscience, 2019. **41**(6): p. 895-906.
270. Carrard, J., et al., *Metabolic View on Human Healthspan: A Lipidome-Wide Association Study.* Metabolites, 2021. **11**(5).
271. Papandreou, C., et al., *Circulating Metabolites Associated with Body Fat and Lean Mass in Adults with Overweight/Obesity.* Metabolites, 2021. **11**(5).
272. Ragonnaud, E. and A. Biragyn, *Gut microbiota as the key controllers of "healthy" aging of elderly people.* Immun Ageing, 2021. **18**(1): p. 2.
273. Ley, R.E., et al., *Obesity alters gut microbial ecology.* Proc Natl Acad Sci U S A, 2005. **102**(31): p. 11070-5.
274. Chyan, Y.J., et al., *Potent neuroprotective properties against the Alzheimer beta-amyloid by an endogenous melatonin-related indole structure, indole-3-propionic acid.* J Biol Chem, 1999. **274**(31): p. 21937-42.
275. Benson, J.M. and D.M. Shepherd, *Dietary ligands of the aryl hydrocarbon receptor induce anti-inflammatory and immunoregulatory effects on murine dendritic cells.* Toxicol Sci, 2011. **124**(2): p. 327-38.
276. Jennis, M., et al., *Microbiota-derived tryptophan indoles increase after gastric bypass surgery and reduce intestinal permeability in vitro and in vivo.* Neurogastroenterol Motil, 2018. **30**(2).
277. Tuomainen, M., et al., *Associations of serum indolepropionic acid, a gut microbiota metabolite, with type 2 diabetes and low-grade inflammation in high-risk individuals.* Nutr Diabetes, 2018. **8**(1): p. 35.
278. Zhang, B., et al., *The Mechanism Underlying the Influence of Indole-3-Propionic Acid: A Relevance to Metabolic Disorders.* Front Endocrinol (Lausanne), 2022. **13**: p. 841703.
279. Serger, E., et al., *The gut metabolite indole-3 propionate promotes nerve regeneration and repair.* Nature, 2022. **607**(7919): p. 585-592.
280. Zhang, L. and P. Romero, *Metabolic Control of CD8(+) T Cell Fate Decisions and Antitumor Immunity.* Trends Mol Med, 2018. **24**(1): p. 30-48.
281. Phan, A.T., et al., *Constitutive Glycolytic Metabolism Supports CD8(+) T Cell Effector Memory Differentiation during Viral Infection.* Immunity, 2016. **45**(5): p. 1024-1037.
282. Gabriel, S.S., et al., *Transforming growth factor-beta-regulated mTOR activity preserves cellular metabolism to maintain long-term T cell responses in chronic infection.* Immunity, 2021. **54**(8): p. 1698-1714 e5.
283. Raskov, H., et al., *Cytotoxic CD8(+) T cells in cancer and cancer immunotherapy.* Br J Cancer, 2021. **124**(2): p. 359-367.
284. Wang, D., et al., *A comprehensive profile of TCF1(+) progenitor and TCF1(-) terminally exhausted PD-1(+)CD8(+) T cells in head and neck squamous cell carcinoma: implications for prognosis and immunotherapy.* Int J Oral Sci, 2022. **14**(1): p. 8.
285. Petrova, V., et al., *The hypoxic tumour microenvironment.* Oncogenesis, 2018. **7**(1): p. 10.
286. Zhai, L., et al., *Immunosuppressive IDO in Cancer: Mechanisms of Action, Animal Models, and Targeting Strategies.* Front Immunol, 2020. **11**: p. 1185.
287. Sharma, M.D., et al., *Plasmacytoid dendritic cells from mouse tumor-draining lymph nodes directly activate mature Tregs via indoleamine 2,3-dioxygenase.* J Clin Invest, 2007. **117**(9): p. 2570-82.
288. Peng, Q., et al., *PD-L1 on dendritic cells attenuates T cell activation and regulates response to immune checkpoint blockade.* Nat Commun, 2020. **11**(1): p. 4835.
289. Iwai, Y., et al., *Involvement of PD-L1 on tumor cells in the escape from host immune system and tumor immunotherapy by PD-L1 blockade.* Proc Natl Acad Sci U S A, 2002. **99**(19): p. 12293-7.
290. Philip, M., et al., *Chromatin states define tumour-specific T cell dysfunction and reprogramming.* Nature, 2017. **545**(7655): p. 452-456.

291. Matloubian, M., et al., *Molecular determinants of macrophage tropism and viral persistence: importance of single amino acid changes in the polymerase and glycoprotein of lymphocytic choriomeningitis virus.* J Virol, 1993. **67**(12): p. 7340-9.
292. Bergthaler, A., et al., *Viral replicative capacity is the primary determinant of lymphocytic choriomeningitis virus persistence and immunosuppression.* Proc Natl Acad Sci U S A, 2010. **107**(50): p. 21641-6.
293. Kapasi, Z.F., et al., *Defective generation but normal maintenance of memory T cells in old mice.* Eur J Immunol, 2002. **32**(6): p. 1567-73.
294. Green, W.D., et al., *Metabolic and functional impairment of CD8(+) T cells from the lungs of influenza-infected obese mice.* J Leukoc Biol, 2022. **111**(1): p. 147-159.
295. Khan, S.H., et al., *Diet-induced obesity does not impact the generation and maintenance of primary memory CD8 T cells.* J Immunol, 2014. **193**(12): p. 5873-82.
296. Shan, Q., et al., *Tcf1 preprograms the mobilization of glycolysis in central memory CD8(+) T cells during recall responses.* Nat Immunol, 2022. **23**(3): p. 386-398.
297. Peters, M.J., et al., *The transcriptional landscape of age in human peripheral blood.* Nat Commun, 2015. **6**: p. 8570.
298. Simar, D., et al., *DNA methylation is altered in B and NK lymphocytes in obese and type 2 diabetic human.* Metabolism, 2014. **63**(9): p. 1188-97.
299. Vaena, S., et al., *Aging-dependent mitochondrial dysfunction mediated by ceramide signaling inhibits antitumor T cell response.* Cell Rep, 2021. **35**(5): p. 109076.
300. Ron-Harel, N., et al., *Defective respiration and one-carbon metabolism contribute to impaired naive T cell activation in aged mice.* Proc Natl Acad Sci U S A, 2018. **115**(52): p. 13347-13352.
301. Jheng, H.F., et al., *Mitochondrial fission contributes to mitochondrial dysfunction and insulin resistance in skeletal muscle.* Mol Cell Biol, 2012. **32**(2): p. 309-19.
302. Turbitt, W.J., et al., *Obesity and CD8 T cell metabolism: Implications for anti-tumor immunity and cancer immunotherapy outcomes.* Immunol Rev, 2020. **295**(1): p. 203-219.
303. Leon-Ponte, M., G.P. Ahern, and P.J. O'Connell, *Serotonin provides an accessory signal to enhance T-cell activation by signaling through the 5-HT7 receptor.* Blood, 2007. **109**(8): p. 3139-46.
304. Luo, J., et al., *Effect of melatonin on T/B cell activation and immune regulation in pinealectomy mice.* Life Sci, 2020. **242**: p. 117191.
305. Roager, H.M. and T.R. Licht, *Microbial tryptophan catabolites in health and disease.* Nat Commun, 2018. **9**(1): p. 3294.
306. Kowalczyk, A.P., et al., *The amino-terminal domain of desmoplakin binds to plakoglobin and clusters desmosomal cadherin-plakoglobin complexes.* J Cell Biol, 1997. **139**(3): p. 773-84.
307. Maeda, O., et al., *Plakoglobin (gamma-catenin) has TCF/LEF family-dependent transcriptional activity in beta-catenin-deficient cell line.* Oncogene, 2004. **23**(4): p. 964-72.
308. Yang, L., et al., *Desmoplakin acts as a tumor suppressor by inhibition of the Wnt/beta-catenin signaling pathway in human lung cancer.* Carcinogenesis, 2012. **33**(10): p. 1863-70.
309. Aktary, Z., M. Alaee, and M. Pasdar, *Beyond cell-cell adhesion: Plakoglobin and the regulation of tumorigenesis and metastasis.* Oncotarget, 2017. **8**(19): p. 32270-32291.
310. Mahendram, S., et al., *Ectopic gamma-catenin expression partially mimics the effects of stabilized beta-catenin on embryonic stem cell differentiation.* PLoS One, 2013. **8**(5): p. e65320.
311. Driessens, G., et al., *Beta-catenin inhibits T cell activation by selective interference with linker for activation of T cells-phospholipase C-gamma1 phosphorylation.* J Immunol, 2011. **186**(2): p. 784-90.
312. Lovatt, M. and M.J. Bijlmakers, *Stabilisation of beta-catenin downstream of T cell receptor signalling.* PLoS One, 2010. **5**(9).

313. Harly, C., et al., *A Shared Regulatory Element Controls the Initiation of Tcf7 Expression During Early T Cell and Innate Lymphoid Cell Developments.* Front Immunol, 2020. **11**: p. 470.
314. Kwon, H., et al., *Androgen conspires with the CD8(+) T cell exhaustion program and contributes to sex bias in cancer.* Sci Immunol, 2022. **7**(73): p. eabq2630.
315. Generoso, S.F., et al., *Pharmacological folding chaperones act as allosteric ligands of Frizzled4.* Nat Chem Biol, 2015. **11**(4): p. 280-6.
316. Huang, J., et al., *Activation of Wnt/beta-catenin signalling via GSK3 inhibitors direct differentiation of human adipose stem cells into functional hepatocytes.* Sci Rep, 2017. **7**: p. 40716.
317. Tsui, C., et al., *MYB orchestrates T cell exhaustion and response to checkpoint inhibition.* Nature, 2022.
318. Leeming, E.R., et al., *Effect of Diet on the Gut Microbiota: Rethinking Intervention Duration.* Nutrients, 2019. **11**(12).
319. Menni, C., et al., *Circulating levels of the anti-oxidant indoleproprionic acid are associated with higher gut microbiome diversity.* Gut Microbes, 2019. **10**(6): p. 688-695.

Supplements

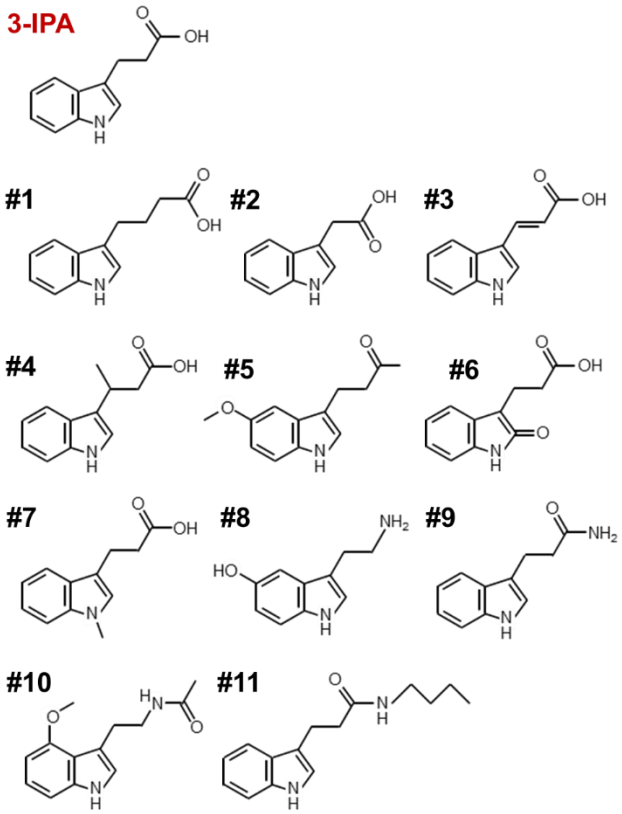

1	Indole-3 butyric acid
2	Indole-3-acetic acid
3	Trans-Indole-3-acrylic acid
4	3-(1H-Indol-3-yl)butanoic acid
5	3-(5-Methoxy-1H-indol-3-yl)propanoic acid
6	3-(2-Oxo-2,3-dihydro-1H-indol-3yl) propanoic acid
7	3-(1-Methyl-1H-indol-3-yl)propanoic acid
8	3-(β-Aminoethyl)-5-hydroxyindole (Serotonin)
9	1H-indole-3-propanamide
10	N-Acetyl-5-methoxytryptamine (Melatonin)
11	Screening Compound ($C_{15}H_{20}N_2O$)

Supplementary Figure 1: Chemical structures of 3-IPA and structurally similar molecules.

List of figures

List of tables